IVW - Schriftenreihe Band 47

Institut für Verbundwerkstoffe GmbH - Kaiserslautern

Juha Hartikainen

Tailoring of the properties of long glass fibre reinforced thermoplastics

Bibliografische Information Der Deutschen Bibliothek

Die Deutsche Bibliothek verzeichnet diese Publikation in der Deutschen Nationalbibliografie; detaillierte bibliografische Daten sind im Internet über http://dnb.ddb.de abrufbar.

Herausgeber: Institut für Verbundwerkstoffe GmbH
Prof. Dr.-Ing. Alois K. Schlarb
Erwin-Schrödinger-Straße
TU Kaiserslautern, Gebäude 58
67663 Kaiserslautern
http://www.ivw.uni-kl.de

Verlag: Institut für Verbundwerkstoffe GmbH

Druck: Technische Universität Kaiserslautern
ZBT – Abteilung Foto-Repro-Druck

D 386

Als Manuskript gedruckt. Printed in Germany.

ISSN 1615-021X
ISBN 3-934930-43-3

Tailoring of the properties of long glass fibre reinforced thermoplastics

Vom Fachbereich für Maschinenbau und Verfahrenstechnik

der Technischen Universität Kaiserslautern

zur Verleihung des akademischen Grades

Doktor-Ingenieur (Dr.-Ing.)

genehmigte Dissertation

von

Dipl.-Ing. Juha Hartikainen

aus Espoo, Finnland

Tag der mündlichen Prüfung:	23. Juli 2004
Prüfungsvorsitzender:	Prof. Dr.-Ing. D.-H. Hellmann
1. Berichterstatter:	Prof. Dr.-Ing. K. Friedrich
2. Berichterstatter:	Prof. Dr.-Ing. S. Toll

D 386

ACKNOWLEDGEMENTS

The present thesis reports the results of the experiments that were carried out during the years 2001-2004 at the company FACT GmbH and at Institut für Verbundwerkstoffe GmbH (IVW) of Kaiserslautern University of Technology. The study was carried out under Marie Curie Fellowships program of the European Commission (contract number G5TR-CT2001-00052).

First of all, I thank sincerely the European Commission and the company FACT GmbH for the financial support.

Prof. K. Friedrich I want to thank for supervising my thesis and for collaboration. The group of Prof. O. Ikkala and Prof. J. Ruokolainen of Helsinki University of Technology and the group of Prof. A. Duckett of University of Leeds I wish to thank for fruitful cooperation. Additionally, I am grateful to Prof. J. Karger-Kocsis for discussions, advices and guidance on many scientific questions. Also, I wish to thank Prof. S. Toll for correcting my thesis and Prof. D.-H. Hellmann for heading the examination committee.

Most of all, I extend my deepest gratitude to Dr. T. Harmia, whose practical guidance and constructive criticism were particularly important for the success of this work. I am especially grateful for his untiring support, encouragement and positive attitude throughout the project. Thank you very much.

I am also indebted to my colleagues at FACT and at IVW for numerous discussions, experimental help, comments and encouragement. Especially Mr. M. Lindner, Mr. J. Ibach and Mr. G. Hens of FACT, and Dr. P. Tsotra and Dr. O. Gryshchuk of IVW are thanked.

Finally, I want to thank my wife Jenny for support and understanding.

Kaiserslautern in August 2004 Juha Hartikainen

INDEX

ABBREVIATIONS

ABS	Acrylonitrile-butadiene-styrene copolymer
AE	Acoustic emission
AN	Acrylonitrile
ASA	Acrylonitrile-styrene-acrylate copolymer
BOPP	Biaxially oriented polypropylene (film)
BSSE	Basis set superposition error
DBSA	Dodecylbenzenesulfhonic acid
DFT	Density functional theory
DMTA	Dynamic mechanical thermal analysis
DSC	Differential scanning calorimetry
ESP	Electrostatic potential
ESR	Electron spin resonance (spectroscopy)
FTIR	Fourier transform infrared (spectroscopy)
GMT	Glass-mat reinforced thermoplastics
HIPS	High-impact polystyrene (rubber modified polystyrene)
HMTA	Hexamethylene tetramine
IPN	Interpenetrating network
LEFM	Linear elastic fracture mechanics
LFT	Long fibre reinforced thermoplastics
LFT-D	Direct process for long fibre reinforced thermoplastics
LGF	Long glass fibres
MAH	Maleic acid anhydride
MFD	Melt flow direction
MP2	Second-order Møller-Plesset perturbation theory

NMA	N-methylacetamide
NMR	Nuclear magnetic resonance (spectroscopy)
PA	Polyamide
PA6	Polyamide-6
PA66	Polyamide-66
PBT	Poly(butylene terephtalate)
PC/ABS	Polycarbonate/acrylonitrile-butadiene-styrene copolymer blend
PEEK	Polyether etherketone
PFR	Phenol formaldehyde resin
PMMA	Poly(methyl methacrylate)
PP	Polypropylene
PPS	Polyphenylenesulfide
PS	Polystyrene
PS-*co*-MAH	Styrene-maleic acid anhydride copolymer (=SMA)
PSU	Polysulfone
SAN	Styrene-acrylonitrile copolymer
SAN-*co*-MAH	Styrene-acrylonitrile-maleic acid anhydride copolymer
SAXS	Small angle X-ray scattering
SEM	Scanning electron microscopy
SEN-T	Single edge notched tensile
SFT	Short fibre reinforced thermoplastics
SGF	Short glass fibres
SMA	Styrene-maleic acid anhydride copolymer
STO	Slater type orbital
TEM	Transmission electron microscopy
γ-MPS	γ-methacryloxypropyltrimethoxysilane

SYMBOLS

ϕ	[°]	In-plane orientation angle
θ	[°]	Out-of-plane orientation angle
ρ	[g/cm^3]	Density of the specimen
α		Mark-Howink constant for molecular weight
ρ_0	[g/cm^3]	Density of water
σ_c	[MPa]	Gross fracture stress
ω_i		Weight fraction of component i
η_r		Relative viscosity
η_{sp}		Specific viscosity
$[\eta]$	[dl/g]	Solution viscosity
a	[mm]	Notch length
E*	[MPa]	Complex modulus
F_{max}	[N]	Maximum force
G_c	[J]	Critical fracture energy
K	[dl/g]	Mark-Howink constant for molecular weight
K_c	[MPa$\sqrt{m}$]	Critical stress intensity factor
L/D		Length/diameter ratio (fibre aspect ratio)
m_{air}	[g]	Weight of the specimen in air
M_v	[g/mol]	Viscosity averaged molecular weight
P	[g]	The buoyancy of the specimen in water
t	[s]	Effux time
tan δ		Mechanical loss factor
T_c	[°C]	Crystallisation (peak) temperature
T_g	[°C]	Glass transition temperature

T_m	[°C]	Melting temperature
W	[mm]	Specimen width
Y		Geometrical factor for SEN-T specimens
ΔE	[kJ/mol]	Complexation energy

ABSTRACT

The fact that long fibre reinforced thermoplastic composites (LFT) have higher tensile strength, modulus and even toughness, compared to short fibre reinforced thermoplastics with the same fibre loading has been well documented in literature. These are the underlying factors that have made LFT materials one of the most rapidly growing sectors of plastics industry. New developments in manufacturing of LFT composites have led to improvements in mechanical properties and price reduction, which has made these materials an attractive choice as a replacement for metals in automobile parts and other similar applications. However, there are still several open scientific questions concerning the material selection leading to the optimal property combinations. The present work is an attempt to clarify some of these questions. The target was to develop tools that can be used to modify, or to "tailor", the properties of LFT composite materials, according to the requirements of automobile and other applications.

The present study consisted of three separate case studies, focusing on the current scientific issues on LFT material systems. The first part of this work was focused on LGF reinforced thermoplastic styrenic resins. The target was to find suitable maleic acid anhydride (MAH) based coupling agents in order to improve the fibre-matrix interfacial strength, and, in this way, to develop an LGF concentrate suitable for thermoplastic styrenic resins. It was shown that the mechanical properties of LGF reinforced "styrenics" were considerably improved when a small amount of MAH functionalised polymer was added to the matrix. This could be explained by the better fibre-matrix adhesion, revealed by scanning electron microscopy of fracture surfaces. A novel LGF concentrate concept showed that one particular base material can be used to produce parts with different mechanical and thermal properties by diluting the fibre content with different types of thermoplastic styrenic resins. Therefore, this concept allows a flexible production of parts, and it can be used in the manufacturing of interior parts for automobile components.

The second material system dealt with so called hybrid composites, consisting of long glass fibre reinforced polypropylene (LGF-PP) and mineral fillers like calcium carbonate and talcum. The aim was to get more information about the fracture behaviour of such hybrid composites under tensile and impact loading, and to observe the influence of the fillers on properties. It was found that, in general, the addition of fillers in LGF-PP, increased stiffness but the strength and fracture toughness were decreased. However, calcium carbonate and talcum fillers resulted in different mechanical properties, when added to LGF-PP: better mechanical properties were achieved by using talcum, compared to calcium carbonate. This phenomenon could be explained by the different nucleation effect of these fillers, which resulted in a different crystalline morphology of polypropylene, and by the particle orientation during the processing when talc was used. Furthermore, the acoustic emission study revealed that the fracture mode of LGF-PP changed when calcium carbonate was added. The characteristic acoustic signals revealed that the addition of filler led to the fibre debonding at an earlier stage of fracture sequence when compared to unfilled LGF-PP.

In the third material system, the target was to develop a novel long glass fibre reinforced composite material based on the blend of polyamide with thermoset resins. In this study a blend of polyamide-66 (PA66) and phenol formaldehyde resin (PFR) was used. The chemical structure of the PA66-PFR resin was analysed by using small molecular weight analogues corresponding to PA66 and PFR components, as well as by carrying out experiments using the macromolecular system. Theoretical calculations and experiments showed that there exists a strong hydrogen bonding between the carboxylic groups of PA66 and the hydroxylic groups of PFR, exceeding even the strength of amide-water hydrogen bonds. This was shown to lead to the miscible blends, when PFR was not crosslinked. It was also found that the morphology of such thermoplastic-thermoset blends can be controlled by altering ratio of blend components (PA66, PFR and crosslinking agent). In the next phase, PA66-PFR blends were reinforced by long glass fibres. The studies showed that the water absorption of the blend samples was considerably decreased, which was also reflected in higher mechanical properties at equilibrium state.

KURZFASSUNG

Wie man aus zahlreichen Untersuchungen und Anwendungsbeispielen entnehmen kann, besitzen langfaserverstärkte Thermoplaste (LFT) eine bessere Zugfestigkeit, Biege- und Schlagzähigkeit im Vergleich zu kurzfaserverstärkten Thermoplasten. Die Vorteile in den mechanischen Eigenschaften haben die LFT zu einem schnellwachsenden Bereich in der Kunststoffindustrie gemacht. Neue Entwicklungen in Bereich der Herstellung von LFT haben für zusätzliche Verbesserungen der mechanischen Eigenschaften sowie eine Preisreduzierung der Materialien in den vergangenen Jahren gesorgt, was die LFT zu einer attraktiven Wahl u.a. als Ersatz von Metallen in Automobilteilen macht. Es stellen sich allerdings immer noch einige offene wissenschaftliche Fragen in Bezug auf z.B. die Materialbeschaffenheit, um optimale Eigenschaftskombinationen zu erreichen. Die vorliegende Arbeit versucht, einige dieser Fragen zu beantworten. Ziel war es, Vorgehensweisen zu entwickeln, mit denen man die Eigenschaften von LFT gezielt beeinflussen und so den Anforderungen von Automobilen oder anderen Anwendungen anpassen oder „maßschneidern“ kann.

Die vorliegende Arbeit besteht aus drei Teilen, welche sich auf unterschiedliche Materialsysteme, angepasst an den aktuellen Bedarf und das Interesse der Industrie, konzentrieren.

Der erste Teil der Arbeit richtet sich auf die Eigenschaftsoptimierung von langglasfaserverstärkten (LGF) thermoplastischen Styrolcopolymeren und von Blends aus diesen Materialien. Es wurden passende, auf Maleinsäureanhydride (MAH) basierende Kopplungsmittel gefunden, um die Faser-Matrix-Haftung zu optimieren. Weiterhin wurde ein LGF Konzentrat entwickelt, welches mit verschiedenen thermoplastischen Styrolcopolymeren kompatibel ist und somit als „Verstärkungsadditiv“ eingesetzt werden kann.

Das Konzept für ein neues LGF-Konzentrat auf Basis des kompatiblen Materialsystems konzentriert sich insbesondere darauf, dass ein Basismaterial für die Herstellung von Bauteilen bereit gestellt werden kann, mit dessen Hilfe gezielt verschiedene mechanische und thermomechanischen Eigenschaften durch das Zumischen von verschiedenen Styrolcopoylmeren und Blends verbessert werden können. Dieses Konzept ermöglicht eine sehr flexible Produktion von Bauteilen und wird seine Anwendung bei der Herstellung von Bauteilen u.a. im Interieur von Autos finden.

Das zweite Materialsystem basiert auf sogenannten hybriden Verbundwerkstoffen, welche aus Langglasfasern und mineralischen Füllstoffen wie Kalziumkarbonat und Talkum in einer Polypropylen (PP) - Matrix zusammengesetzt sind. Ziel war es, durch detaillierte bruchmechanische Analysen genaue Informationen über das Bruchverhalten dieser hybriden Verbundwerkstoffe bei Zug- und Schlagbelastung zu bekommen, um dann die Unterschiede zwischen den verschiedenen Füllstoffen in Bezug auf ihre Eigenschaften zu dokumentieren. Es konnte beobachtet werden, dass bei Zugabe der Füllstoffe zum LGF-PP normalerweise die Steifigkeit weiter verbessert wurde, jedoch die Festigkeit und Schlagzähigkeit abnahmen. Weiterhin zeigten die verschiedenen Füllstoffe wie Kalziumkarbonat und Talkum unterschiedliche mechanische Eigenschaften auf, wenn sie zusammen mit LGF Verstärkung eingesetzt wurden: Bei der Zugabe von Talkum wurde u.a. eine deutlich bessere Schlagzähigkeit als bei der Zugabe von Kalziumkarbonat festgestellt. Dieses Phänomen konnte durch das unterschiedliche Nukleierungsverhalten des PPs erklärt werden, welches in einer unterschiedlichen Kristallmorphologie von Polypropylen resultierte. Weiterhin konnte man durch Messungen der akustischen Emmissionen während der Zugbelastung eines bruchmechanischen Versuchskörpers aufzeigen, dass die höhere Bruchzähigkeit von LGF-PP ohne Füllstoffe daraus resultiert, dass Faser-Pullout schon bei geringeren Kräften vorhanden war.

Im dritten Materialsystem war es das Ziel, eine neue Gruppe von langglasfaserverstärkten Thermoplasten zu entwickeln, welche auf einer Mischung aus Polyamid und duroplastischen Kunststoffen oder Harzen basiert. Die Untersuchungen wurden anhand einer Mischung aus Polyamid-66 (PA66) und Phenolformaldehyd-Harz (PFR) durchgeführt. Die chemische Struktur des PA66-PFR Systems wurde mit Modellmaterialien mit ähnlichem chemischen Aufbau untersucht. Theoretische Berechnungen und experimentelle Untersuchungen weisen auf, dass eine starke Wasserstoffverbindung zwischen der Carboxylgruppe von PA66 und der Hydroxylgruppe von PFR vorhanden ist, welche sogar die Stärke von Amid-Wasserstoff-Bindungen übersteigt. Dies konnte mit Mischungen aufgezeigt werden, bei denen PFR nicht chemisch vernetzt wurde. Es wurde weiterhin festgestellt, dass die Morphologie dieser thermoplastischen Blends mit Duroplasten anhand des Verhältnisses der Bestandteile und der Menge der vernetzenden Reaktionspartner kontrolliert werden kann. In einem weiteren Schritt wurden diese PA66-PFR Mischungen mit Langglasfasern verstärkt. Die Versuche ergaben eine Reduzierung der Wasseraufnahme und damit verbundene, bessere mechanische Eigenschaften.

1 INTRODUCTION TO THE TOPIC

Thermoplastic composites form a material class which was discovered in 1960's when Menges replaced epoxy with polyamide as a composite matrix [1]. Later other thermoplastics like polyphenylenesulfide (PPS), polyether etherketone (PEEK), polysulfone (PSU) and polypropylene (PP) were reinforced with glass, carbon and other types of fibres. Nowadays thermoplastic composites are increasingly replacing corresponding thermosets and other materials. There are 3 main reasons for this [2-6]. Firstly, thermoplastics allow, in principle, fast processing of the composites, without the curing reaction of thermosets. Thermoplastic polymers only need to be melted, brought into contact with the fibres, then shaped and cooled, which minimises the cycle times compared to epoxy and other thermosets where curing can take several hours. Secondly, thermoplastic matrices offer attractive properties like high impact toughness, good fatigue resistance and excellent chemical resistance. Third factor is that thermoplastic matrices offer environmental benefits in the sense that they can be easily recycled and have low toxicity [7].

Table 1 presents some properties of thermosets and thermoplastics, comparing the differences between these two types of matrices. One can observe that the use of thermoplastic resins instead of thermosets offers many benefits. These include good stability of the prepregs during the storing, high fracture toughness, and short consolidation time. Additionally, good recyclability is becoming more and more important in the future, due to the tightening environmental legislation. This makes thermoplastic composites a highly potential material class for several applications, such as automobile components. It must be noted, however, that impregnation, *i.e.* the process where the polymer melt is introduced between the individual fibres, is not straightforward in the case of thermoplastics due to the high melt viscosity. This generally results in poor wetting of the applied fibres with these polymers. The full potential of these materials will only be realised when efficient processes and high quality thermoplastic materials are used.

Table 1.1: Comparison between the properties of thermoplastic and thermoset matrices [8]

	Thermosets	*Thermoplastics*
Prepreg production	Very good	Poor
Prepreg tack	Very good	No
Prepreg storability	Poor	Very good
Shrinkage	Little	Little
Fracture toughness	Low	High
Solvent resistance	Good	Poor-good
Crystallisation problems	No	Yes
Recycling	Poor	Good
Consolidation time	High	Very short

Traditionally reinforcing fibres in thermoplastic composites are short in length, the average fibre length varying typically from 0.2 to 0.5 mm. However, mechanical properties of these materials can be further improved by using longer fibres [9]. Therefore, an increasing number of scientists, engineers and companies are working today with discontinuous long fibre reinforced thermoplastics, where fibre length can be up to 25 mm, or with composites with continuous fibres (Figure 1.1). In the latter case fibre length actually reflects the geometry of the manufactured part. Different methods have been presented in literature in order to manufacture long fibre thermoplastic composites. The basic issue is to wet, *i.e*. impregnate, the applied fibres with the chosen thermoplastic matrix. Today many methods are used: continuous melt impregnation, solvent impregnation, powder impregnation and different methods resulting in thermoplastics with mat-like reinforcements. A common feature of most methods is that reinforcing fibres are assembled into intimate contact with the resin so that the flow length of the viscous melt is as short as possible (see also chapter 2.12).

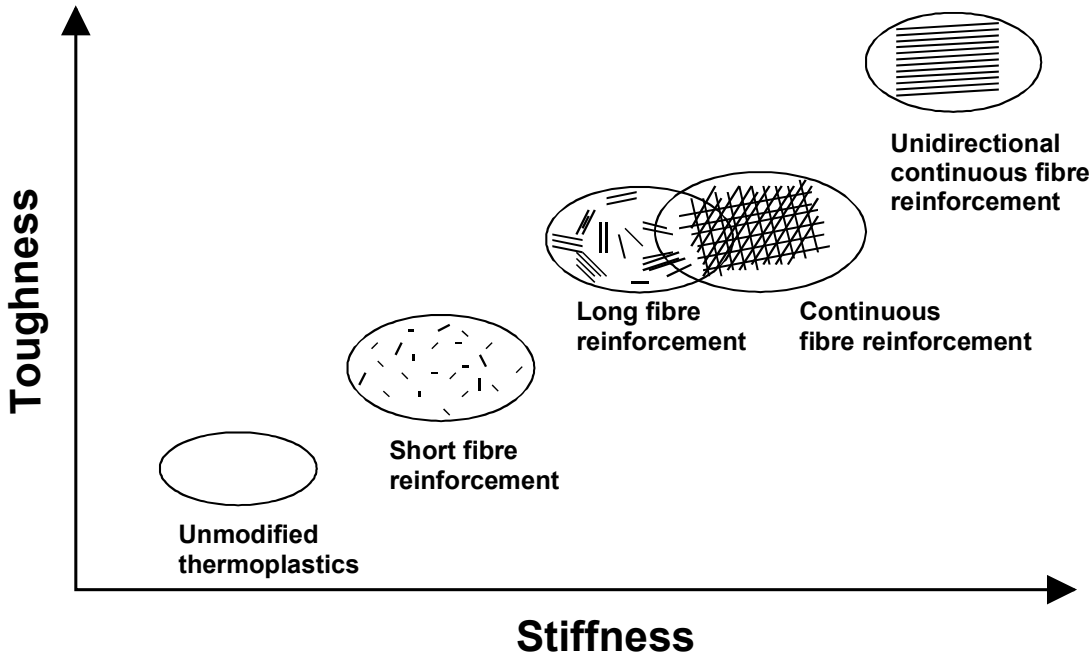

Figure 1.1: Comparison of the properties of long and short glass fibre thermoplastics. In the case of unidirectional continuous fibre reinforcement the toughness/stiffness relationship is a function of loading direction.

At the moment, the most common fibre/matrix combination in long fibre reinforced thermoplastic composites is polypropylene together with glass fibre reinforcement. To evaluate mechanical properties is a complex process due to many different affecting factors. For example, the basic properties of the fibres used, the matrices and additives, as well as the manufacturing process of the actual part, all need to be taken into account. In general, fibre reinforced thermoplastics are better in strength and toughness compared to thermoset counterparts, and the best mechanical performance is achieved with unidirectional glass mat reinforcement. A typical end-user of LFT materials is automotive industry. Figure 1.2 shows some automobile components where LFT composites have found use: instrumental panels, sunroof structures, trunk coverings, bumper beams, underbody panels, front-ends etc. The manufacture and properties of thermoplastic composites based on long glass fibre reinforcement are reviewed and discussed in more detail in the following chapters.

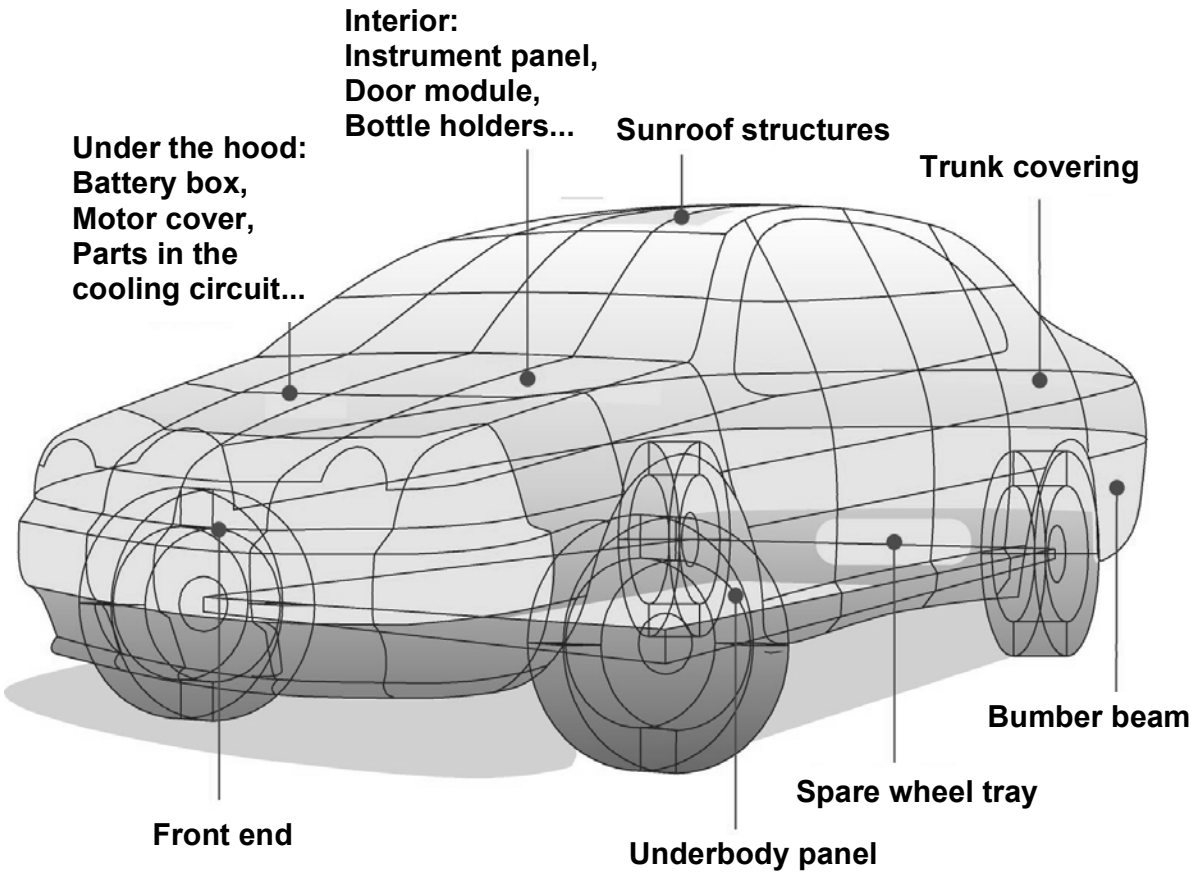

Figure 1.2: Typical automotive components where LFT materials can be applied. Courtesy of FACT GmbH.

2 DISCONTINUOUS LONG GLASS FIBRE REINFORCED THERMOPLASTICS (LFT) : PROPERTIES AND THEIR MODIFICATION

2.1 Manufacture and properties of LFT composites

2.1.1 LFT manufacturing methods

Control of the fibre wet-out is one of the most essential issues in the manufacturing of thermoplastic composite materials, mainly due to the high viscosity of the melt (200-2000 Pa) compared to the low viscosity of thermoset pre-polymers (< 50 Pa) [10-13]. Other important considerations are the complex rheological properties caused by a non-Newtonian behaviour and the high processing temperatures of up to 450 °C. Nowadays there exists three base methods of impregnation technology in LFT manufacture:

1) Traditional glass-mat reinforced thermoplastics (GMT) [14]
2) So called direct or in-line processes (LFT-D) [15]
3) Various pre-impregnation processes [13]

GMT is typically sold as a plate shaped pre-product, which can be compression moulded to final shape. On the other hand, in a typical direct in-line method continuous glass fibres are fed into an extruder, which chops them to the required length and mixes them with the polymer melt [15]. The plate shaped extrudate is then fed into the mould, pressed to a final shape and cooled. Pre-impregnation processes may be further divided into processes based on semi-impregnated intermediates (commingled yarns, powder impregnation *etc.*) and on completely impregnated intermediates (solvent based methods, melt impregnation). Furthermore, semi-impregnated preforms can be used either to produce injection mouldable pellets or GMT sheets. Figure 2.2 schematically presents two different approaches to accomplish complete fibre wetting in processes based on pre-impregnation, showing the changes in material temperature during the manufacturing cycle. In a direct GMT type process based on semi-impregnated preforms (Figure 2.2a) there exists one heating cycle, and the impregnation takes place during the consolidation step.

Apparently, direct process is beneficial regarding possible degradation of the polymer matrix, since a thermoplastic matrix polymer needs to be melted only once during the whole process cycle. On the other hand, significant variations in the fibre length distribution have been reported when continuous fibres were fed into a twin screw extruder. In the first step during the two-step process (Figure 2.2b), fibres are impregnated separately so that two heating cycles are required. In this specific case, starting material is a continuous fibre rowing, which is impregnated with molten thermoplastic polymer, cooled and cut to pellets. Composite parts are then processed typically by injection moulding (step II), where fibre spreading and orientation takes place. The advantages of two-step processes are shorter moulding time, due to pre-impregnation, and a high freedom of part design. Also noteworthy is that the quality control for the impregnated composite material may be carried out before the production of the parts, which reduces the risks for part producer. Various two-step processes have increasingly been the subject of studies, not least due to their commercial potentiality [13].

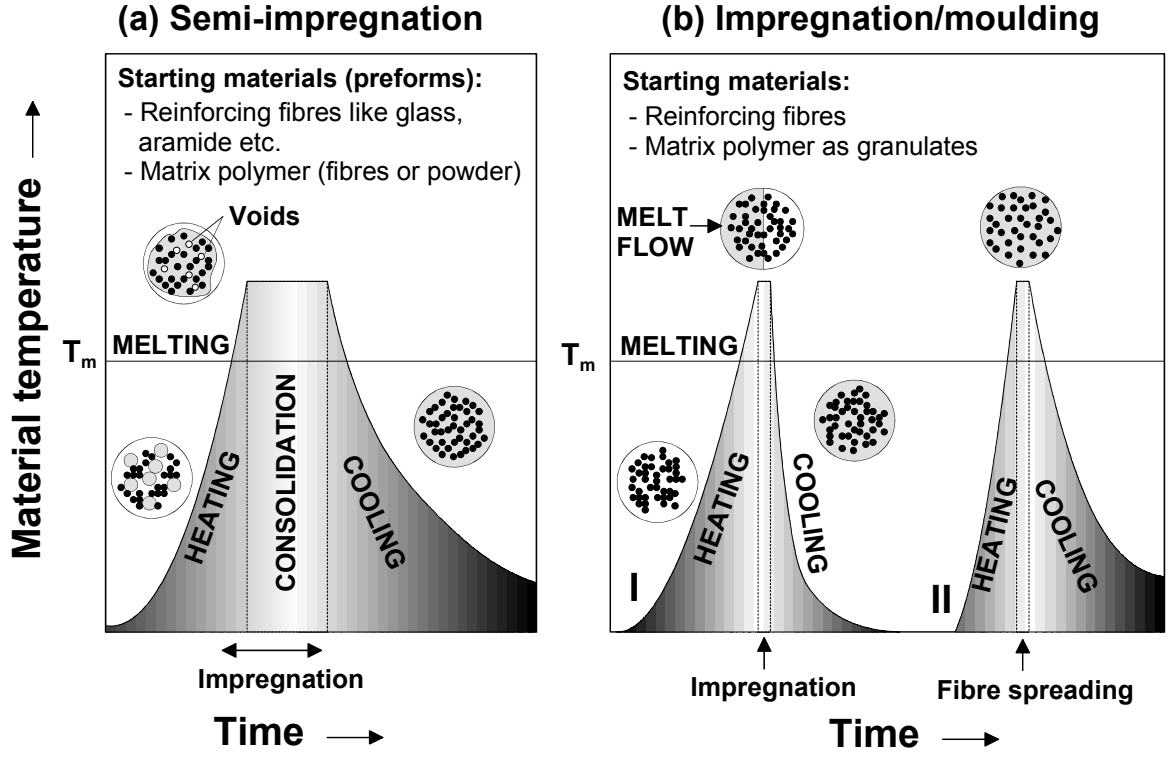

Figure 2.2: Schematics about the processing cycles in manufacture of LFT parts from fibre impregnation point of view: a) direct, one-step process based on semi-impregnated preforms and b) twofold process based on complete pre-impregnation (I) and part production by injection moulding (II). Figure is based on reference [16].

2.1.2 Properties

It is a characteristic of fibre reinforced thermoplastic composites that the mechanical properties can vary drastically, depending not only on the properties of ingredients (matrix and fibre) but also on manufacturing method and fibre length, content and orientation [17-19]. For example, during the injection moulding of the fibre reinforced thermoplastics fibre orientation is layered so that near the walls of the mould main direction of orientation is parallel to the melt flow direction, whereas in core layer the fibres are mainly oriented perpendicularly to the melt flow direction [20-24]. As a consequence, anisotropic mechanical properties are obtained [17, 21, 25]. Table 2.1 shows the values of some important properties describing the mechanical behaviour of thermoplastic polymers and of corresponding glass fibre reinforced composite materials, in current commercial materials. Standard injection moulded bone shaped test specimens are used in these tests. As can be noticed, the mechanical properties can be clearly improved by reinforcing with glass fibres. Additionally, the properties are better when long glass fibres are used as a reinforcement, compared to short fibre reinforced composites.

Table 2.1: Typical mechanical properties of common thermoplastic composite materials. In the case of polyamides, values for non-conditioned materials are given. Fibre contents in wt %. The data were collected from commercial datasheets.

Material	*Tensile strength [MPa]*	*Tensile modulus [GPa]*	*Charpy at 23 °C [kJ/m^2]*
PP	30 *	1.5	n.b. **
LGF-PP 30 %	110	7.5	60
SGF-PP 30 %	85	7	45
PA66	85 *	3	n.b.
LGF-PA66 50 %	260	18	95
SGF-PA66 50 %	230	16	85
PA6	85 *	3	n.b.
LGF-PA6 50 %	240	17	100
SGF-PA6 50 %	225	15	90

* Yield stress ** n.b. = not breaking

Fibre length in relation to diameter (so called aspect ratio) is one important factor affecting the properties of fibre reinforced thermoplastics. This issue has been extensively discussed in literature [23, 24, 26-32], with the conclusion that with longer fibres it is possible to achieve higher levels of mechanical behaviour. It must be emphasised that there are some fundamental differences in material ingredients and manufacturing methods between short fibre materials and long fibre materials. LFT composites are often produced by pultrusion methods based on continuous fibres, whereas short fibre reinforced thermoplastics are usually manufactured by direct extrusion processes based on chopped fibres. This leads to different requirements and restrictions concerning the treatment and diameter size of the fibres. In the case of glass fibres this means that the grades which are meant for the production of short fibre reinforced thermoplastics have a fibre diameter of 14 to 17 µm, but in the case of LFT composites the diameter typically lies between 16-20 µm [26]. Also the requirements of the matrix types are different; in the case of LFT composites low viscosity polymers are required, whereas in short fibre compounding the viscosity of the polymer is usually higher. Therefore the mechanical properties of LFT materials are superior to SFT composites. However, these sort of comparisons between SFT and LFT materials must be carried out with care (*e.g.* the same amount of reinforcing fibres and same type of matrix must be used).

Figure 2.1 shows the typical tensile strength behaviour of short and long glass fibre reinforced thermoplastics. In this case the effect of fibre diameter was not taken into account, since the data were collected from commercial sources. The diagram shows increasing tensile strength as a function of fibre content. It can also be noticed that LGF-PP results in clearly higher tensile strength compared to corresponding SGF-PP, and the difference between the two is larger at higher fibre levels. This phenomenon is also frequently reported in literature, *e.g.* [26]. The maximum values are achieved typically at fibre levels of 40 to 50 wt %, both in short and long fibre reinforced thermoplastics.

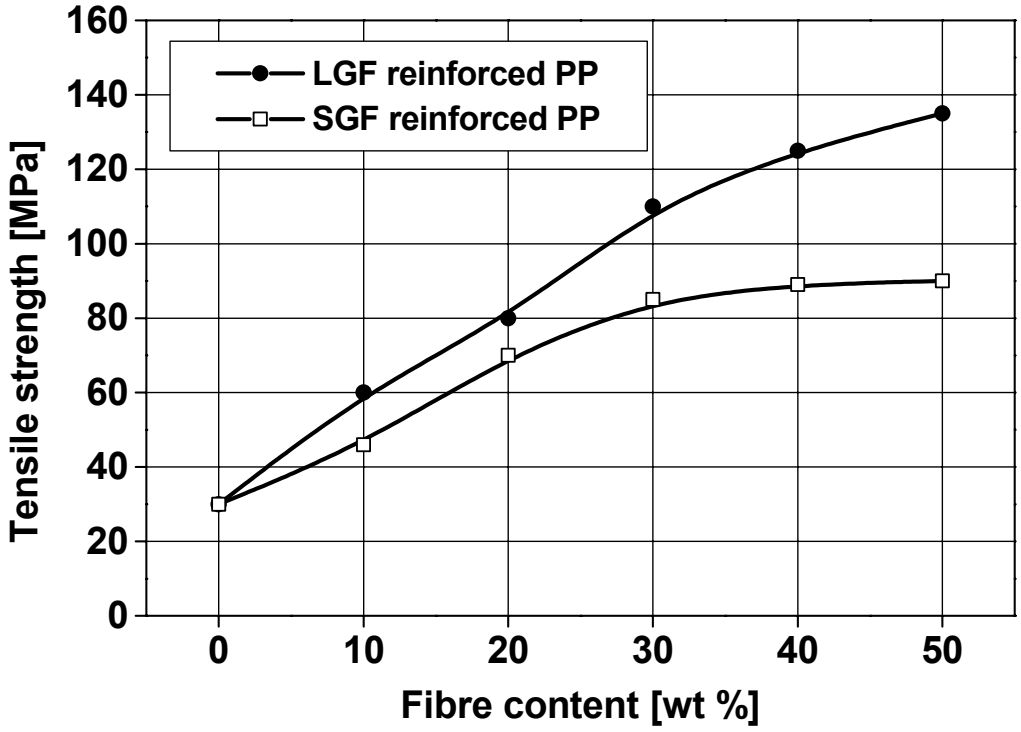

Figure 2.1: Typical tensile strength behaviour of SGF and LGF reinforced polypropylene composites as a function of glass fibre concentration. The data were collected from commercial datasheets.

In addition to fibre orientation, good interfacial adhesion between fibres and polymer matrix is required in fibre reinforced thermoplastics, in order to facilitate stress transfer during impact or tensile loading [33]. This requirement applies both to SFT and LFT composites, and it has a pronounced effect on mechanical behaviour. The main methods to promote the adhesive strength in fibre reinforced thermoplastics are:

1) Coating of the fibre surface with specific chemicals which offer adhesion sites (so called fibre sizing)
2) The addition of compatibilising chemicals to a polymer matrix (so called coupling agents).

Typical sizing agents for glass fibres are based on silanes [34-39], but also other systems like titanates [35, 38, 40], zirconates [35] and even plasma treatment [41] have been studied. The most common coupling agents for polyolefins containing aliphatic carbons are based on maleic anhydride (MAH) crafted polymers, which are compatible both with sizing agents and polymer matrix [35-37, 42]. Mechanical properties of composites based on thermoplastic styrenics are also improved by using MAH based compatibilisers [43-45].

2.2 Composite materials based on thermoplastic styrenic resins

2.2.1 Thermoplastic styrenic resins

Thermoplastic polymers based on styrene monomer have been available for several decades, forming one of the broadest polymer classes with various copolymers and blends [46]. The simplest polymer in the family of styrenic thermoplastics is polystyrene (PS). Despite its desirable properties like relatively good mechanical properties and optical clarity, neat PS is rarely used in applications due to the poor toughness, thermal properties and chemical resistance. To improve impact toughness of PS, it can be modified by rubber particles, resulting in high impact PS (HIPS) [47]. However, copolymerising of PS with other, more polar substances is a preferred method to improve mechanical behaviour and other properties of polystyrene. It has been noticed that the introduction of polar groups in PS enhances strength and modulus [48], but also thermal properties and chemical resistance are simultaneously improved [46]. The most common comonomer in PS copolymers is acrylonitrile (AN), resulting in styrene-acrylonitrile copolymer (SAN). Another copolymer type is styrene-maleic acid anhydride (SMA), which is used in lesser extend. Also rubber modified SAN is often used as a terpolymer, where the rubber part (butadiene) is copolymerised in polymer chain, or as a heterogeneous system with a separate elastomer phase. Rubber modified grades of SAN are known under a common name acrylonitrile-butadiene-styrene copolymers (ABS). Chemical structures of PS, SAN and SMA are presented in Figure 2.3, illustrating the origin of polarity difference of co-polymers compared to PS homopolymer.

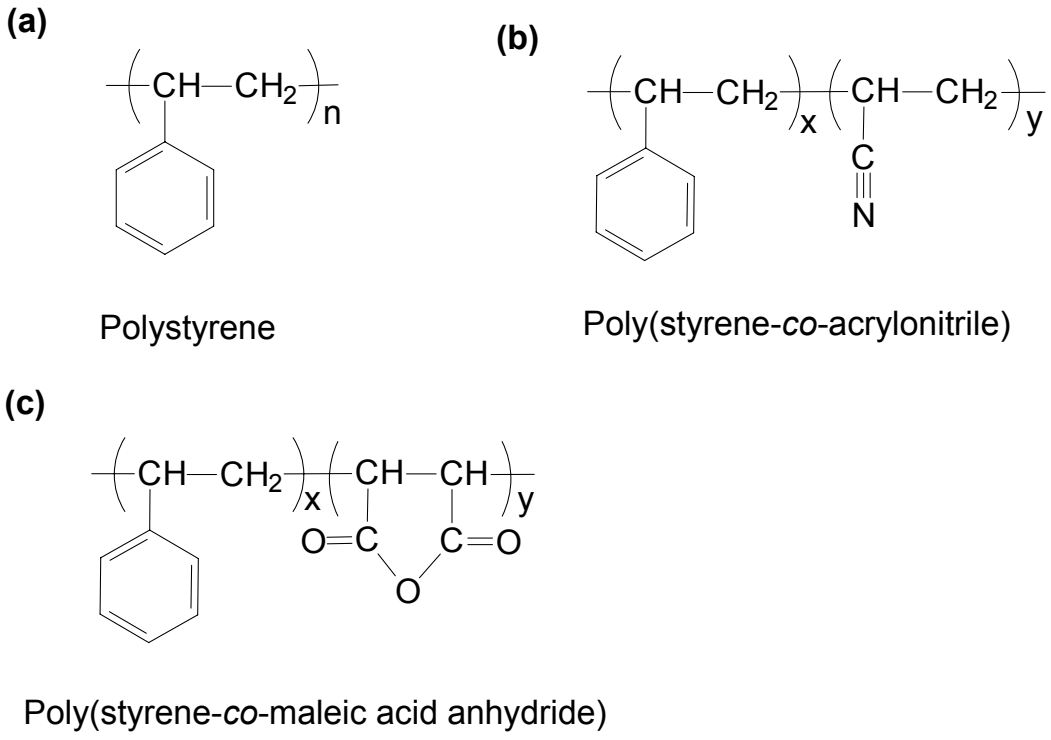

Figure 2.3: Chemical structures of three thermoplastic styrenic resins: a) PS, b) SAN and c) SMA.

SAN copolymers are frequently formulated with additives or fillers to improve stability, to facilitate processing, or to enhance mechanical properties. In ABS, the main function of rubber part is to improve impact toughness of SAN [48]. Unfortunately the addition of elastomer leads to decreased values of strength and stiffness, which can be seen in the property comparison of Table 2.2. From these values it can be seen that the strength and modulus of ABS are 20-30 % lower compared to neat SAN without a rubber phase. SMA copolymer, on the other hand, is said to fill the gap between SAN and ABS, especially in terms of thermal properties [46]. This is clearly indicated in the HDT values shown in Table 2.2. The chemical resistance of SMA copolymers is similar as that of PS homopolymer. Due to the maleic acid anhydride part, SMA is readily reactive even in copolymer form with various chemicals like alkalis and amines, and it is also directly compatible with glass fibres. Commercial SMA grades contain typically 5-12 % of anhydride part.

Table 2.2: Comparison of the mechanical properties of PS, SAN, ABS and SMA based composites. References: commercial datasheets and [46].

Material	*Tensile Strength [MPa]*	*Tensile Modulus [GPa]*	*Notched IZOD, 23 °C [J/m]*	*HDT, 1.8 MPa [°C]*
PS	45	3.0	10-13	83
SAN	57-82	3.0-3.9	13-27	99-109
SGF-SAN 30	140	11.0	60	100
ABS	35-40	2.0-2.3	200-400	75-85
SMA	50	3.4-3.7	11-16	91-107
SGF-SMA 30	100	7.5	120	120

2.2.2 Composites based on thermoplastic styrenic resins

Also thermoplastic styrenic resins can be reinforced with glass fibres, which increases the mechanical properties like strength and modulus (Table 2.2). Main dilemmas in development and manufacture of thermoplastic styrenic composites are very similar as in the case of other thermoplastic composites and therefore, much work has been devoted to the processing related issues [49-51] and to the improvement of fibre-matrix adhesion [43, 44, 52, 53]. Lately, it was demonstrated that PS-glass fibre composites can be produced in pultrusion process by using a low molecular weight pre-polymer as a starting material [49, 50]. The pre-polymer can be polymerised *in-situ* during the manufacturing process, leading to composite materials with good mechanical properties. Mechanical behaviour of short glass fibre reinforced SMA copolymers were also studied recently [51, 54]. It was shown that the elastic modulus, strength and fracture toughness of SGF-SMA composites increased considerably as a function of increasing fibre content (up to 22 vol %) [54]. Also, it was demonstrated that the recycling of SMA composites led to a grater decrease in mechanical properties compared to that of the neat SMA copolymer, which was attributed to the fibre length degradation taking place during the recycling process [51]. Very similar mechanical behaviour was found in SGF reinforced acrylonitrile-styrene-acrylate (ASA) copolymers, but the fracture toughness of ASA was noticed to be essentially unaffected by the addition of short glass fibres [55].

It has been recognised that the fibre-matrix adhesion plays a key role in achieving good mechanical properties of thermoplastic styrenics reinforced with glass fibres, due to the reason that there is a large difference between the polarity of styrenic group and glass. The polarity of the matrix is higher in the cases of styrenic copolymers like SAN and SMA, but the correct fibre surface treatment (sizing) is yet essential. It has been reported that by modifying glass fibre surface by silane based chemicals such as γ-methacryloxypropyltrimethoxysilane (γ-MPS), it is possible to achieve good compatibility between fibre and the thermoplastic styrenic resins [43]. By copolymerising γ-MPS with polystyrene provides poly(γ-MPS-*co*-styrene) copolymer, which was successfully used to improve fibre-matrix adhesion in LGF reinforced polystyrene composites [44]. In another study it was shown that the interfacial adhesion between glass fibres and PS can be improved by introducing small amount (1-2 wt %) of low molecular weight poly(styrene-*co*-maleic anhydride) copolymer as a coupling agent in matrix [52]. A model describing the mechanism was suggested (Figure 2.4), indicating that the optimal coverage of the fibre surface is attained at high level of maleic acid anhydride (MAH) content in coupling agent. It was proposed that SMA oligomers with low MAH content form loops on the glass fibre surface (Figure 2.4a), whereas at higher MAH content SMA oligomers the surface becomes saturated, resulting in better adhesion. Thus, fibre-matrix interfacial properties are identified as a central issue in composites based on thermoplastic styrenic resins.

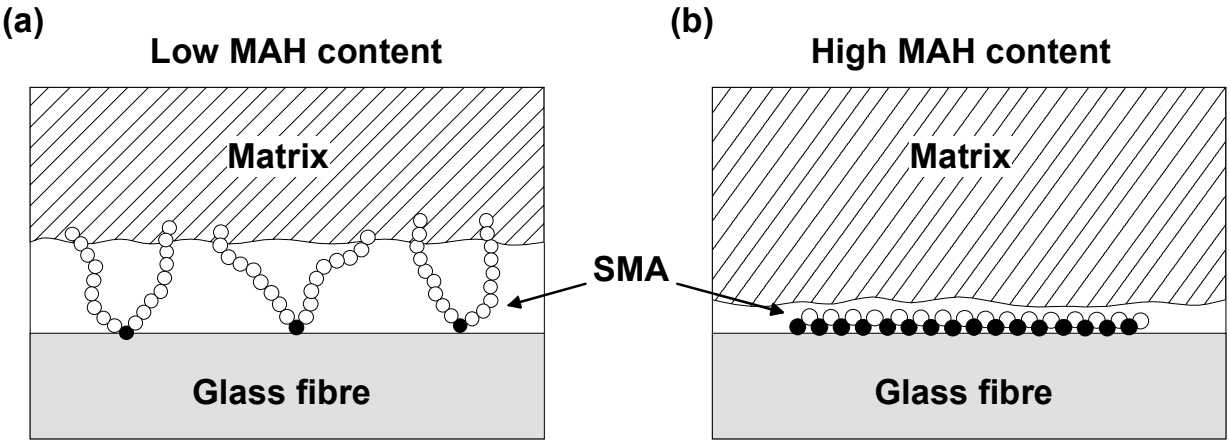

Figure 2.4: Coupling mechanism of low molecular weight SMA adhesion promoter in glass fibre reinforced PS composites at a) low MAH content and b) high MAH content [52].

2.3 Polypropylene hybrid composites

2.3.1 Polypropylene

Polypropylene (PP) is the most widely used thermoplastic material worldwide. Originally it was developed in 1950's after new discoveries in the field of coordination catalysis by Ziegler and Natta, which made possible to produce polymers with unusual stereospecific structures [56]. Yet today vast majority of the commercial PP is produced by Ziegler-Natta catalyst systems from cracked gas streams of crude petroleum, in spite of the recently emerged metallocene catalysis systems [57]. The reason behind the success of PP has been its extremely wide application possibilities, as well as potentiality for new innovations and modifications. Besides new developments in production technology, also modification with fillers, fibres and elastomers have expanded the usage of PP in a variety of applications. The applications can be roughly divided to extrusion and moulding technologies, which both account about 50 % of the industrial consumption. Figure 2.5 presents the application segments of polypropylene in 2001, showing that in extrusion technologies PP fibre is dominating with 46 % share, followed by biaxially oriented PP *i.e.* BOPP film (19 %) and cast film (11 %). Moulding technologies are more fragmented, automotive applications taking largest share (21%). According to estimates, the usage of PP will increase in the future especially in household, packaging, automotive and pipe sectors [57].

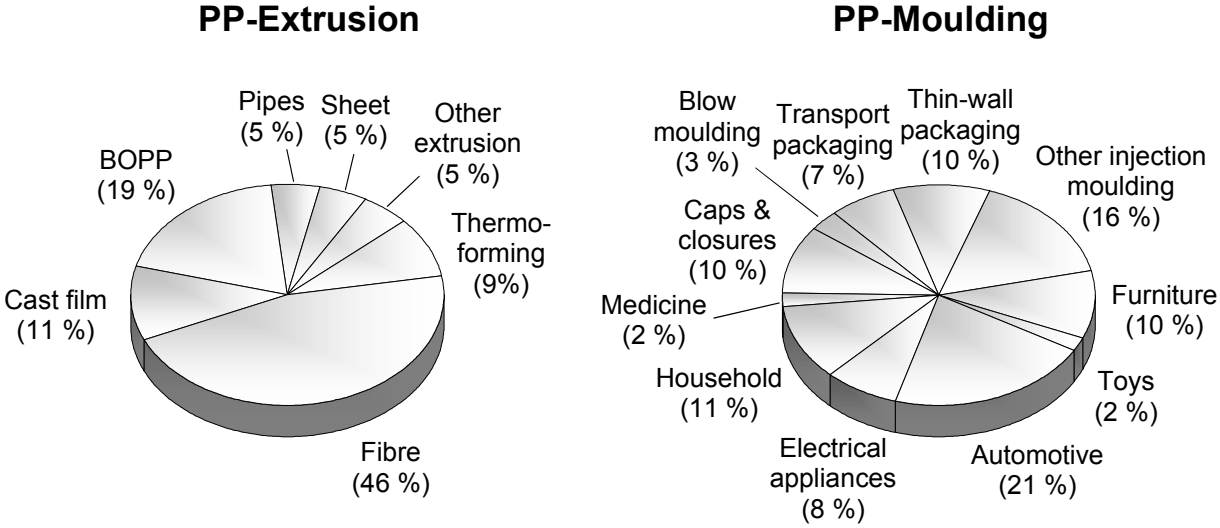

Figure 2.5: Industrial usage of polypropylene in Western Europe in 2001 [57].

2.3.2 Polypropylene composites

PP is traditionally reinforced with short glass fibres, which is known to improve stiffness, strength and fracture toughness [58], but the use of long glass fibres has become more and more popular due to the improved mechanical properties that they can provide (*e.g.* references [14, 17, 18, 28, 59]). Irrespective of the fibre length, one of the most important parameters, affecting on the mechanical properties of glass fibre reinforced PP, is interfacial bonding between the reinforcing fibres and the matrix [60]. Figure 2.6 presents the effect of different coupling conditions on tensile strength of LGF reinforced polypropylene. Without coupling or with incompatible sizing, polar glass fibres are essentially unbonded to the PP matrix, and, as a consequence, the strength is not improved upon addition of the reinforcement. On the other hand, as the fibres are treated with a sizing agent compatible with PP, a major improvement in strength is obtained as a function of LGF concentration. Even a higher level of strength can be achieved by adding adhesion promoting agents into the matrix, such as PP crafted with maleic acid anhydride, himic acid anhydride or acrylic acid [33, 37]. This example reflects the importance of the correctly chosen compatibilising system in the case of unpolar PP matrix and highly polar glass fibres.

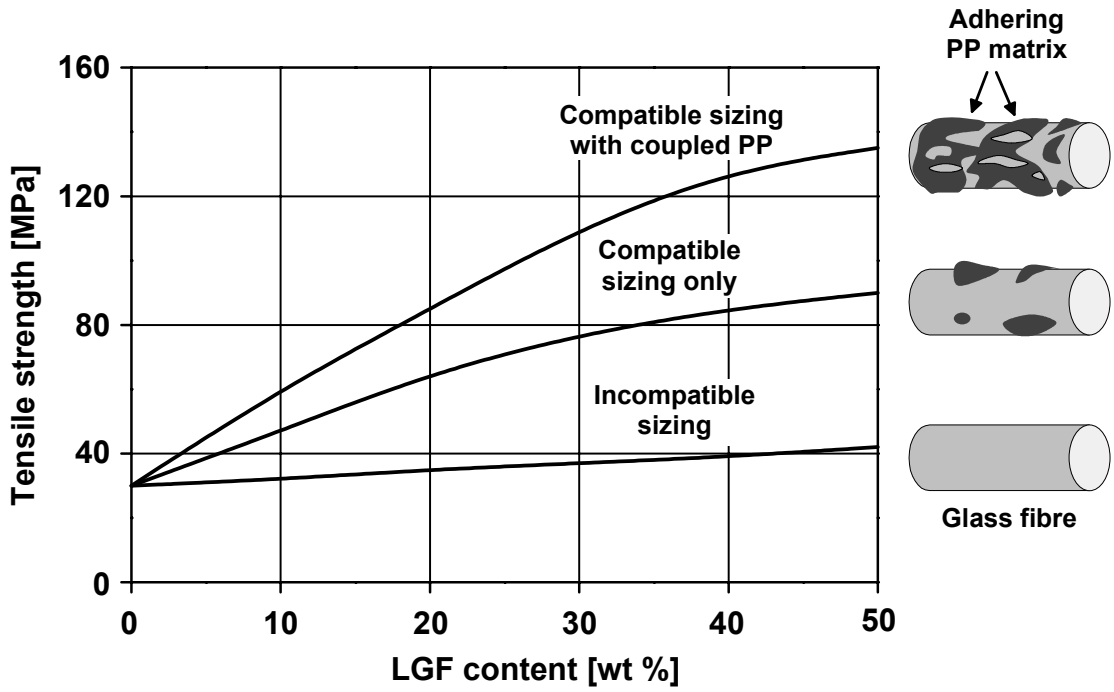

Figure 2.6: Effect of adhesion promotion on tensile strength of LGF-PP [60].

A second characteristic feature of chopped fibre reinforced PP composites is the flow induced alignment of the fibres taking place during the processing by injection moulding [21, 22]. The structuring of the layering is a complex issue, being strongly affected by the mould design and processing parameters [58], but generally the fibre structuring consists of three separate alignment layers as shown in Figure 2.7 [23, 59]. In this case the alignment structure is composed of two surface layers (S) and one core layer (C). As a consequence of the alignment, unisotropic mechanical properties are obtained, which is well documented and reviewed in literature [22-24, 61-64]. Also one important feature in chopped fibre reinforced thermoplastics is that the degree of fibre orientation depends strongly on the fibre volume fraction. It has been observed that the degree of orientation increases as a function of increasing fibre volume fraction [65].

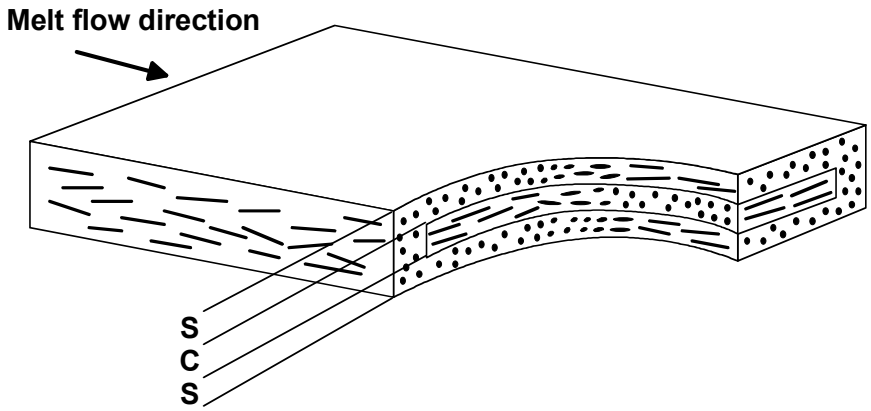

Figure 2.7: Schematic drawing of the layered fibre orientation in injection moulded glass fibre reinforced PP composites [59].

2.3.3 Particle filled polypropylene

In addition to fibres, mineral fillers are frequently used to modify the properties of polypropylene and to decrease the price. Though the most common fillers for PP are talc and calcium carbonate, also several other materials have been reported as potential PP fillers, such as mica, glass beads, sepiolite, magnesium hydroxide, wollastonite, carbon black, metal powders and silicium carbide [66]. In the light of literature it can be stated that the effect of fillers on the mechanical response of PP is a relatively complex matter, due to the considerable amount of affecting parameters

like characteristics of the filler itself (chemical composition, geometrical shape, particle size), interfacial adhesion between the particles and polypropylene matrix, homogeneity of the particle distribution and the effect of the used filler on the crystallinity of the matrix, among others [66]. Nevertheless, it is widely reported that the Young's modulus of PP increases upon filler addition, but often with the cost of decreased strength and toughness [58, 66]. Changes in mechanical properties can be explained by the higher modulus and more brittle nature of filler particles compared to PP, but also by changes in fracture sequence (Figure 2.9) and in crystalline morphology when filler is added [67]. It is known, for example, that particulate fillers work as nucleation agents in semi-crystalline thermoplastics [66], and the nucleation effect differs strongly by filler type, particle size (*i.e.* surface area) and filler surface treatment. It has been observed that talc is an active filler, affecting strongly on crystalline morphology of polypropylene [68]. Calcium carbonate, instead, has typically little effect on crystallinity and can be considered as an inactive filler in sense of nucleation effect [68-70]. The differences between talc and calcium carbonate fillers can be seen in diagram of Figure 2.8, showing the changes in crystalline peak temperatures (T_c) of PP as a function of filler concentration [68].

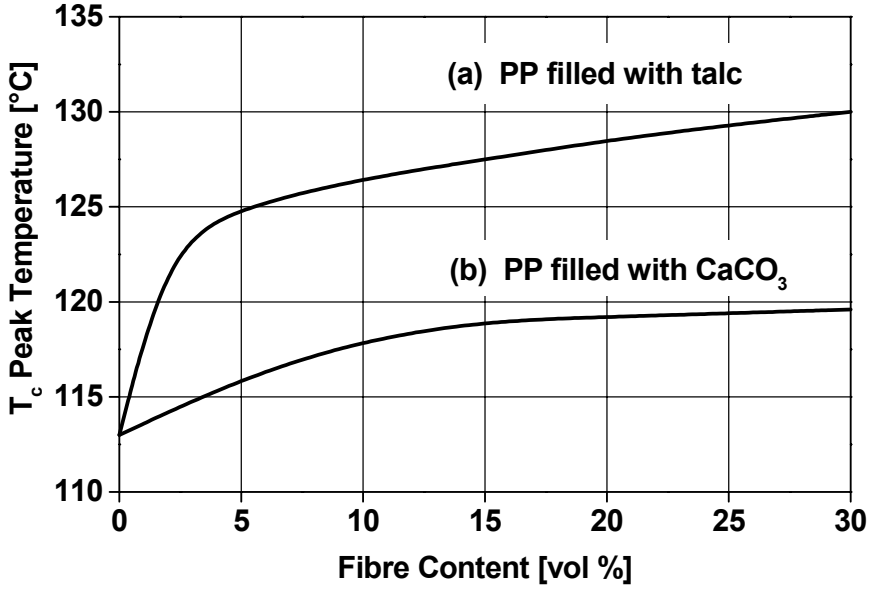

Figure 2.8: Effect of two different mineral fillers on crystallisation peak temperature (by differential scanning calorimetry, DSC): a) PP filled with talc and b) PP filled with $CaCO_3$ [68].

There are few publications where both the modulus and impact toughness of PP have been simultaneously improved by using particulate fillers [71, 72]. General idea in this novel concept is to imitate the toughening mechanism of thermoplastic-rubber blends, where the void formation (*i.e.* cavitation) around the rubber particles is responsible for the increased impact energy. The basic idea is presented in schematic drawing of Figure 2.9, illustrating the cavity formation upon loading of PP filled with rigid particles [67, 72]. In the first phase, filler particles form stress concentration sites due to the different elastic properties compared to PP. In second phase the stress concentration induces triaxial stress around the particles, resulting in filler-matrix debonding. Shear yielding of PP takes place in third phase and the cavitation lengths around the particles increase. Finally, in phase IV the voids coalesce, which leads to the failure of the material.

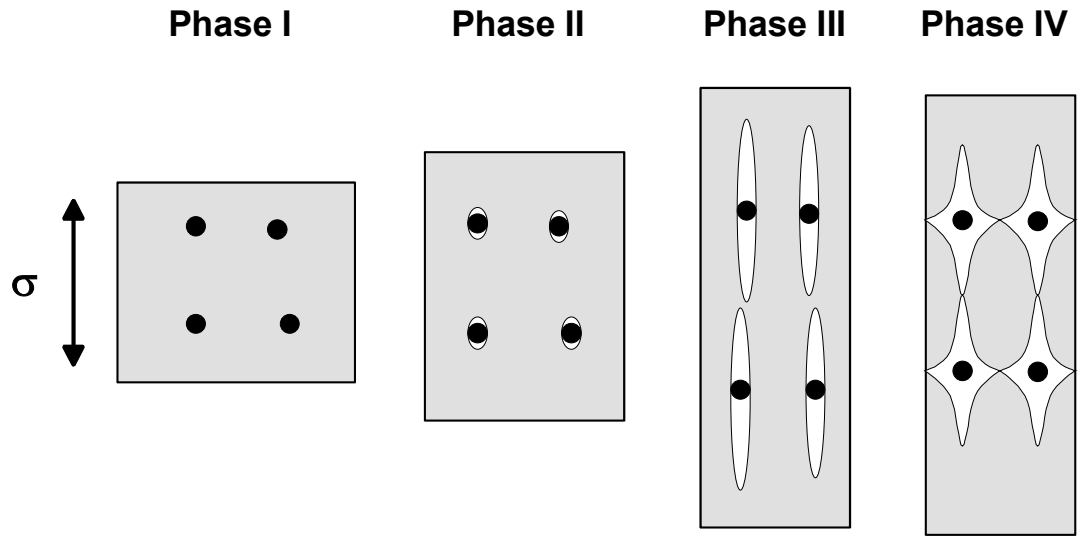

Figure 2.9: Cavitation mechanism of the rigid particle filled polypropylene during the loading [67, 73].

2.3.4 Thermoplastic hybrid reinforcement systems

During the recent years also multicomponent systems containing both reinforcing fibres and mineral fillers have been demonstrated [74-77], referred as hybrid reinforcement composites. It has been observed that by incorporating filler particles into the matrix of fibre reinforced composites, synergistic effects may be achieved in form of higher modulus and reduced material costs, yet accompanied with decreased strength and impact toughness [66, 78]. Such multicomponent hybrid composites

based on poly(butylene terephtalate) (PBT) [74], acrylonitrile-butadiene-styrene co-polymer (ABS) [75, 76] and PP [77, 78] matrices have been demonstrated in literature. Schematic drawing of Figure 2.10 illustrates the dimensions and geometries of the different reinforcements. Typically long glass fibres possess an aspect ratio up to 1000 before processing. Calcium carbonate has almost spherical particle shape, thus having an aspect ratio of 1-2, whereas plate shaped talcum particles have an aspect ratio which varies from 20 up to 50. The dimensions of long glass fibres and fillers are of different order of magnitude, for which reason the effects on matrix crystalline morphology and failure modes are based on different principles in LGF reinforced PP and filler filled PP. Thus, hybrid composites form a very complex system.

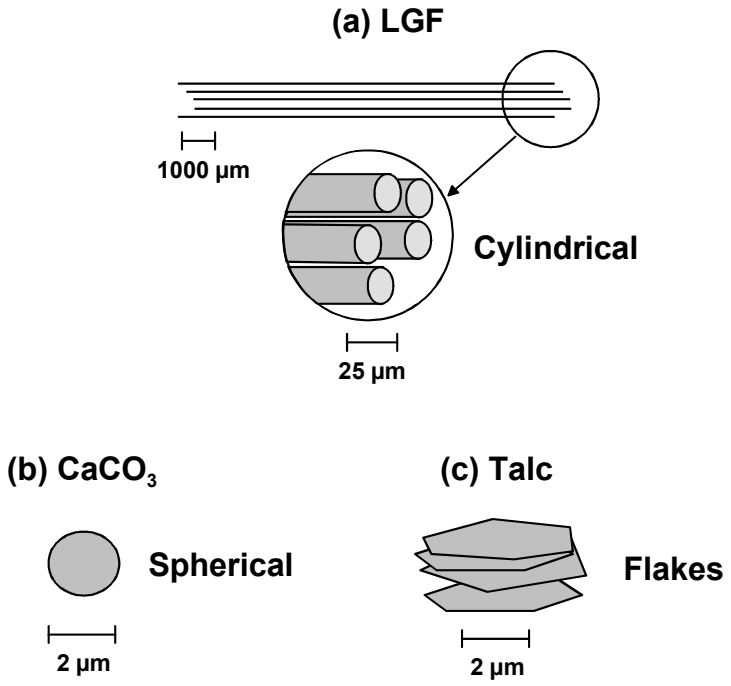

Figure 2.10: Schematic drawing presenting the geometries and dimensions of long glass fibres (a) and two different types of mineral fillers, $CaCO_3$ (b) and talc (c).

One additional advantage of the hybrid material is the reduced warpage of the manufactured parts. Such warpage of the composite parts can be determined for example by using the modelling approach, or experimentally by scanning the profile of the part, followed by the image analysis [79]. This improved dimensional stability is important in several automotive and other applications.

2.4 Water resistance of long glass fibre reinforced polyamide composites

2.4.1 Polyamide and its blends

Aliphatic polyamides are widely used semi-crystalline polymers, characterised by their excellent mechanical performance combined with good resistance to chemicals. The properties also remain over wide temperature scale ranging from sub-zero to 150 °C. These are the underlying factors that have made aliphatic polyamides as one of the most successful class of plastic materials in the market, commercially the most important types being polyamide 6 (PA6), which is chemically poly(ω-aminocaproic acid), and polyamide 66 (PA66), which is a product of reaction between adipic acid and hexamethylene diamine [80]. Figure 2.11 shows the chemical structures of some synthetic (a-d) and naturally occurring (e, f) polyamides.

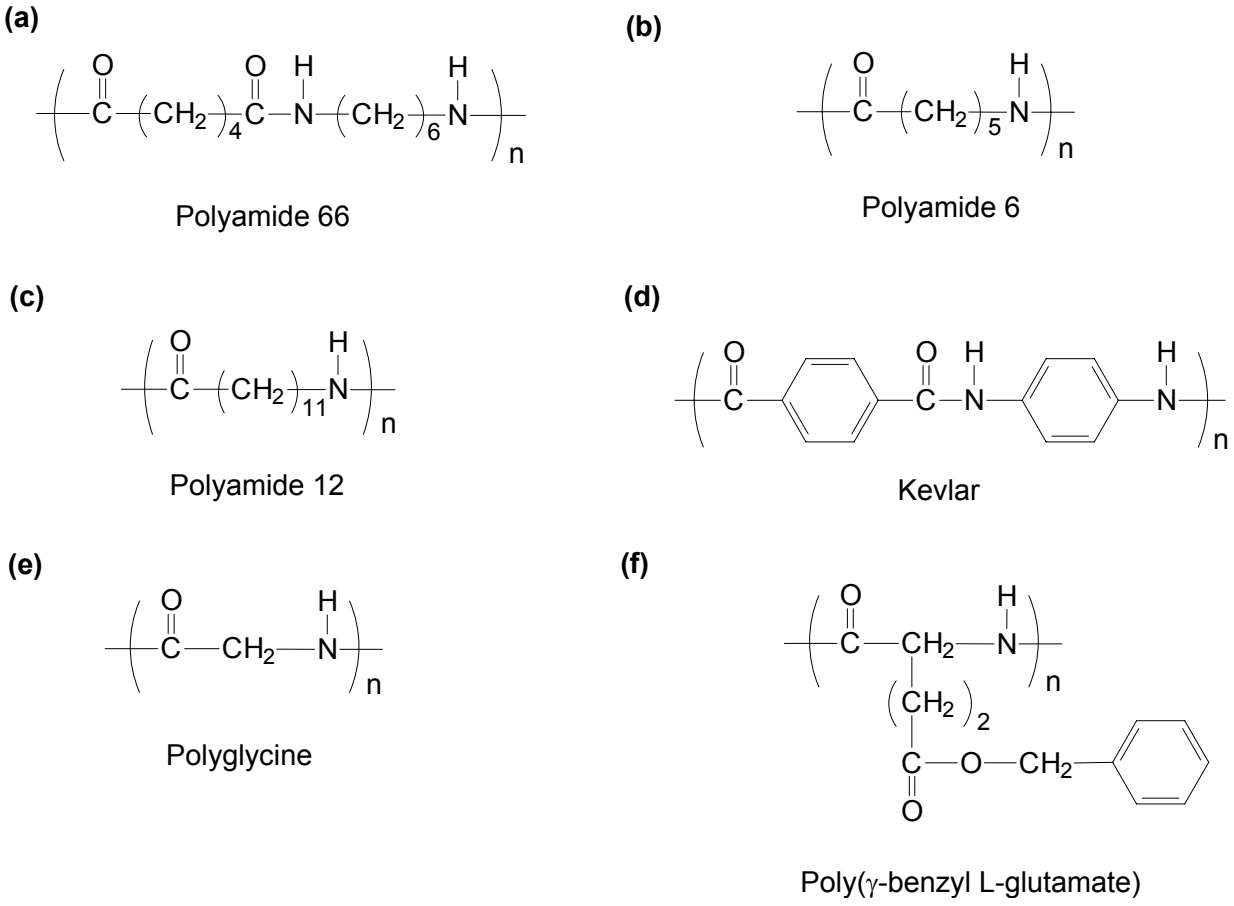

Figure 2.11: Chemical structures of some synthetic (a-d) and natural occurring (e-f) polyamides: a) PA66, b) PA6, c) PA12, d) polyaramid (Kevlar), e) polyglycine and f) poly(γ-benzyl L-glutamate) [81].

The properties of aliphatic polyamides are greatly influenced by the degree and morphology of crystallinity. The crystallisation of polyamides results in the spherulite type structure, the size and number of spherulites being dependent on the molecular weight of the polymer, and on the presence of possible nucleation sites (*e.g.* fibres, fillers or voids) [82, 83]. In the case of PA66, the crystalline lattice is formed of fully extended chains, the most usual crystal type being α-form where the molecules are lying antiparallel to each others in sheets, *e.g.* [56, 82]. This conformation allows a high density hydrogen bonding between the adjacent chains. Another important parameter in addition to crystallinity is the glass transition temperature, T_g, resulting in large changes of polymer properties like stiffness and impact toughness. In the case of polyamides, T_g values increase with increasing crystallinity degree and with increasing degree of chain orientation (unisotropy) in amorphous phase [82].

During the recent years, several attempts to modify aliphatic polyamides in order to further improve mechanical performance or to achieve new desirable properties have been published in literature, one of the most studied methods being blending of PA with other thermoplastic polymers or rubbers [84-86]. Large number of possible variations in blends lead to a very broad range of properties, which has made blending a popular modification method also in industrial scale. Usually the targets in blending of PA with other polymers are improvement of impact toughness in dry state and at low temperature, decrease of water absorption and improvement of dimensional stability [87, 88]. Basically the properties of the blends depend on the component properties and on their interaction between each others, but also on mixing ratio and the final morphology of the blend [88]. For example, blending of polyamide with unpolar polymers like polyethylene or polypropylene leads to a rough blend morphology and poor mechanical properties, but finer morphology and better properties are achieved by adding small amount of graft copolymers of polyolefins as a compatiblising agent [89]. Blends of aliphatic polyamides, *e.g.* with polyethylene [87, 89], polypropylene [90, 91] and various rubbers [92, 93], have been demonstrated in literature, but also blending with phenol based thermosets has recently attained attention as a novel route to achieve new property combinations.

2.4.1.1 Polyamide-phenolic resin blends

Driving force for the miscibility in blends of thermopalstic polymers with phenol based resins is a strong hydrogen bonding formed between hydroxyl group of phenolic resin (donor) and functional group of thermoplastic counterpart (acceptor) [94]. Poly(methyl methacrylate), PMMA, was one of the first polymers which was noticed to form miscible blends with oligomeric phenol formaldehyde resins (PFR) [94, 95]. By crosslinking of the thermoset counterpart it was possible to achieve even interpenetrating network (IPN) type structures, though only when PFR was rich in composition [96, 97]. In PMMA rich region it is not possible to achieve thermoset network structure over the whole material, for which reason phase separation takes place upon curing, especially if the crosslinking density is high [97].

Similarly, miscible blends between PFR and a variety of other thermoplastics have been reported, including poly(vinyl acetate) [94], ethylene-vinyl acetate copolymers [98, 99], poly(ε-carpolactone) [100] and poly(adipic ester) [101]. In the recent reports it was demonstrated that PFR and poly(2-vinylpyridine)-polystyrene and poly(2-vinylpyridine)-poly(isoprene) block-copolymers form miscible blends with self-organised spherical, cylindrical and lamellar nanostructures [102, 103]. Also various polyamides have been blended with PFR type thermosets recently, showing miscibility due to the hydrogen bonding between hydroxyl group of phenolic resin and carbonyl group of amide functionality [104-108].

Figure 2.12 shows how the hydrogen bonding connection is formed in some thermoplastic-PFR blends, as demonstrated by studies with Fourier transform infrared spectroscopy (FTIR), nuclear magnetic resonance spectroscopy (NMR) and DSC. It can be seen that in most cases there exist a physical, hydrogen bond between carboxylic group of amide and hydroxyl group of phenolic resin. As an exception, in the case of poly(2-vinylpyridine)-poly(isoprene) block-copolymer complexation takes place *via* nitrogen-hydroxyl hydrogen bonding.

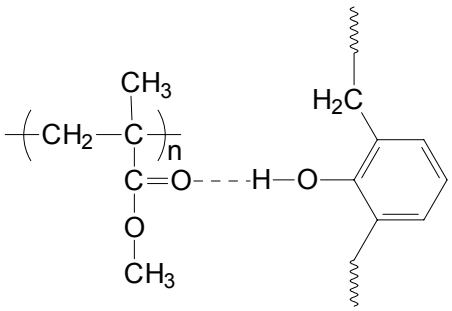

Poly(methlyl methacrylate)

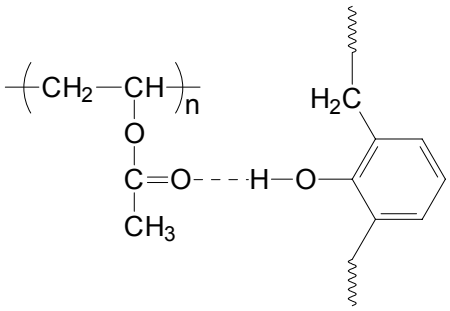

Poly(vinyl acetate)

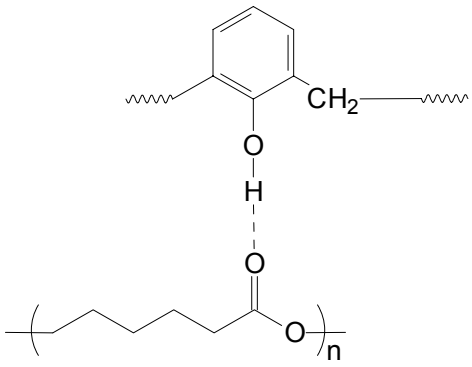

Poly(ε-caprolactone)

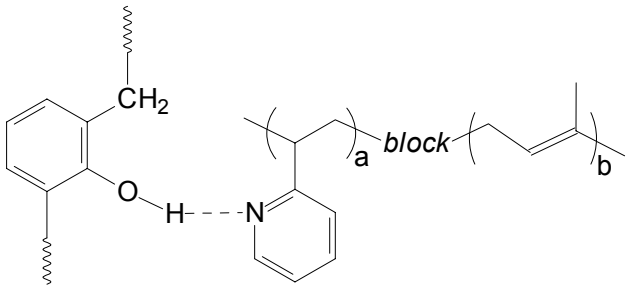

Poly(2-vinylpyridine)-*block*-poly(isoprene)

Figure 2.12: Examples of the chemical structures of thermoplastic resins which may form a hydrogen bonding complex with phenolic resins [94, 95, 100, 103].

In light of the recent publications it seems that the addition of PFR affects both the crystalline and the amorphous phase of semi-crystalline polymers like polyamide, which in turn may be reflected in the final properties of the blends. Recently Huang et *al.* studied the morphological changes in PA6 blended with poly(4-vinyl phenol) and with oligomeric, chlorinated novolac type phenolic resin, concluding that phenol containing counterparts locate largely in amorphous phase [107, 108]. This assumption is based on small angle X-ray scattering (SAXS) patterns, indicating that the thickness of the crystalline layer is essentially unchanged upon blending. In another study it was observed that small amount of oligomeric novolac type PFR in PA6 1) decreased water absorption considerably and 2) induced spherulite growth rate: the size of the spherulites increased compared to neat PA6, but the nucleation density decreased simultaneously [106]. Thus, blending of polyamides with PFR type resins offers a convenient route for property modification.

2.4.2 Polyamide composites

Glass fibre reinforced polyamide composites are considered as excellent materials in terms of high stiffness and strength, good chemical resistance and thermomechanical properties. Further enhancement of mechanical properties like strength, modulus and creep resistance can be achieved by reinforcing polyamides with various fibre reinforcements or fillers [82]. Table 2.3 summarises the mechanical properties of PA66 containing same volume fraction of different reinforcements and fillings, showing how the properties of polyamide composites can be modified in a very wide range by changing the types of the material components. The most common reinforcement for aliphatic polyamides is based on short glass fibres, with a typical fibre content of about 30 wt % and with a maximum of about 45 wt % [61]. The mechanical properties of the resulting composite are at high level, but still too low to fulfil the requirements of many load bearing applications. For this reason, long glass fibre reinforced polyamides have gained more and more attention during the recent years [20, 64, 109]. The commercial grades of PA6 and PA66 typically contain 30 to 60 wt % of LGF.

Table 2.3: Mechanical properties of reinforced and filled PA66 composites at 30 wt % reinforcement content. Source: reference [82] and commercial datasheets.

Reinforcement type	*Tensile strength [MPa]*	*Tensile modulus [GPa]*	*Density [g/cm^3]*
Long glass fibres	190	10.5	1.35
Short glass fibres	160	7.8	1.35
Short carbon fibres	230	17.5	1.27
Glass spheres	80	3.7	1.35
Mica	39	6.9	1.35
Asbestos	133	9.2	1.30

Since aliphatic polyamides are semi-crystalline polymers, most properties of PA composites are strongly affected by the (process induced) crystalline morphology, but also on molecular weight of the matrix, type of reinforcement and also by processing conditions [82]. Secondly, it is known that due to the polarity of amide

groups, polyamide is able to absorb substantial amount of moisture, and is prone to a chemical attack by water and other polar fluids, thus affecting on the mechanical behaviour, thermal properties, T_g behaviour and long term properties. These factors are fundamental both in the case of polyamides and in their composites, and must be carefully considered when determining the conditions and material limits for applications.

2.4.2.1 Water in polyamide composites

Water absorption by various polyamides has been extensively studied in literature [110-114]. A driving force for absorption is a polar nature of the amide moieties, for which reason they can form strong hydrogen bonds with water molecules. It is also generally accepted that water absorption takes place almost entirely in the amorphous region of polyamide due to the reason that H_2O molecules cannot intrude into the dense crystalline phase, in spite of their small size. However, prolonged exposure in slightly acidic water solution has been noticed to deteriorate crystallinity [115], after which also crystalline regions may take part in sorption. The main parameters affecting on the equilibrium amount of absorbed water are the number of amide groups in polymer backbone, degree of crystallinity, specimen geometry (thickness) and environmental conditions [116].

One of the most pronounced effects of water in polyamide is the plasticization due to the water molecules that replace the intermolecular hydrogen bonds of polyamide in amorphous regions. H_2O molecules increase the space between individual polymer chains, facilitate molecular relaxation and thus softens the polymer [116]. This is reflected in several structural features and macromolecular properties of polyamides. One of the changed properties due to plasticization is the glass transition temperature, which decreases considerably upon water absorption. For example, T_g of PA66 (drawn fibres) is noticed to drop from 106 °C to about 10 °C after treatment in 100 % relative humidity [82, 117]. In polyamide-glass fibre composites, the loss of fibre-matrix adhesion is noticed to take place upon moisture treatment, leading to extensive fibre debonding during the loading [118]. These phenomena lead to

changes in mechanical performance of polyamides and their composites, reported widely in literature: decreased tensile strength and modulus [116, 119], increased tensile elongation, fracture energy G_c and impact toughness [82, 116, 118] and decreased creep resistance [120].

Different means to prevent the effects of water absorption and hydrolysis on polyamide have been demonstrated, one common method being blending of PA with other polymers like polyethylene [87] or polypropylene [91, 121]. However, in order to facilitate decreased water absorption, such blends need to be compatibilised by suitable additives. In uncompatibilised blends even increased water sorption has been reported [91], possible due to the filling of capillary voids that separate PA and PP phases. An other approach to decrease moisture uptake in polyamides is to use blending with thermoset resins that can form strong hydrogen bonding with amide groups, and in this way block water molecules from bonding with PA. As an example, Huang *et* al. demonstrated that the addition of a small fraction of phenol based resin to PA6 decreased water absorption by 44 % [106, 107]. It was suggested that the decreased moisture uptake in such a blend is caused by the interaction between phenolic groups of phenolic resin and amide moieties of PA6, leading to the reduced number of available (“free”) amide groups in blend [107]. This novel route offers a possibility to reduce the water absorption and its negative effects on mechanical properties in polyamides and its composites.

3 AIMS OF THE WORK

Both academic and commercial research of LFT materials has been very intensive for some two decades now, which has led to several novel LFT manufacturing methods, material combinations, improvements in processing of the final parts, and new high-tech applications. Therefore, LFT composites form nowadays a broad material group with a tremendous number of different fibre-matrix-filler-additive variations, making the control of the final properties a challenging task. The present work is an attempt to develop novel tools for property modification of LFT materials. The work is divided in three separate case studies with different target applications and thus, with different material combinations and specific aims:

1) Property modification of LGF composites based on thermoplastic styrenic resins.
2) Mechanical behaviour of LGF polypropylene composites containing mineral fillers as a hybrid reinforcement,
3) Structure and properties of LGF composites based on polyamide-thermoset blends and

The basic guideline of the study is a systematic approach from atomic or molecular level to the mechanical characterisation of the composites (Figure 3.1). Additionally, applicability of the resulting materials in automobile components is discussed.

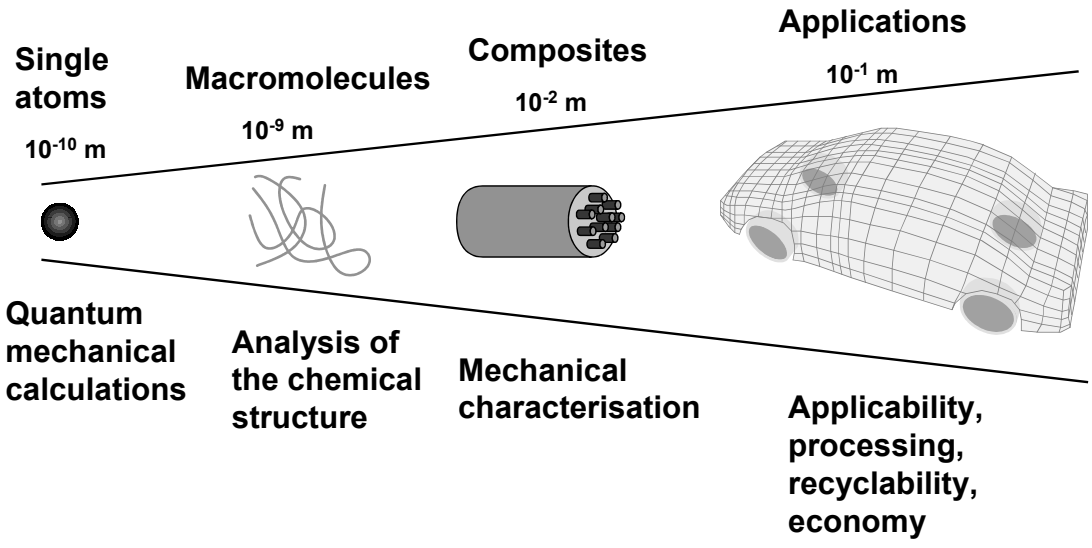

Figure 3.1: A general principle of the present study as a schematic presentation.

The three sub-topics can be clarified in the following scheme (see also Figure 3.2):

1) Aims of material system A: LGF composites based on thermoplastic styrenic resins:

In material system A the target was to develop LGF reinforced thermoplastic styrenic composites with optimised mechanical properties for automobile interior parts, the focus being particularly in the improvement of the interfacial adhesion between the reinforcing glass fibres and various thermoplastic styrenic matrices. More specifically, the aim was to enhance fibre-matrix interaction with help of styrenic copolymers including polar groups that can react with glass fibre surface. Small amount of such copolymers added into the matrix may work as a coupling agent, increasing the adhesive strength, which in turn improves the wetting of the fibres during the composite manufacturing process and lead to the better mechanical properties of the final parts. Thermoplastic LGF styrenics may find usage in several automobile parts, especially in interior applications.

2) Aims of material system B: LGF-PP/filler hybrid composites:

Hybrid composites are known to be complex systems in sense of predicting the mechanical behaviour *e.g.* in applications, which is due to the reason that there are large number of factors that affect on the failure process. In material system A the target was to study the microstructural phenomena behind the property changes in LGF reinforced PP composites containing mineral fillers. Effect of filler addition to the LGF composites on fibre orientation, fibre length degradation, changes in crystalline morphology and changes in failure modes under loading were analysed. Then, the results were compared to the mechanical properties of the hybrid composites, and considered as novel tools to understand the mechanical behaviour of such complex material systems. The applicability of LGF-PP hybrid composites *e.g.* in automobile interior parts is discussed.

3) Aims of material system C: LGF composites based on PA-thermoset blends:

The effect of water absorption is one of the most essential issues in the case of composite materials based on polymers which include polar groups. In this work LGF PA66 composites were modified by using a novel matrix system based on polyamide-thermoset blends, the main target being reduction of moisture absorption of the matrix. The reduced affinity of the new matrix material towards water molecules allows improved mechanical properties under humid conditions and opens possibilities for novel applications. The chemical structure of the polyamide-thermoset blends was analysed by a model compound approach with the target of predicting the chemical connection between the blend components in macromolecular system. Results of the model compound study were then compared to the macromolecular system. Next, PA-thermoset blends were used as a matrix material in LGF composites. The mechanical properties of the composites were studied in dry state, as well as after different treatments. The targeted applications of such a material are components in the automobile cooling system and similar parts that require good mechanical response under water or chemical environment.

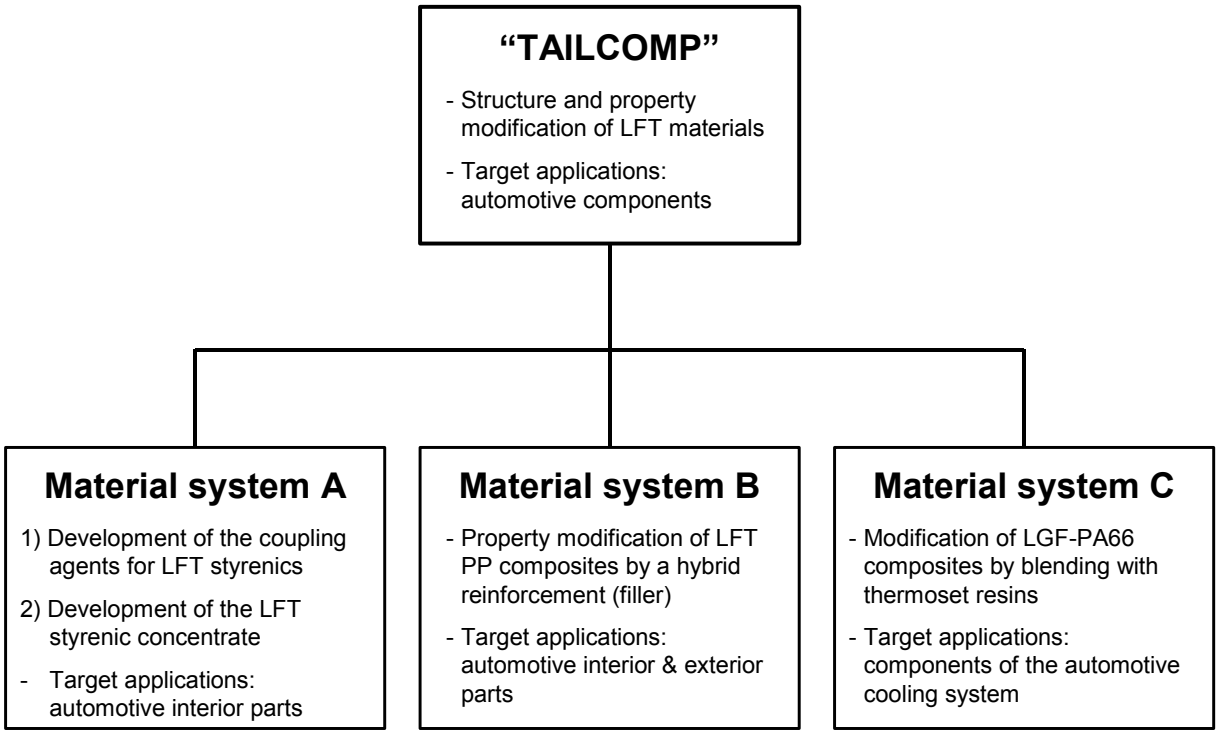

Figure 3.2: The aims of the three material systems studied in the present work as a schematic graphics.

4 MATERIALS AND SAMPLE PREPARATION

4.1 Material system A: Thermoplastic styrenic composites

4.1.1 Materials

SAN-*co*-MAH copolymer was supplied by Bayer Plastics and PS-*co*-MAH copolymer was supplied by Nova Chemicals. PS was supplied by BASF and it was of type Polystyrol 144 C. Other thermoplastic styrenic resins were supplied by Resin Express GmbH, Germany. SAN was a grade Tyril 790 of DOW Chemical Company, ABS was a grade Sicoflex S454 AT of MP compounds and PC/ABS was a grade Pulse A35-105 of DOW Chemical Company.

4.1.2 Sample preparation

LGF composite materials based on thermoplastic styrenics were produced by using a production technology of FACT GmbH. Pellet length was 11 mm. Next, the sample specimens were injection moulded by using an Arburg Allrounder 320 C 600-250 injection moulding machine, with a maximum clamping force of 600 kN. The processing temperature was 250-290 °C and the mould temperature 50 °C.

4.2 Material system B: Polypropylene hybrid composites

4.2.1 Materials

Long glass fibre reinforced polypropylene pellets were supplied by FACT GmbH. The material was of type FACTOR® PP GF 60 N 11, a long glass fibre reinforced PP with glass fibre content of 60 wt %. The fibre length in the pellets was the same as the pellet length of 11 mm. A calcium carbonate ($CaCO_3$) filler concentrate Omyalene 102 (87 wt% filler content) was supplied by Omya GmbH, Germany. The $CaCO_3$ particles were surface modified (olefin based modifier optimised for PP), and the mean particle size was 2.0 µm. Talcum powder was also supplied by Omya GmbH and it was of type Finntalc M15, the mean particle size being 4.5 µm

4.2.2 Sample preparation

At first, two concentrates with different amounts of fillers in polypropylene (20 and 40 wt %) were compounded using laboratory scale twin screw extruder, Brabender DSE 25. The L/D ratio of the extruder was 22/1, and there were 4 separate heating zones. The temperature profile was adjusted to 180, 220, 240 and 260 °C, and the used rotation speed was 60 rpm. Neat polypropylene granulates were first mechanically mixed with additive granulates or powder, after which the dry blend was fed into the extruder using an automatic feeder provided by Continator Plastic Machinery. Then, the extruded material was granulated into pellets with a length of 11 mm. Additionally, neat PP was processed into 11 mm pellets, in order to facilitate the proper mixing during the injection moulding and also to harmonize the processing histories of the components. Finally, the pellets were dried for a minimum of two hours at 70 °C in order to remove the residual water originating from the cooling step during the compounding process.

Next, the samples were prepared by mechanically mixing the compounded materials in different ratios of fillers, glass fibres and polypropylene. The bone shaped specimens with a geometry as specified in standard ISO 3167 (geometry Type 2 – Figure 4.1) were then injection moulded using an Arburg Allrounder 320 C 600-250 injection moulding machine with a maximum clamping force of 600 kN. The processing temperature was 225-270 °C and the mould temperature 50 °C. For the fracture mechanical tests, a 2 mm deep and 1 mm wide notch was machined in the middle of the sample. Additionally, a razor blade was used to make a small cut in the bottom of the notch to work as a crack initiation point during the fracture mechanical test. Similarly, 2 mm thick plate shaped specimens (Geometry Type 1 - Figure 4.1) were injection moulded for the fibre orientation and fibre length degradation analyses. The mould of the plate specimens has been developed by the companies IB Steiner and HTP Fohnsdorf GmbH in Austria (the shape is not according to a standard). Therefore, the moulding of the plate shaped samples was carried out in Austria by the company Werner GmbH. The melt temperature used during the moulding of the plate specimens was 220-240 °C and the mould temperature was 15 °C. The sample denotion and the formulations are presented in Table 4.1.

Table 4.1: A list of the prepared LGF-PP/filler samples.

Formulation	*Filler*	*Fibre loading [vol %]*	*Filler loading [vol %]*	*ISO 3167 standard specimens*	*Plate shaped specimens*
A	-	0	0	Yes	No
B	$CaCO_3$	0	7.7	Yes	No
C	-	3.7	0	Yes	No
D	-	12.9	0	Yes	Yes
E	$CaCO_3$	4.2	7.4	Yes	No
F	$CaCO_3$	14.6	6.6	Yes	Yes
G	Talc	4.2	7.4	Yes	No
H	Talc	14.6	6.6	Yes	No

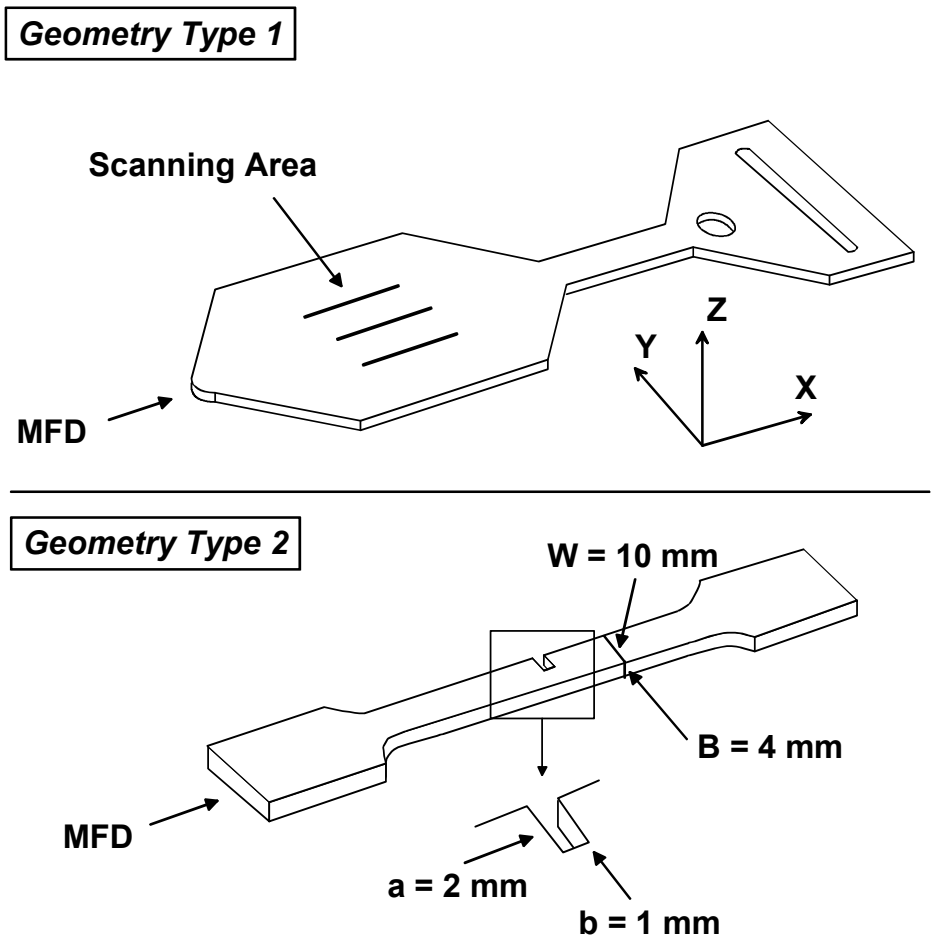

Figure 4.1: A schematic drawing illustrating the sample geometries in the study of LGF-PP/filler hybrid composites.

4.3 Material system C: Polyamide composites

4.3.1 Materials

N-methylacetamide (NMA) and phenol were of 99 % purity and supplied by Aldrich. Zytel PA66 of DuPont was supplied in granulate form by Biesterfeld Plastics GmbH (Germany), and its viscosity averaged molecular weight M_v was 32700 g/mol, as analysed by solution viscosity method in concentrated sulphuric acid. Phenol formaldehyde resin (PFR) was of type Supraplast 1763 and supplied by Süd-West-Chemie GmbH, Germany. It was a novolac type resin having a weight averaged molecular weight M_w of 989 g/mol and number averaged molecular weight M_n of 463 g/mol as analysed by gel permeation chromatography. Also hexamethylene tetramine (HMTA) crosslinking agent was supplied by Süd-West-Chemie GmbH.

4.3.2 Sample preparation

NMA-phenol complex was directly mixed in a molar ratio of 1:1 at 30 °C by a magnetic stirrer for 4 hours in a closed 4 ml glass bottle. The closed sample bottle was stored in a vacuum desiccator before FTIR analysis. To prepare the polymer blends, powdered phenol formaldehyde resin was mechanically mixed with PA66 granulates at ratios varying from 0 to 50 wt % of PFR in PA66. After mixing, the blends were melt processed by using a Haake Buchler Rheocord System 40 laboratory scale twin screw extruder at the company FACT GmbH. Temperature profile was set to 240-290 °C, and the screw speed was 40 rpm. After processing, the blend samples were let to cool slowly to room temperature, dried overnight in vacuum oven at 60 °C and stored in vacuum desiccator until analysed.

LGF composite materials based on polyamide-phenolic resin blends were manufactured by the production technology of FACT GmbH, to give 11 mm long pellets suitable for injection moulding. After this, the bone shaped specimens were injection moulded using Arburg Allrounder 320 C 600-250 injection moulding machine with maximum clamping force of 600 kN. The processing temperature was 260-300 °C and the mould temperature 90 °C.

5 CHARACTERISATION METHODS

5.1 Mechanical testing

5.1.1 Tensile strength test

Tensile tests were carried out according to standard ISO 527 using bone shaped specimens. The testing apparatus was a Zwick UPM 1485 equipped with 250 kN load cell (resolution 50 N), a hydraulic clamping device and an extensiometer (resolution 0.5 µm). The analysis was carried out at a constant crosshead speed of 2 mm/min.

5.1.2 Charpy impact toughness test

Unnotched Charpy impact toughness analysis was performed according to standard ISO 179. The bone specimens were first cut into 4x10 mm^2 plates. Then, the analysis was performed using CEAST pendulum device equipped with a 15 kN Charpy hammer. Notched Charpy impact toughness was performed similarly, but in this case a notch with 0.25 mm notch base radius was machined to the middle of the specimen by using CEAST Notchvis automated notching unit.

5.1.3 Dynamic mechanical thermal analysis

Dynamic mechanical thermal analysis was carried out to find out the effect of temperature on the modulus. DMTA spectra were taken on rectangular specimens (55 x 10 x 4 mm^3; length x width x thickness) in tensile mode at 10 Hz using a Eplexor 25 N device of Gabo Qualimeter. The static and cyclic (sinusoidal) loading components were set to 20 N and $\pm$ 10 N, respectively. Complex modulus (E*) and its constituents (E' and E''), mechanical loss factor (tan δ) were measured at a heating rate of 1 °C/min.

5.1.4 Fracture mechanical test

A Zwick UPM 1485 universal testing apparatus, equipped with a 10 kN load cell, a mechanical clamping device and an extensiometer, was used to analyse the fracture mechanical properties of the LGF-PP/filler samples. Single edge notched tensile (SEN-T) specimens with a machined notch (depth 2 mm) were used, and the crosshead speed was 1 mm/min (Geometry Type 2 – Figure 4.1). Critical stress intensity factor K_c was determined according to the following equation [122]:

$$K_c = \sigma_c Y \sqrt{a} \tag{4}$$

where σ_c is the gross fracture stress, *a* is the length of the notch and *Y* is the geometrical factor. The following equation was used for geometrical factor *Y* [123]:

$$Y = \frac{5\sqrt{\pi}}{\sqrt{20 - 13(a/W) - 7(a/W)^2}} \tag{5}$$

where *W* is the specimen width.

5.2 Microscopic methods

5.2.1 Optical microscopy

Films of PA66/PFR blends and PP/filler samples were cut by using a Leitz 1400 microtome. Film thickness of 25-30 µm was used. Next, the films were analysed by using a Leitz Diaplan polarization microscope, equipped with a video camera.

5.2.2 Scanning electron microscopy

The fracture surfaces after Charpy impact toughness test and fracture mechanical test were analysed using a JEOL JSM 5400 scanning electron microscope. Before the analysis, the fracture surfaces were first cautiously cleaned with an air blow and then coated with an alloy of gold and palladium (ratio 5/1).

5.2.3 Transmission electron microscopy

Ultra thin sections (approximately 100 nm) of PA66/PFR blends for TEM characterization were microtomed at room temperature using a Leica Ultracut UCT ultramicrotome and a Diatome-diamond knife. Bright-field TEM was performed on a JEOL-1200EX transmission electron microscope operating at an accelerating voltage of 60 kV. The analysis was carried out by a group of Prof. O. Ikkala at Helsinki University of Technology, Finland.

5.3 Differential scanning calorimetry

A Mettler Toledo DSC 821 device was used to determine glass transition and melting temperatures of the PA66-PFR blends. The samples were first heated to 270 °C and then cooled back to room temperature to harmonise thermal histories. T_g and T_m values were taken from the second heating scan. The rate of the heating and cooling was 10 °C/min.

5.4 Fourier transform infrared spectroscopy

A Nicolet 510 FTIR spectrometer was used to analyse hydrogen bonding in model compounds and in polymer blends. Model compounds NMA, phenol and NMA(phenol)$_{1.0}$ complex were either mixed and pelletised within KBr (phenol) or “sandwiched” between two KBr pellets (NMA and complex). Polymer blend samples were ground in powder form together with KBr and then pressed to pellets. The minimum number of scans was 32 with resolution of 4 cm^{-1}.

5.5 Optical image analysis

The fibre length and the fibre orientation analyses were carried out by a group of Prof. R. Duckett at University of Leeds, United Kingdom (only Geometry Type 1 – Figure 4.1). The system used is an in-house image analysis facility developed at Leeds University [64]. For fibre orientation investigations, the chosen method is one of optical reflection microscopy of polished 2D sections taken from the areas of interest of the composite. Each fibre that meets the 2D section is seen as an elliptical footprint, and measuring the ellipticity of these images allows to determine the two polar angles, θ and ϕ, that specify the orientation of each fibre to be determined: θ is the angle the fibre makes with the sectioned surface normal (Y), and ϕ is the angle the fibre makes with the Z axis when projected into the XZ plane (Figure 5.1a). Figure 5.1b shows a typical elliptical fibre footprint, and indicates that θ is given by the inverse cosine of the ratio of the semi-minor to semi-major axis of each elliptical image, ϕ is determined by the angle between the major axis and the Z axis. An XY stage allows a large area to be scanned, allowing fibre orientation structures over large areas to be studied and analysed.

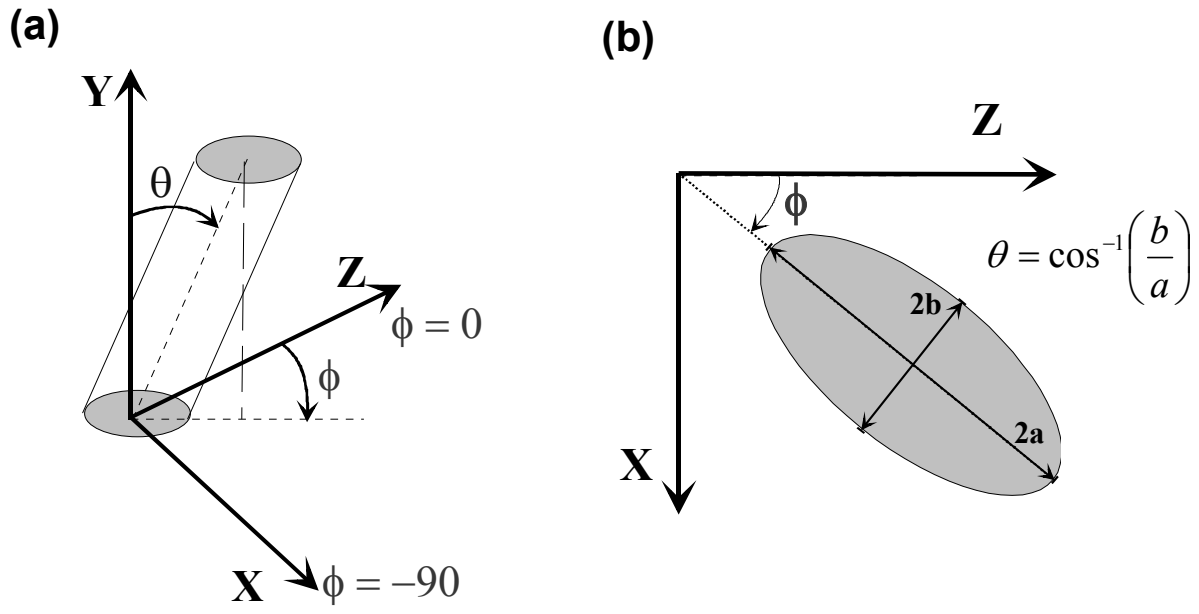

Figure 5.1: Schematic description of the fibre orientation calculations: a) definition of the angles ϕ and θ, and b) the calculation of θ from the elliptical footprint.

Fibre length measurements were carried out for LGF-PP/$CaCO_3$ hybrid composites as taken from the plate shaped samples. The samples were heated in a furnace at 450°C for 8 hours to burn away the matrix. For the $CaCO_3$ filled samples, the ashed fibres/filler mixture was boiled in water for 5 minutes to dissolve the filler. Once ashed a representative fraction of the fibre array was laid onto a glass slide and viewed in transmitted light enabling the length distributions to be measured.

5.6 Acoustic emission analysis

In order to get a deeper understanding on the failure behaviour, acoustic emission (AE) of the notched bone shaped specimens (Geometry Type 2 – Figure 4.1) was recorded *in-situ* (during the loading), by using a miniature sensor (10 mm diameter) attached to the specimen surface and coupled to a Defektophone NEZ 220 device (AEKI, Hungary). The acoustic events were picked up by a wide bandwidth heat-proof transducer in the frequency range 100 to 6001 kHz (peak sensitivity -/ 70dB/V/μbar, type Micro-30D of Dunegan Co., USA). The output signal of the transducer was amplified logarithmically. The transfer function for the whole measuring system (including the logarithmic amplifier and acquisition unit) was:

$$\text{Peak amplitude} = 100 + 20 \lg(U_{inp}/0.4)$$

During the tests the following primary AE signals were measured, calculated and stored: elapsed time, number of events, peak amplitude, AE energy event width and rise time [124].

5.7 Density measurements

The densities of the injection moulded samples were measured from the bone shaped specimens using a Mettler Toledo AG204 Delta Range scale equipped with the density measurement kit (gravimetric method) at FACT GmbH. First, the weights of the samples were measured in air. Next, the nominal weights of the samples were

measured in distilled water at room temperature, after which the densities were calculated by the following equation:

$$\rho = \frac{m_{air}}{P} \cdot \rho_0 \qquad (6)$$

where ρ is the density of the specimen, m_{air} is the weight of the specimen in air, P is the buoyancy of the specimen in water and ρ_0 is the density of water at the test conditions. Density values of the composites were also calculated by using following densities for the ingredients: 2.60 g/cm^3 for glass fibres, 2.75 g/cm^3 for talc, 2.70 g/cm^3 for $CaCO_3$, and 0.90 g/cm^3 for polypropylene.

5.8 Solution viscosity analysis

Solution viscosities of the polyamide samples before and after different treatments were analysed by using a capillary viscometer (Ubbelohde). The solvent used was concentrated sulphuric acid. Relative viscosity was calculated from the efflux times according to the following equation [56]:

$$\eta_r = \frac{t}{t_0} \qquad (7)$$

where t is the efflux time of the sample solution and t_0 is the efflux time of the pure solvent. Similarly, specific viscosity was calculated according to:

$$\eta_{sp} = \frac{t - t_0}{t_0} \qquad (8)$$

Next, intrinsic viscosity *i.e.* limiting viscosity number was calculated from η_r and η_{sp} by using a single point Solomon method [125]:

$$\eta_{\lim} = \frac{1}{c}\sqrt{\left(2(\eta_{sp} - \ln \eta_r\right)} \qquad (9)$$

where η_{lim} is limiting viscosity number and c is polymer concentration. The unit given by the equation (9) is [dl/g]. Finally, viscosity averaged molecular weight can be calculated by using Mark-Houwink equation:

$$\eta_{\lim} = KM_v^{\alpha} \qquad (10)$$

where K and α are constants that depend on the polymer-solvent pair in question, and M_v is viscosity averaged molecular weight. The molecular weights of the samples were calculated by using the parameters for polyamide 66-sulphuric acid pair: 0.741 for α and $5.24 \cdot 10^4$ dl/g for K [126].

5.9 Theoretical calculations

Quantum mechanical calculations for the small molecular weight model compounds of PA66-PFR blend system were carried out by using a Gaussian 03 software [127] running on an SGI Origin 2000 computer system (Finnish IT Center for Science, Finland). All calculations were carried out by a group of Prof. O. Ikkala at Helsinki University of Technology. Two standard computational methods were used in the calculations. The first method was a density functional theory (DFT) with a hybrid functional of Lee, Yang and Parr (LYP), further developed by Becke using a three-parameter least squares fit (B3LYP) [128]. The second method was the second-order Møller-Plesset perturbation theory (MP2). Geometry optimisations and energy calculations of all molecules were done using a B3LYP/6-31+G(d,p) level of theory

with the standard 6-31+G(d,p) basis set. The basis set was comprised of 6 Gaussian functions of the inner shell orbitals, 3 Gaussian functions of the first Slater Type Orbital (STO) of the double zeta function and 1 Gaussian function of the second STO of the double zeta function. The basis set included polarization functions on all elements and diffuse functions on all non-hydrogen elements. The basis set superposition error was estimated using the counterpoise correction [129, 130] with the 6-31+G(d,p) basis set for both B3LYP and MP2 methods.

6 RESULTS AND DISCUSSION

6.1 System A: LGF reinforced thermoplastic styrenic resins

6.1.1 Improvement of the interfacial properties in LGF styrenics

Interfacial adhesion between the reinforcing fibres (most typically glass) and the matrix is a central issue in the case of thermoplastic composite materials. Fibre surface chemistry, as well as the coupling agents often contained in matrix, have to be tailored in a manner which optimises adhesive strength between the components. This is also the case with thermoplastic styrenic resins. These are basically incompatible with glass fibre surfaces because of their unpolar polymer backbone, in contrast to the highly polar glass fibre surfaces.

From previous studies it is known that graft copolymers containing maleic acid anhydride (MAH) groups provide a useful way of improving adhesive strength between the glass fibres and the matrix. For example, it has been proved that PP-*g*-MAH copolymers considerably improve the mechanical properties, when added to glass fibre reinforced PP [33]. Therefore, this method has received already plenty of attention in literature. In the present work the purpose was to use the compatibilisation concept *via* MAH groups to improve the properties of LGF reinforced thermoplastic styrenics. PS and SAN were chosen as matrix materials, to demonstrate the functionality of the concept. PS-*co*-MAH copolymer (SMA) was used in the case of LGF-PS composites and SAN-*co*-MAH copolymer in the case of LGF-SAN composites to improve the compatibility between the fibres and the matrix. Figure 6.1 shows the effect of the compatibilisation on the tensile strength. It can be seen that the strength of the materials increases constantly as a function of additive content. A total increase of 28 % was achieved in the case of LGF-PS composites and 22 % increase in the case of LGF-SAN composites, when compared to the corresponding uncompatibilised materials. This result shows that good compatibility between the components is essential in order to achieve the high tensile strength.

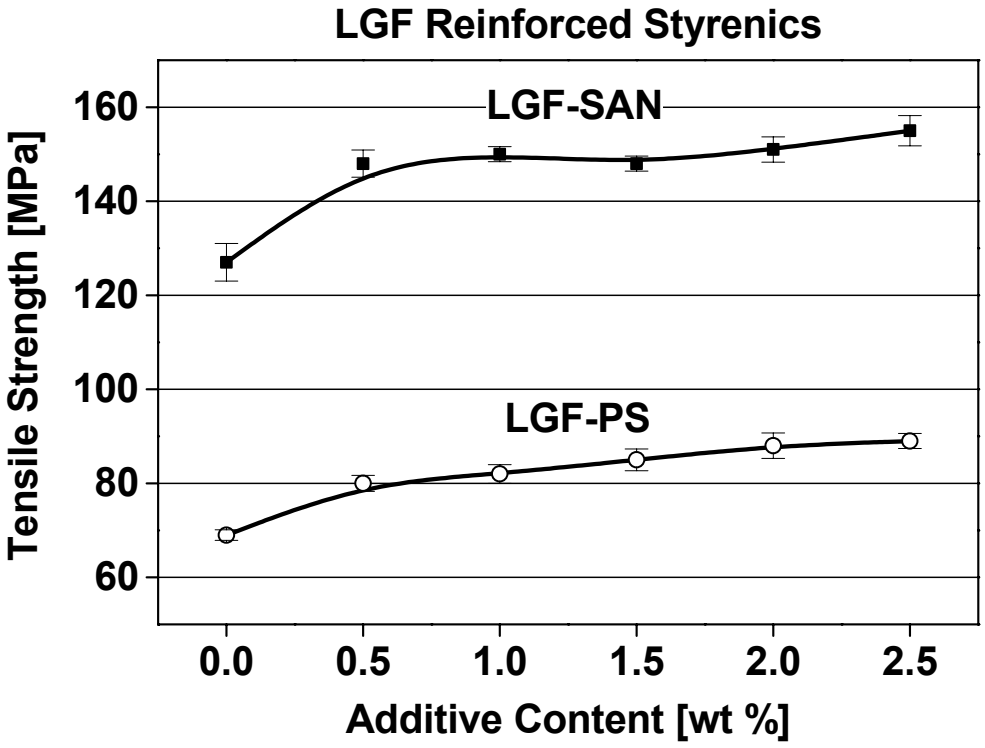

Figure 6.1: Tensile strength of PS reinforced with 15 vol % of LGF and SAN copolymer reinforced with 17 vol % of LGF as a function of coupling agent concentration in the matrix (PS-MAH or SAN-MAH).

Figure 6.2 shows the tensile modulus of LGF-PS and LGF-SAN composites as a function of copolymer concentration. In the case of LGF-SAN composites, the modulus increases up to 1.5 wt % SAN-*co*-MAH concentration. The maximum value of 12 GPa corresponds to a total increase of 11 % compared to an uncompatibilised LGF reinforced SAN. On the other hand, the modulus of LGF-SAN composites remains unchanged until 2.0 wt % PS-*co*-MAH content. After this, a slight increase of 6 % is detected. Therefore, only minor changes in material stiffness are observed upon copolymer addition, especially in the case of PS composites. This phenomenon is known from other thermoplastic composite systems like glass fibre reinforced PP, and can be explained by the fact that the modulus is mainly determined by the volume fraction of glass fibres rather than by the fibre-matrix adhesion [33].

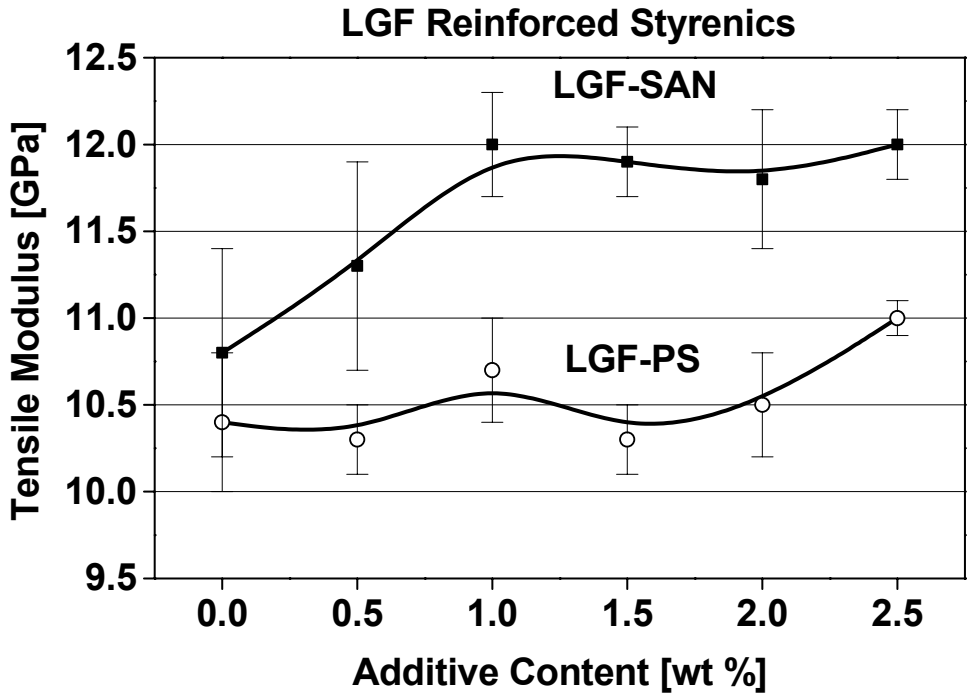

Figure 6.2: Tensile modulus of PS reinforced with 15 vol % of LGF and SAN copolymer reinforced with 17 vol % of LGF as a function of coupling agent concentration in the matrix (PS-*co*-MAH or SAN-*co*-MAH).

The impact energy of the studied LGF styrenic composites as a function of additive content is shown in Figure 6.3. It can be noticed that there is a clear difference in the toughness behaviour of LGF-PS and LGF-SAN composites. The unnotched Charpy impact energy of LGF-SAN composites increases dramatically as SAN-*co*-MAH copolymer is added to the matrix. The maximum value of 32 kJ/m^2 is reached at 1.5 wt % additive concentration, which corresponds to an increase of 62 % as compared to the uncompatibilised material. On the other hand, the toughness of LGF-PS composites is unchanged as PS-*co*-MAH is added to the matrix. In the case of GF-PP composites it has been noticed that both strength and the toughness can be improved simultaneously by optimising the fibre-matrix adhesion [34, 131]. On the other hand, it has been reported that impact toughness may even be reduced as adhesion promoters are added into the matrix [33]. Therefore, it can be concluded that SAN-*co*-MAH is an optimal coupling agent for LGF-SAN composites, whereas SMA improves only the strength and modulus of LGF-PS but does not affect toughness.

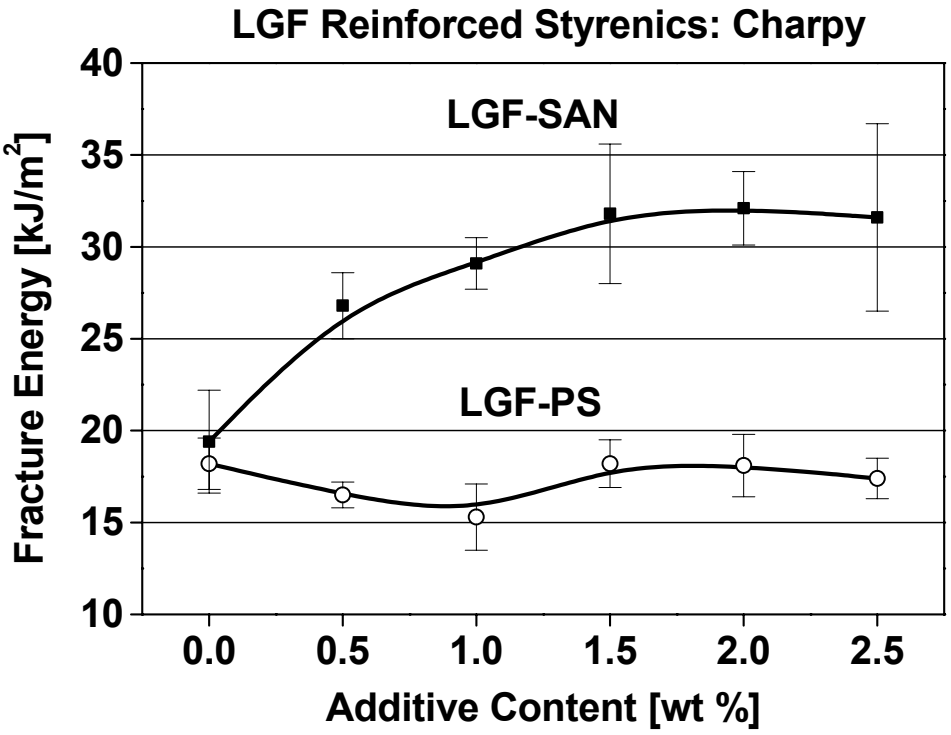

Figure 6.3: Unnotched Charpy impact energy of PS reinforced with 15 vol % of LGF and SAN copolymer reinforced with 17 vol % of LGF as a function of coupling agent concentration in the matrix (PS-*co*-MAH or SAN-*co*-MAH).

SEM fractrographs of Figure 6.4 show the changes in fracture surfaces of LGF-SAN composites, as MAH functionalised SAN copolymer is added into the matrix. Similarly, Figure 6.5 shows the fracture surfaces of LGF-PS composites with and without a PS-*co*-MAH coupling agent. Without a coupling agent, the fibres are loosely connected to the matrix polymer. The fibre surfaces are smooth and without much polymer matrix connected to them. In the case of LGF-SAN composites, the addition of SAN-co-MAH causes obvious changes. Figure 6.4b shows that the fibres are strongly attached to the matrix, and the fibre surfaces are covered with the SAN resin. In contrast, PS-*co*-MAH changes the morphology only slightly. Figure 6.5b indicates that the PS matrix adheres somewhat better to the fibre surface than the uncompatibilised PS resin (Figure 6.5a). Additionally, using SEM it was observed that the fibre pull-out lengths were about 30-50 % higher in the case of the uncoupled samples compared with the samples containing functionalised polymers. These qualitative observations agree well with the mechanical test results.

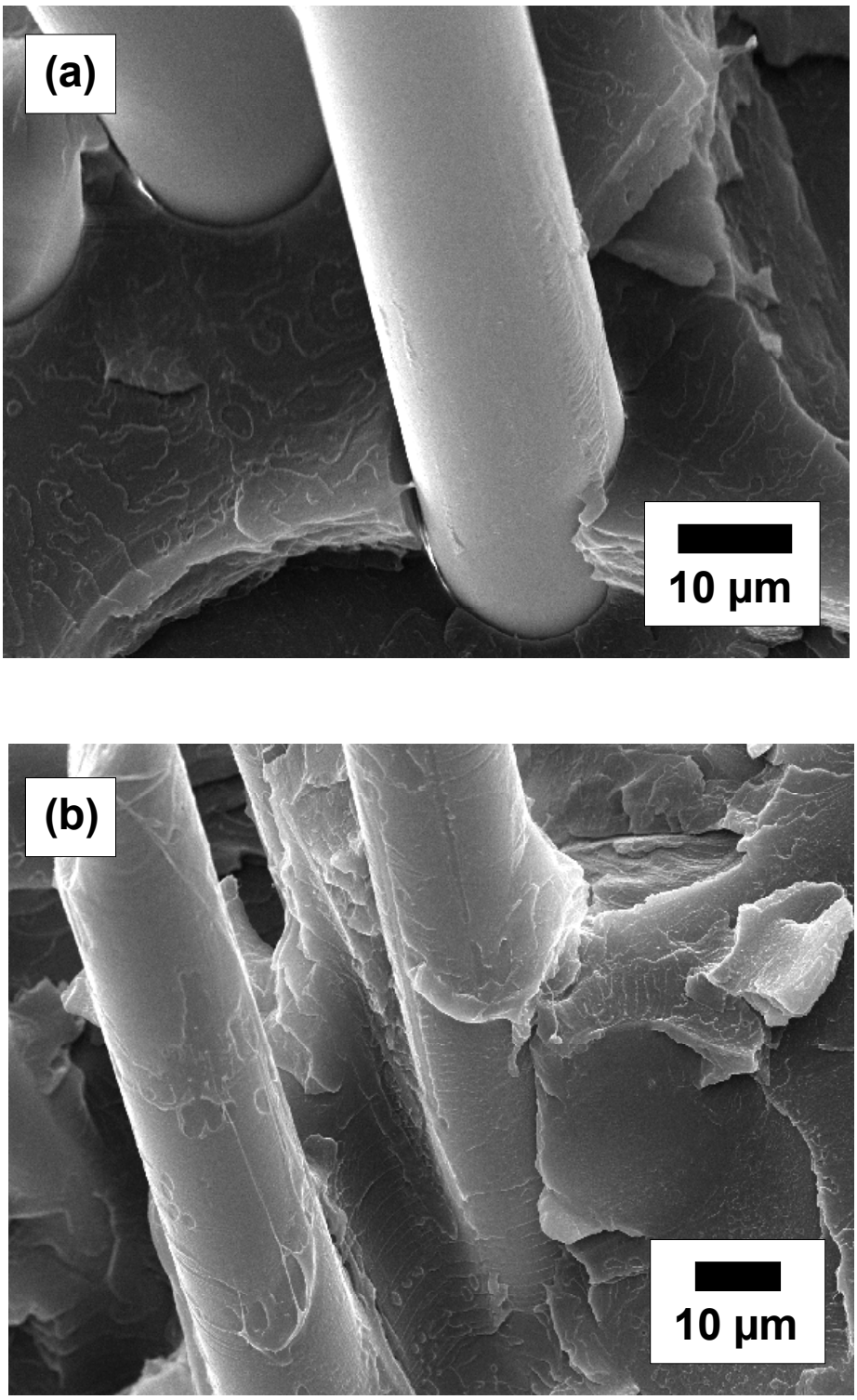

Figure 6.4: SEM micrographs of impact fracture surfaces of LGF-SAN composite including 17 vol % of fibres: a) without a coupling agent and b) with 1.5 wt % of SAN-MAH.

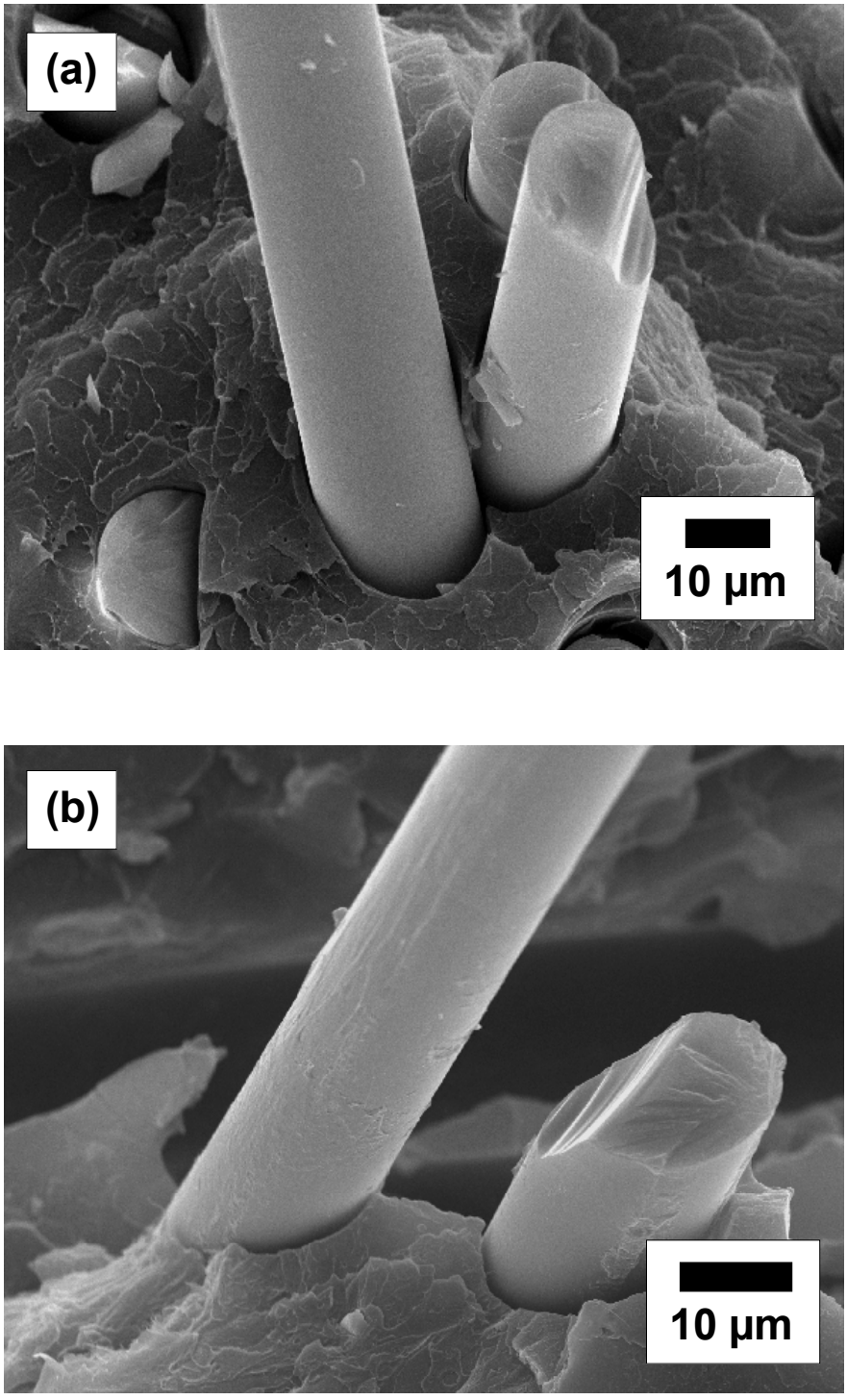

Figure 6.5: SEM micrographs of impact fracture surfaces of LGF-PS composite including 15 vol % of fibres: a) without a coupling agent and b) with 1.5 wt % of PS-MAH.

6.1.2 Development of LGF concentrate for thermoplastic styrenics

There is a wide variety of thermoplastic styrenic resins, due to the fact that PS is often copolymerised with other monomers like acrylonitrile, maleic acid anhydride and butadiene. Additionally, styrenic resins are frequently blended with other thermoplastics like polycarbonate, to improve the mechanical and thermal properties. Therefore, the production of composite materials based on these resins requires that each resin is first impregnated before being processed into final parts. A novel concept developed during this work offers an alternative way of introducing the fibres to the matrix (Figure 6.6). The concept is based on LGF concentrate pellets containing 60 wt % of LGF (about 40 vol %). This base material is compatible with several thermoplastic styrenic resins, which are used to dilute the fibre concentration to the required level. This approach allows a flexible production of the parts, since the final properties can be tailored according to the particular application by changing the "diluent" resin type and by adjusting the level fibre concentration. Therefore, the concept is very similar to the addition of colorants and other additives, which are often used in the form of masterbatches.

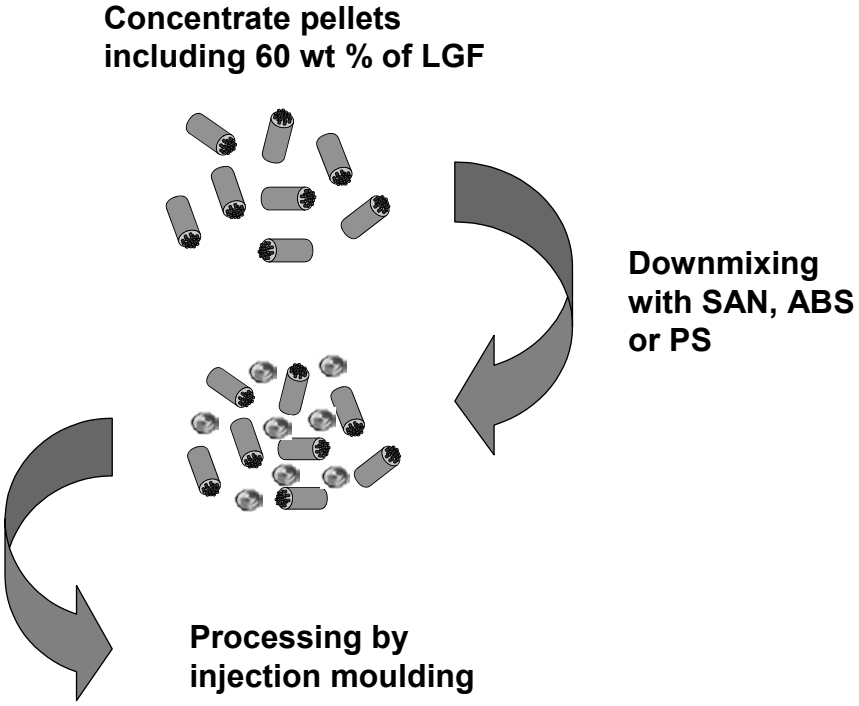

Figure 6.6: The concept of using a general purpose LGF concentrate in the production of thermoplastic styrenic composites.

Figures 6.7-6.9 show the tensile strength of the composite materials based on the LGF styrenic concentrate as a function of fibre content. Fibre content was adjusted by mixing the LGF concentrate with the neat SAN, PC/ABS and ABS resins. For comparison, also the values of the commercial, short glass fibre reinforced styrenic resins are shown in the diagrams. It can be seen that, in general, the tensile strength values increase as the fibre concentration increases. However, there are distinct differences between the different diluent resins. The strength of the samples diluted with the SAN resin are higher compared to the PC/ABS and ABS based materials, and this is reflected in the mechanical behaviour of the corresponding LGF composites. The maximum strength reached with SAN diluent was 105 MPa, whereas in the case of PC/ABS the maximum strength was 90 MPa. Similarly, in the case of ABS the strength of 82 MPa was reached at *ca.* 7 vol % fibre content. Therefore, the strength of the composites is strongly dependent, in addition to the fibre loading, on the type of the dilution resin.

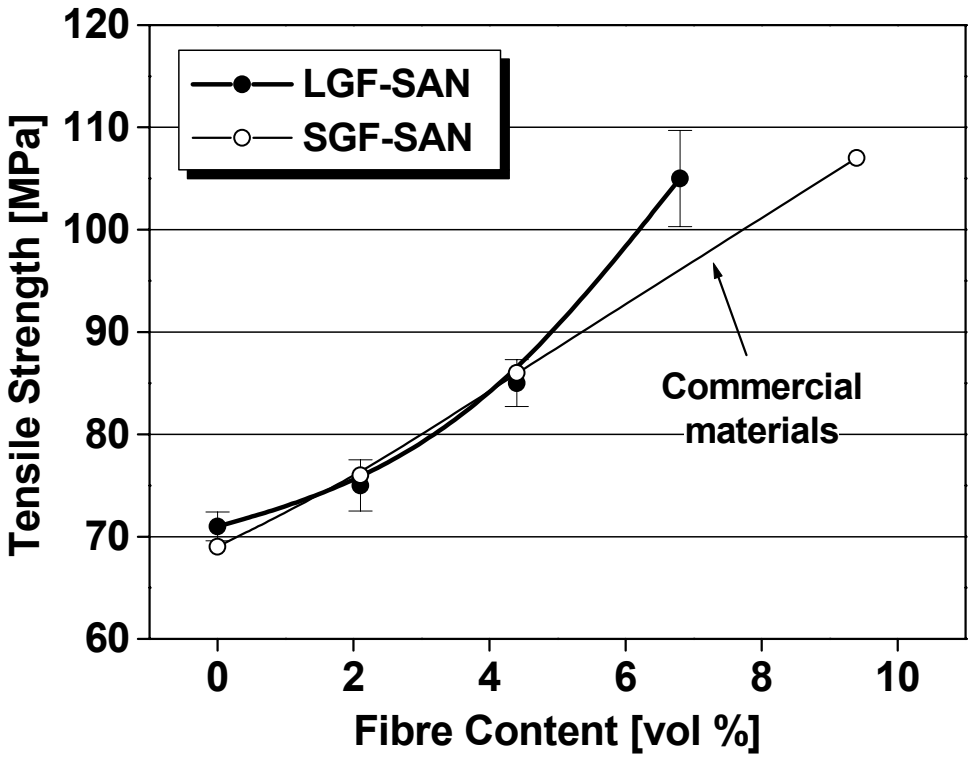

Figure 6.7: Tensile strength of LGF-SAN based on the LGF concentrate compared to the strength values of the commercial SGF-SAN composites (datasheet values).

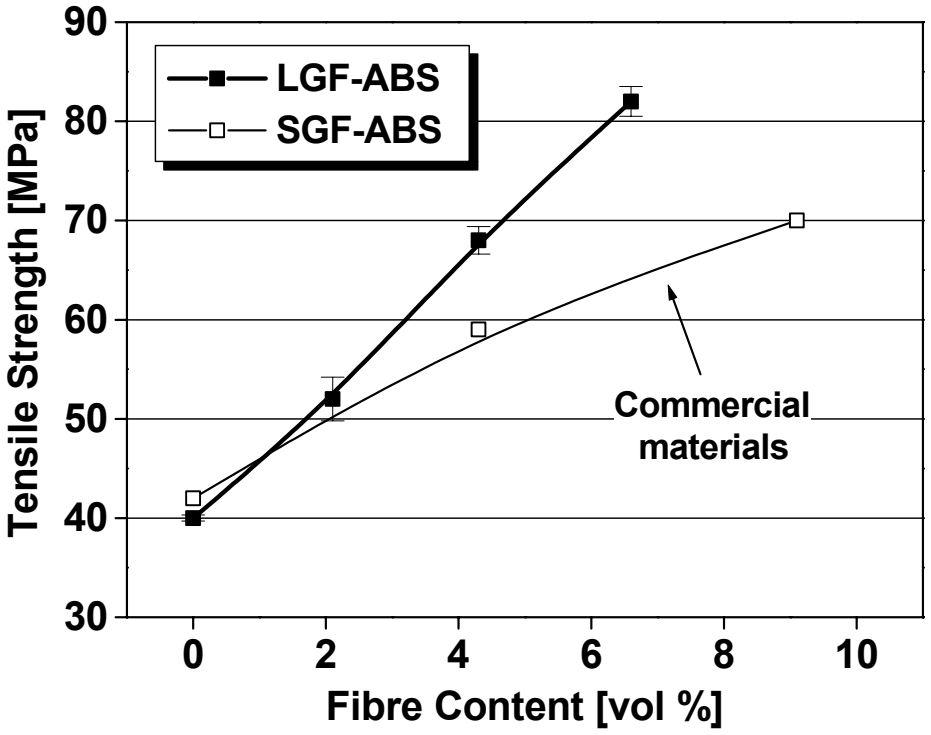

Figure 6.8: Tensile strength of LGF-ABS based on the LGF concentrate compared to the strength values of the commercial SGF-ABS composites (datasheet values)

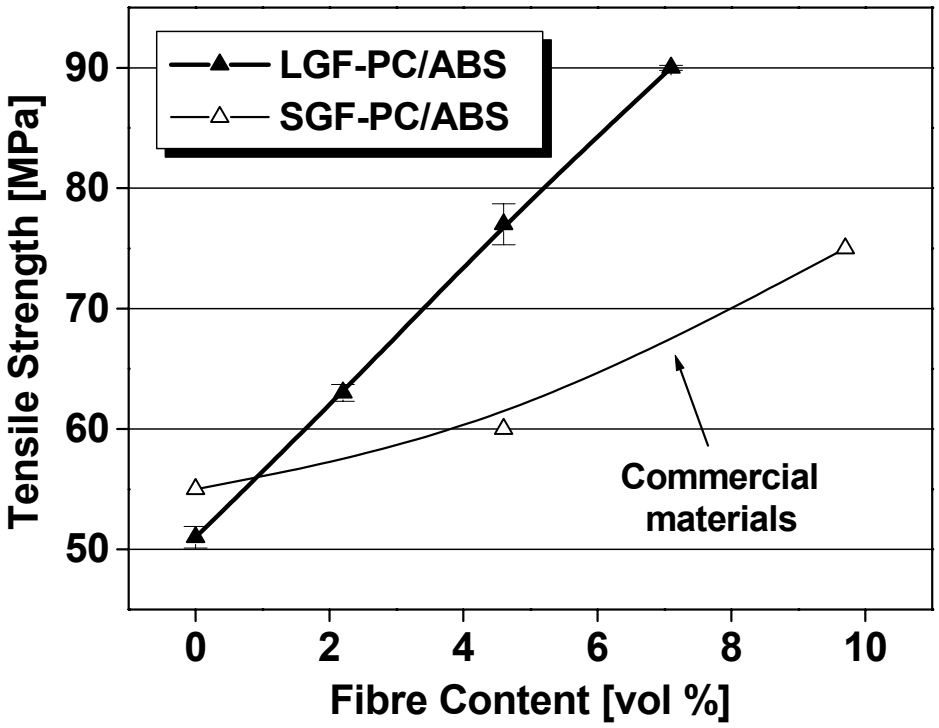

Figure 6.9: Tensile strength of LGF-PC/ABS based on the LGF concentrate compared to the strength values of the commercial SGF-PC/ABS composites (datasheet values)

Second important notion on the basis of Figures 6.7-6.9 is that the long fibre reinforced materials end up to higher strength materials, when compared to the commercial SGF thermoplastic styrenics. Also noteworthy is that the difference between the SGF and LGF composites is larger at higher fibre content. This can be explained by the fact that at higher fibre loading the strength is mainly determined by the reinforcing fibres rather than the matrix. Therefore, the benefit origination from the higher fibre aspect ratio is more clearly detected at higher fibre volume fractions.

Figure 6.10 presents the modulus behaviour of the studied materials. As it can be seen, the tensile modulus of composite materials using SAN resin remains 1.5 GPa higher than the modulus of composite materials using PC/ABS and ABS resins, throughout the studied composition range. This can be explained by the fact that the modulus of SAN resin is much higher than that of the PC/ABS or ABS resins, since the modulus of the composite materials is strongly dependent on the modulus of the single components.

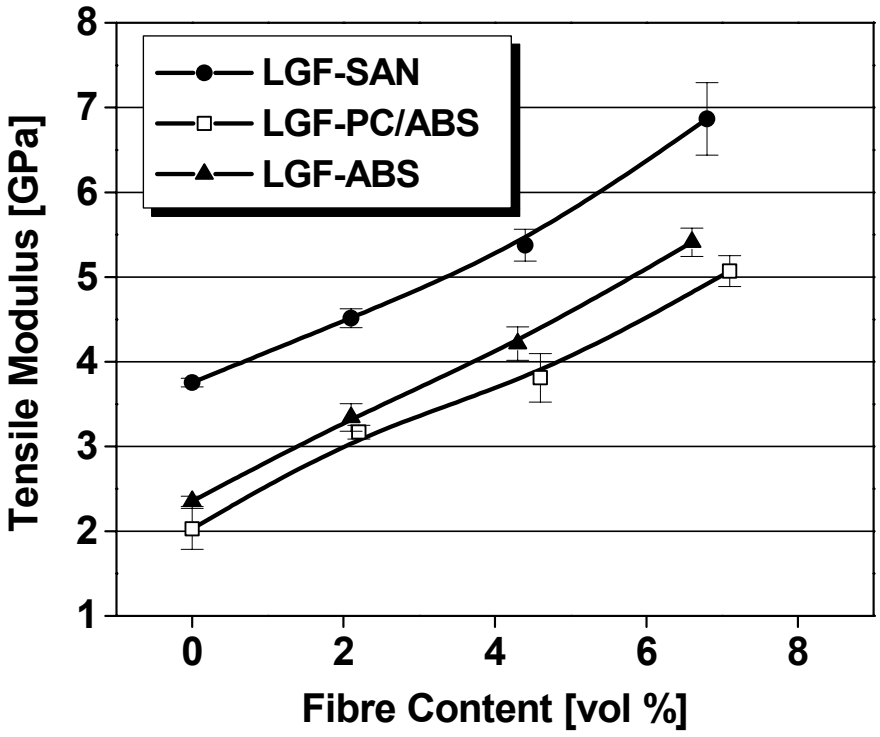

Figure 6.10: Tensile modulus of LGF reinforced styrenic resins based on LGF concentrate method.

The unnotched and notched Charpy impact energy values of LGF styrenic composites based on LGF concentrate are shown in Table 6.1. It can be seen that ABS and PC/ABS resins result in better toughness compared to when SAN resin is used as a diluent. What is also worth noting is that the addition of LGF in matrices results in different changes in toughness, depending on the diluent resin used. In the case of SAN, which is known the be a brittle thermoplastic polymer, the unnothced Charpy impact energy is almost unaffected by the addition of LGF. On the other hand, the notched Charpy impact energy shows a clear increase in this case. In contrast, as more ductile PC/ABS and ABS resins are used to dilute the fibre concentration, the toughness of the LGF composites are lower than that of neat matrices. This clearly shows that the effect of LGF reinforcement depends strongly on whether the matrix is intrinsically ductile or brittle.

Table 6.1: Charpy impact energy of LGF styrenic composites.

Formulation	*Unnotched Charpy* $[kJ/m^2]$	*Notched Charpy* $[kJ/m^2]$
SAN	15.3 ± 0.3	< 2
LGF-SAN 4 vol %	11.6 ± 2.7	3.0 ± 1.0
SAN LGF 7 vol %	18.6 ± 2.2	6.7 ± 0.7
ABS	n.b.	24.0 ± 0.1
LGF/ABS 4 vol %	27.4 ± 2.4	12.5 ± 0.1
LGF/ABS 7 vol %	32.6 ± 3.1	13.8 ± 0.5
PC/ABS	n.b.	n.b.
LGF/PC/ABS 4 vol %	37.7 ± 1.5	21.9 ± 4.7
LGF/PC/ABS 7 vol %	37.5 ± 2.7	14.5 ± 0.7

Finally, a DMTA analysis was carried out to establish the behaviour of the LGF styrenics at elevated temperatures. Figure 6.11 shows DMTA spectra of LGF reinforced SAN, PC/ABS and ABS composites at about 4 vol % fibre content. At room temperature, the absolute value of complex modulus $|E^*|$ was higher when SAN is used as a diluent, compared to the PC/ABS and ABS resins. However, above

120 °C the modulus of PC/ABS was clearly higher, indicating better thermal resistance. Thus, in applications that require better thermal properties, PC/ABS resin would be the suitable dilution resin.

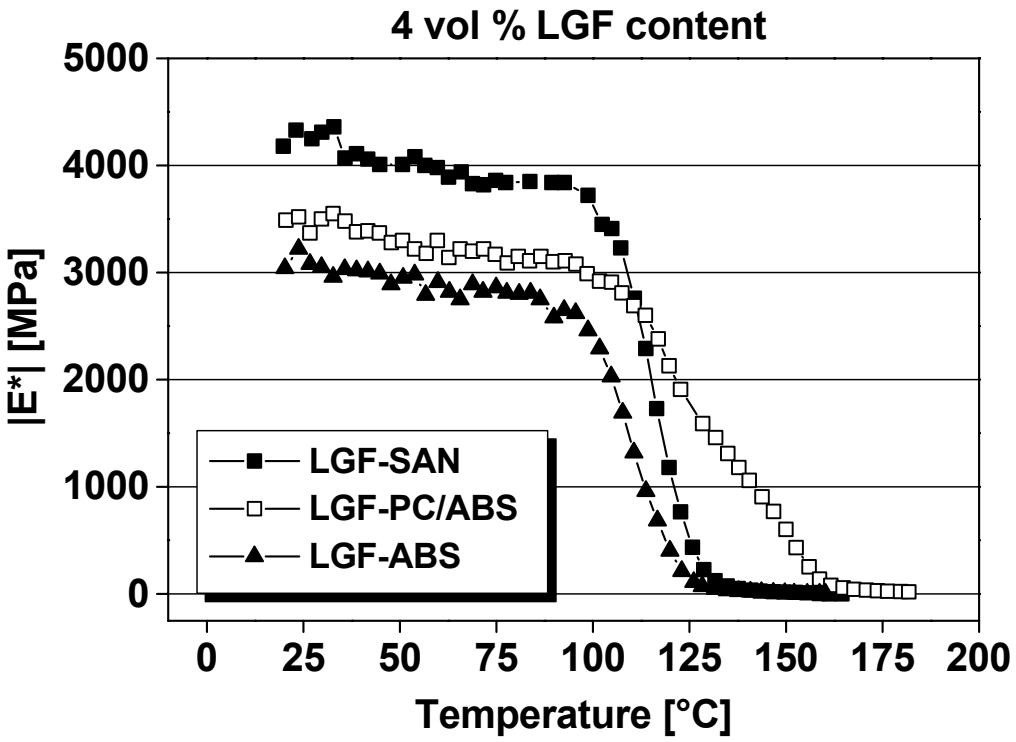

Figure 6.11: DMTA spectra of LGF reinforced styrenic composites based on LGF concentrate.

6.1.3 Conclusions

It was shown that compatibility issues are very important in order to achieve good mechanical behaviour in LGF reinforced thermoplastic styrenic resins. The addition of MAH functionalised resins to PS or SAN resins resulted in improved strength, stiffness and toughness. By using scanning electron microscopy it was shown that improved mechanical properties are related to improved interfacial adhesion between the reinforcing fibres and the SAN or PS matrix. In the case of LGF reinforced SAN, the adhesion was dramatically improved by the addition of small amount of SAN-*co*-MAH copolymer. This resulted in improved mechanical properties compared to corresponding uncompatibilised composite material.

The mechanical properties of LGF-PS composites were also improved by the addition of PS-*co*-MAH. However, a fractography by SEM revealed that adhesion between the long glass fibres and styrenic matrices was improved only slightly in the case of LGF-PS, which may explain why the increase of the mechanical properties was not so impressive as in LGF-SAN composites. Nevertheless, it was shown that the method of adding functionalised resin to the thermoplastic styrenic matrix generally resulted in an improved compatibility between glass fibres and the matrix.

In the next phase of the study a novel concept was introduced using an LGF concentrate to produce thermoplastic styrenic composite parts. It was shown that by using different styrenic resins to dilute the LGF concentration, different properties can be achieved. Therefore, the concept allows a flexible production method of the parts. It was shown that SAN resins as a diluent result in a better strength (Figures 6.7-6.9) and modulus (Figure 6.10), but lower toughness than the corresponding PC/ABS and ABS resins (Table 6.1). Therefore, in applications where high strength or stiffness are required, SAN diluent should be used. On the other hand, if high impact toughness is needed, PC/ABS or ABS resins give the best results. Additionally, it was found that thermomechanical properties are better when PC/ABS rather than SAN or PS resins were used as a dilution polymer (Figure 6.11). In conclusion, this process allows a new, flexible and economic way to manufacture parts based on LGF reinforced thermoplastic styrenic composites. The possible applications of such materials would be interior automotive parts such as instrumental panels, decoration panels, door modules *etc*.

6.2 System B: LGF-PP/mineral filler hybrid composites

6.2.1 Effect of fillers on crystalline morphology of PP

The nucleation effect of the two fillers, calcium carbonate ($CaCO_3$) and talcum, on the crystalline morphology of PP was studied using differential scanning calorimetry. Figure 6.12 depicts DSC thermograms during the 2nd cooling cycle of pure PP (a), and of PP containing 7.7 vol % of calcium carbonate (b) or talc (c), at a temperature interval of 100-150 °C. Crystallisation exotherm appears as a single, distinct peak in each case. The crystallisation temperature T_c was 125 °C for neat PP, whereas in the case of $CaCO_3$ filled PP it was slightly lower *i.e.* 123 °C. Thus, it seems that the $CaCO_3$ used in this study is inactive regard a nucleation effect, probably due to the facts that firstly, the average particle size of the used filler was relatively high (2 μm), and secondly, the filler particles were surface treated to decrease the surface energy, which both are known to reduce the "activity" of calcium carbonate.

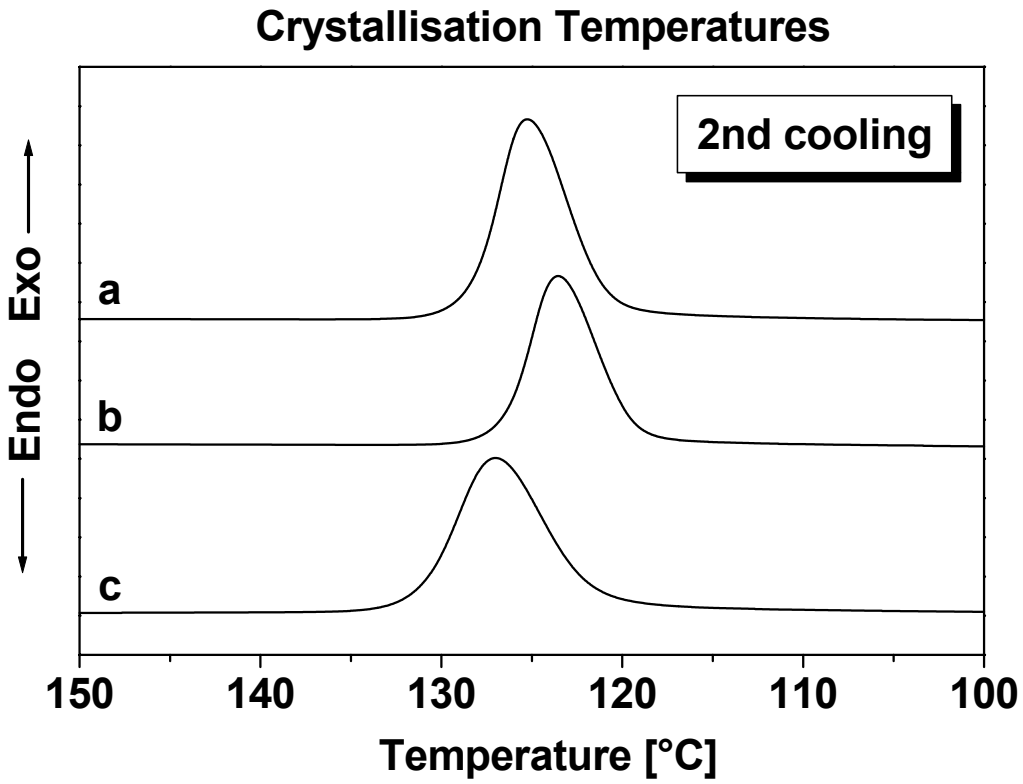

Figure 6.12: DSC scans of the 2nd cooling cycle showing the crystallinity exotherms of a) neat PP, b) PP with 7.7 vol % of $CaCO_3$ and c) PP with 7.7 vol % of talc.

In contrast, the addition of talcum in PP results in a different crystallisation behaviour. Firstly, the shape of the T_c exotherm is broader than in the cases of neat PP or calcium carbonate filled PP, which indicates that the crystallisation takes place during a longer period of time. Secondly, the peak of T_c has increased to 127 °C. These findings show that talc has a more pronounced effect on the crystallisation behaviour of polypropylene. Therefore, a DSC analysis offers one possibility to explain the different properties of $CaCO_3$ and talc filled materials.

Further evidence of the different nucleation effects of $CaCO_3$ and talc in PP is obtained by carrying out optical polarisation microscopy studies. Figure 6.13 shows the micrographs taken from 3 thin films of a) neat polypropylene, b) PP filled with *ca.* 7 vol % of $CaCO_3$ and c) PP filled with *ca*. 7 vol % of talc. All samples are birefringent, but the morphology of the talc filled sample differs from the others; the birefringence is much more intense compared to neat PP, or to PP with calcium carbonate. Furthermore, no difference can be detected between neat PP and $CaCO_3$ filled samples. Therefore, it is evident that the addition of talc affects the crystalline morphology of PP more than the addition of calcium carbonate.

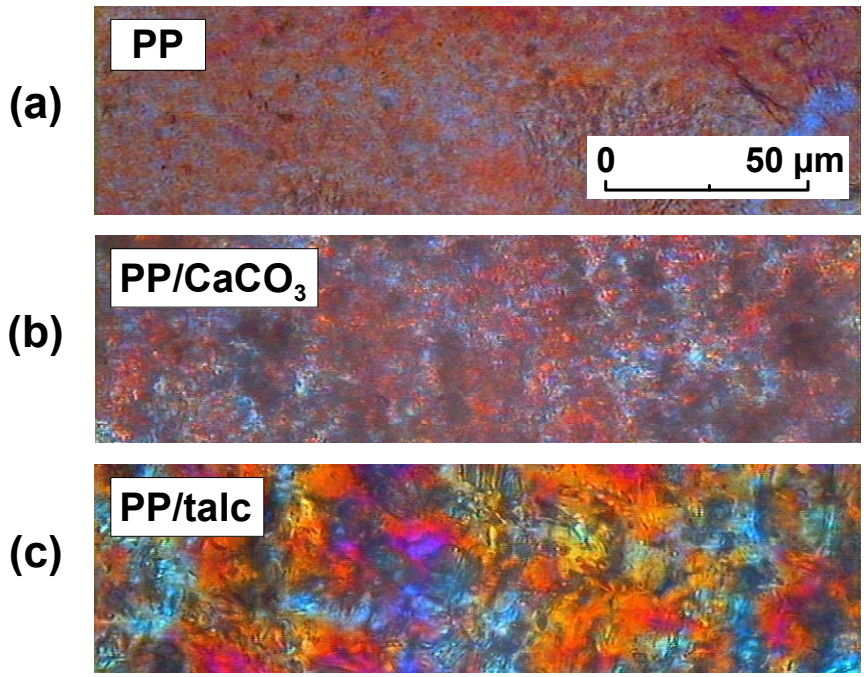

Figure 6.13: Optical micrographs of the a) PP, b) PP $CaCO_3$ and c) PP talc samples (filler content 7.7 vol %).

6.2.2 Effect of fillers on fibre orientation and length in LGF-PP composites

6.2.2.1 Fibre orientation

Fibre orientation in moulded LGF-PP components with and without $CaCO_3$ filler was analysed at the areas shown in Figure 4.1 (Geometry Type 1). The area scanned was located in the middle of the part, where three sections were investigated, all through thickness (XZ plane, see the coordinate system in Figure 4.1). Each section was 30 mm long and 15 mm apart from each others. Figure 6.14 shows a reconstruction of the scanned section (2 mm thick and 15 mm long), using LGF-PP with 12.9 vol % fibre content and a hybrid composite containing 14.6 vol % of LGF and 6.6 vol % of $CaCO_3$. In common with the majority of injection moulded plates, at the centre the fibres are aligned perpendicularly to the melt flow direction (MFD), whereas in the outer shell regions the fibres are more preferentially aligned along the MFD.

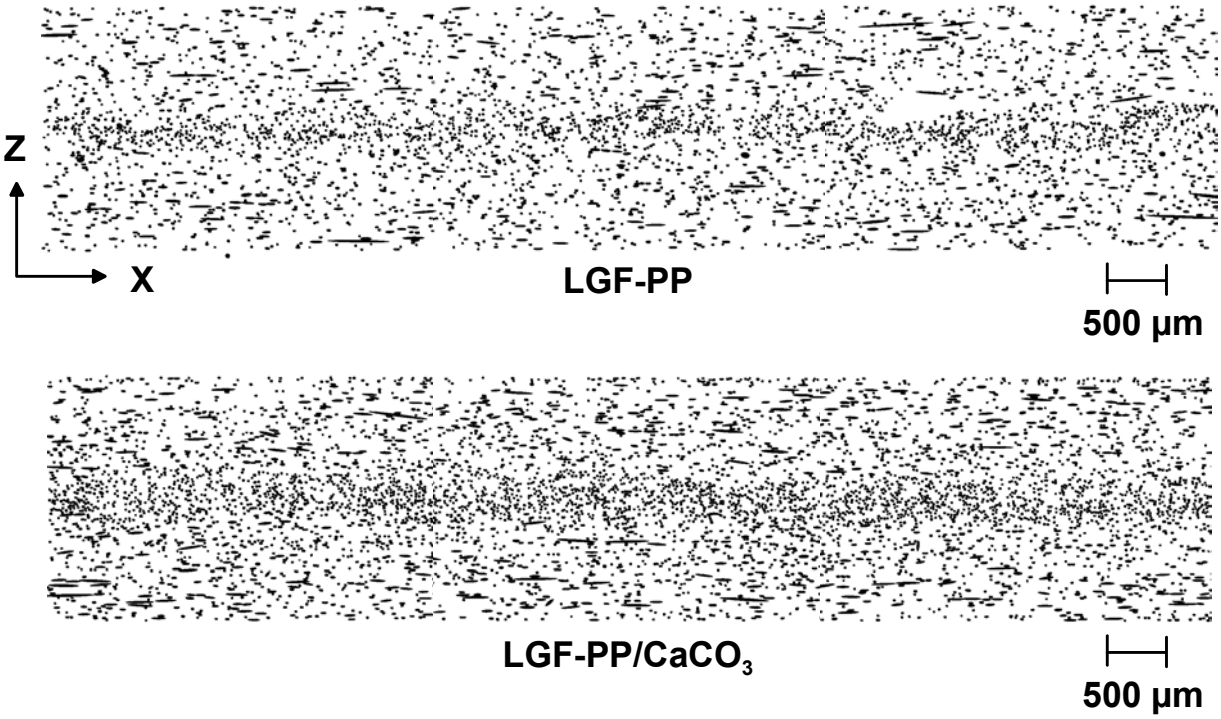

Figure 6.14: Reconstructed image scans showing the fibre orientation in LGF-PP (12.9 vol % fibre content) and LGF-PP/$CaCO_3$ (14.6 vol % fibre content, 6.6 vol % filler content) hybrid composite specimens. Both specimens were of the Geometry Type 1.

In the case of LGF-PP with 12.9 vol % of fibres (formulation D, see Table 4.1) an analysis of the three sections showed very little difference, suggesting that the fibre orientation was homogeneous over a 30 mm square region at the central section. A similar analysis of the corresponding sample containing $CaCO_3$ (formulation F) showed the same result. Figure 6.15 shows a comparison of the fibre orientation at the central section for these two samples. The data is presented as a histogram of the angle θ (that is, the frequency of the each θ throughout the scanned section). The angle θ was determined by using the elliptical fibre footprints and the equation shown in Figure 5.1. As can be seen, the fibre orientation in the two sample formulations is not identical but very similar. Therefore, it can be concluded that the addition of calcium carbonate in LGF reinforced PP has only a slight influence on the orientation behaviour of the fibres during injection moulding.

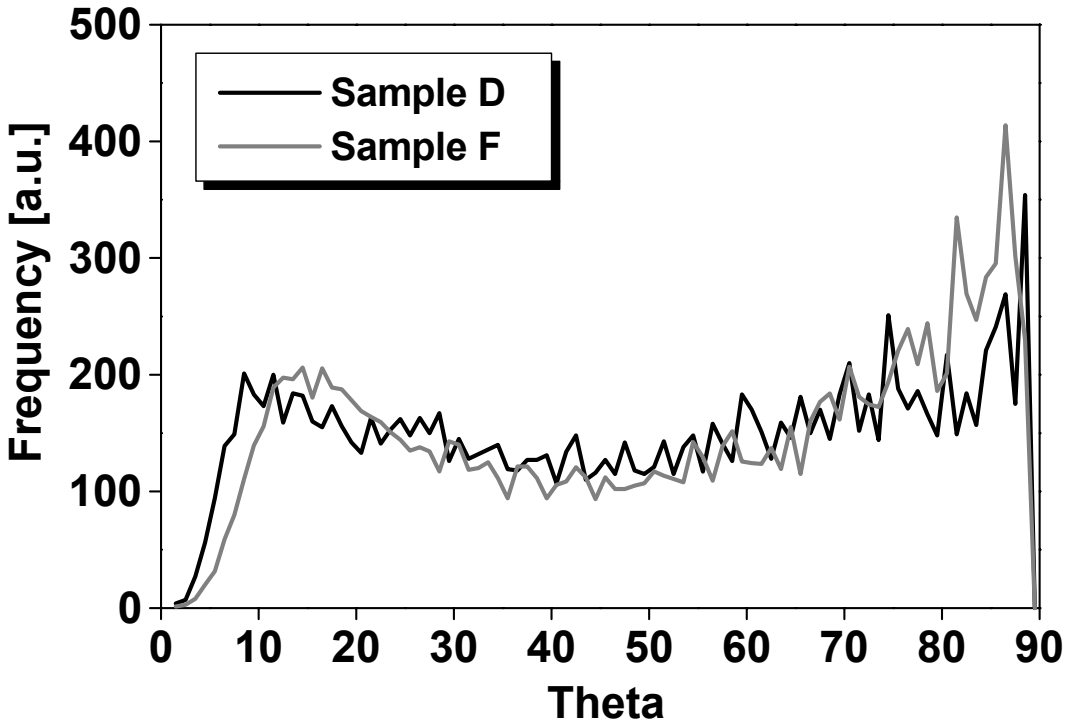

Figure 6.15: A comparison of the histogram of θ for samples D (LGF/$CaCO_3$ = 12.9/0 vol %) and F (LGF/$CaCO_3$ = 14.6/6.6 vol %).

6.2.2.2 Fibre length distribution

Normalised fibre length distribution in LGF-PP composites (Geometry Type 1) with and without a $CaCO_3$ filler are shown in Figures 6.16 and 6.17. In previous studies it has been observed that filler addition to the glass fibre reinforced thermoplastics may lead to process induced fibre length degradation [75]. A similar trend was observed in the present study, comparing the number average fibre lengths (l_{avg}) in unfilled (887 µm) and filled (648 µm) LGF-PP samples. As can be seen, in this material system there was a 25 % decrease in average fibre length, which may lead to decreased mechanical response. In general, the obtained average fibre lengths are shorter than expected, since the initial length of the glass fibre in the starting material was 11 mm. The unexpectedly high amount of fibre length degradation during injection moulding can be explained.

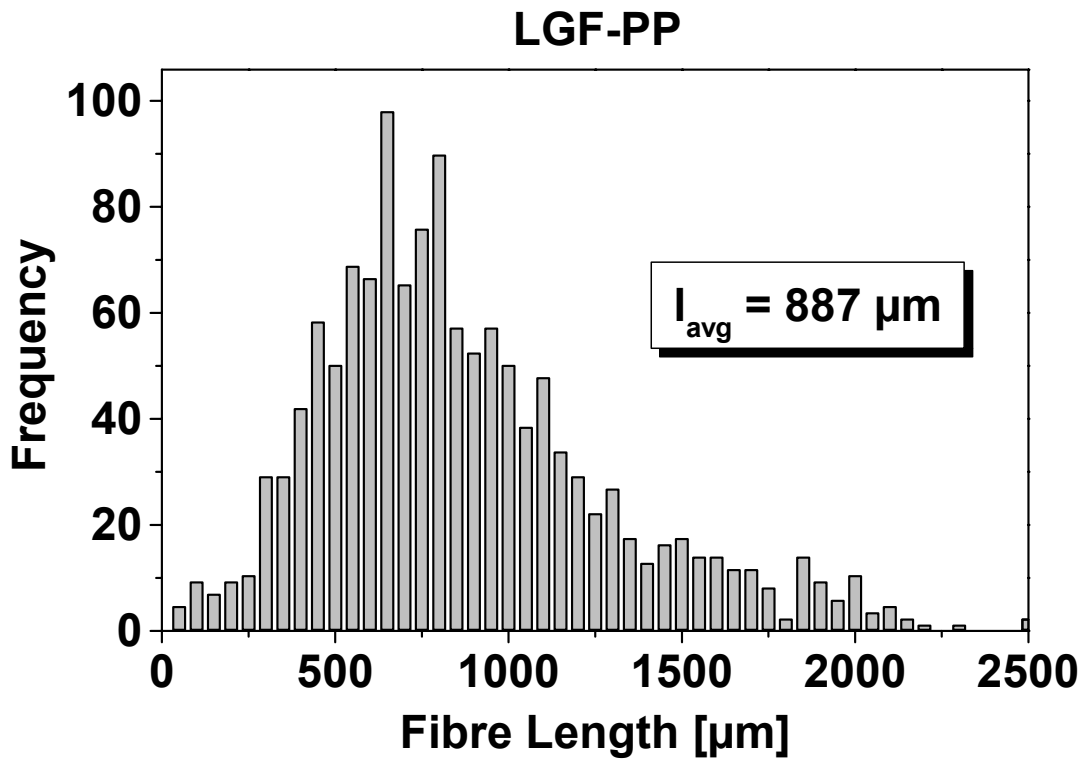

Figure 6.16: Fibre length distribution of PP reinforced with 12.9 vol % of LGF.

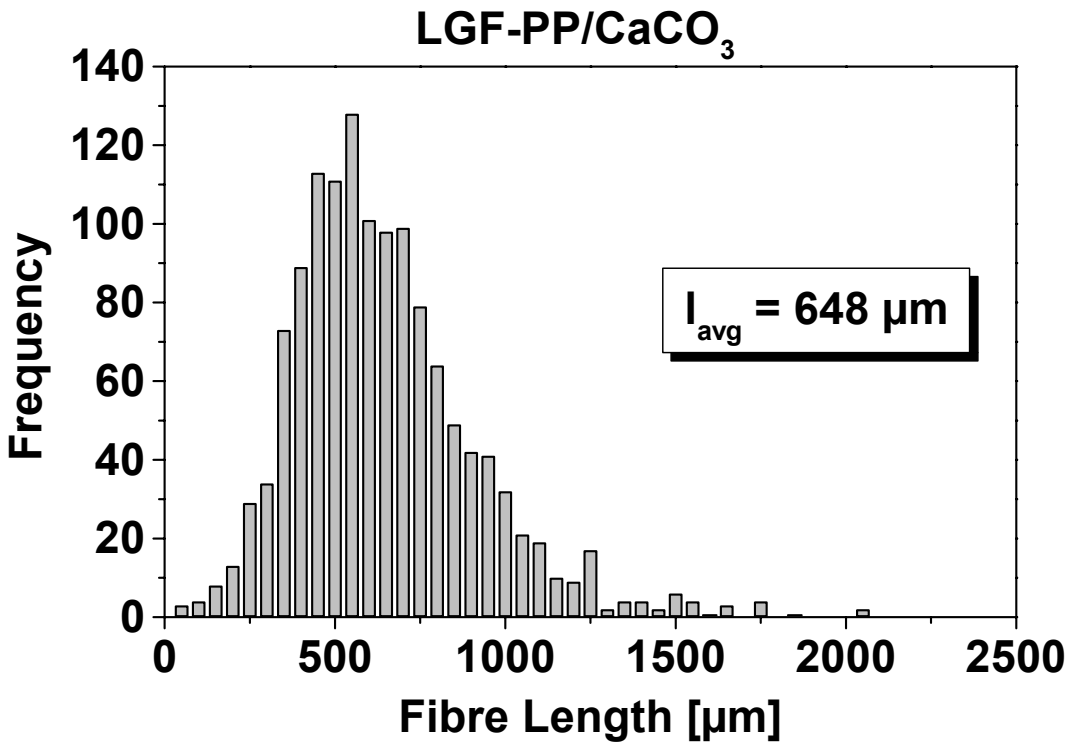

Figure 6.17: Fibre length distribution of a LGF-PP/$CaCO_3$ hybrid composite containing 14.6 vol % of LGF and 6.6 vol % of $CaCO_3$.

It should be noted that the fibre volume fraction differs in the samples shown in Figures 6.16 and 6.17. In the case of the hybrid sample containing a filler it is 14.6 vol %, whereas in the case of unfilled LGF-PP it is 12.9 vol %. The effect of the higher fibre volume fraction on the fibre length degradation was not studied in this work. Therefore, it cannot be said that the decreased average fibre length was wholly a result of filler addition, and/or the higher fibre volume fraction. In any case, it can be expected that fillers lead to some decrease in the average fibre length, as observed also in earlier studies on this subject [75].

6.2.3 Tensile properties of LGF-PP/filler hybrid composites

Tensile stress-strain values of LGF-PP/$CaCO_3$ and LGF-PP/talc composites at different levels of fibre and filler contents are shown in Table 6.2. It can be seen that both the strength and modulus distinctly increase as the LGF content increases. On the other hand, the modulus values show that by using filler addition the stiffness of the LGF composite may be further enhanced. In the case of calcium carbonate filled PP the modulus increases by about 5 %, which agrees with values reported elsewhere [68, 132]. On the other hand, when filler is added to LGF reinforced composites, the modulus increase is more distinct, *i.e.* of the order of 15-25 % in the case of $CaCO_3$ and 30-40 % in the case of talc. Thus, it seems that by incorporating particulate filler into the matrix, there is a synergy effect leading to a higher stiffness than would normally be expected. Furthermore, tensile strength decreases as $CaCO_3$ is added to the LGF composites, but in the case of talc the strength remains unaffected.

Table 6.2: Tensile properties of LGF-PP/filler hybrid composites.

Formulation	*Filler*	*Fibre loading [vol %]*	*Filler loading [vol %]*	*Tensile strength [MPa]*	*Tensile modulus [GPa]*
A	-	0	0	38 *	1.68
B	$CaCO_3$	0	7.7	27 *	1.76
C	-	3.7	0	60	3.26
D	-	12.9	0	90	6.25
E	$CaCO_3$	4.2	7.4	44	3.83
F	$CaCO_3$	14.6	6.6	63	7.75
G	Talc	4.2	7.4	59	4.63
H	Talc	14.6	6.6	88	8.14

* yield stress

The strength and modulus of particle filled PP is known to depend strongly on the physical properties, such as the modulus of the filler itself, particle or fibre orientation, and on the effect of the filler on crystallinity [68, 74]. The fibre orientation analysis carried out in the present work showed that the addition of a filler into the matrix of the LGF-PP composite does not essentially affect the orientation of the fibres during processing. On the other hand, DSC and optical microscopy studies suggested that the effect of talc on the crystallinity of PP is more pronounced than the effect of $CaCO_3$ (Figures 6.12 and 6.13). Furthermore, an SEM analysis of fracture surfaces was carried out to detect a possible orientation of talc particles (Figure 6.18). It was observed, firstly, that talc particles orient during injection moulding and, secondly, that the main direction of the orientation is parallel to the melt flow direction. It must be noted, however, that quantitative determination of particle orientation is difficult when using SEM. More sensitive methods like electron spin resonance (ESR) spectroscopy would give more accurate results [66, 68, 133]. Nevertheless, although ESR spectroscopy was not used in the present study, it is suggested that higher strength and modulus values in the case of LGF-PP/talc hybrid composites is a consequence of the higher L/D ratio of talc (compared to $CaCO_3$), resulting in particle orientation, and that this filler has a higher tendency to work as a nucleating agent in PP.

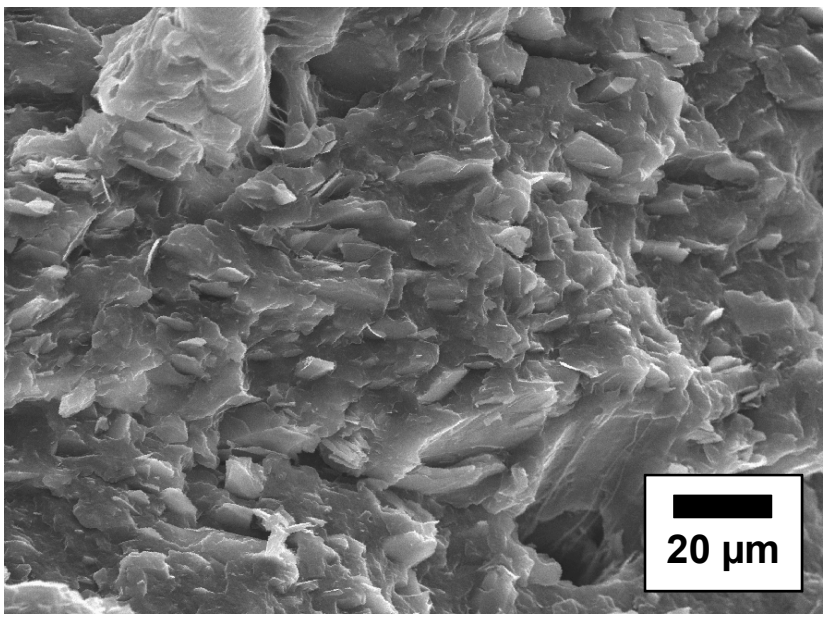

Figure 6.18: SEM micrograph of an impact fracture surface of PP reinforced with 4.2 vol % of LGF and filled with 7.4 vol % of talc (formulation G), showing the flow induced orientation of talc particles.

6.2.4 Impact energy of LGF-PP/filler hybrid composites

Figure 6.19 presents the results of the unnotched Charpy impact test for hybrid composites. It can be observed that unnotched impact energy increases considerably as the fibre content increases. On the other hand, the impact energy decreases with the addition of $CaCO_3$ to the LGF reinforced PP. The impact energy decreases also when talc is added (samples G and H), but the relative change is minor compared to the calcium carbonate.

It is widely accepted that fibre related phenomena, rather than matrix deformation, form a main contributor in energy absorption during the impact loading of fibre reinforced thermoplastics [30, 72, 134]. In the case of LGF reinforced thermoplastics, fibre related failure mechanisms include fibre debonding, pull-out, fracture, multiple fibre debonding or fracture and even slippage of the fibres within a bundle [58]. On the other hand, in particulate filler filled semi-crystalline thermoplastics matrix deformation also plays an important role in determining impact energy. On the basis of the Charpy impact tests carried out in this work it can be noticed that whereas talc has little influence on impact energy of hybrid composites, $CaCO_3$ causes a notable decrease. As evidenced by the optical microscopy and DSC studies, talc had a more pronounced effect on the crystalline morphology of PP compared to calcium carbonate; higher level of the total crystallinity and the smaller spherulite size were reached in the talc filled samples. On the other hand, it is known that the finer spherulitic structure (smaller spherulite size) leads to the higher impact energy of PP, *e.g.* [58, 135]. Though the optical microscopy did not enable explicit conclusions to be made about the changes in spherulite size, it can be assumed that the crystalline morphology contributes to the better impact energy of the talc filled samples compared to the samples with calcium carbonate.

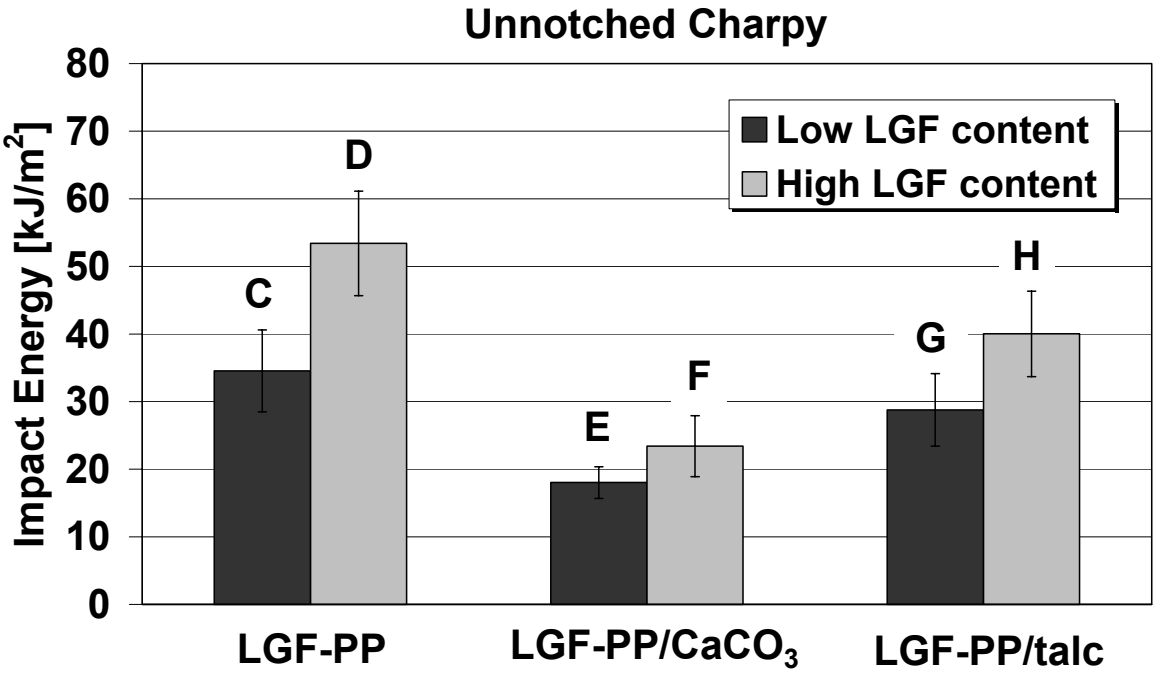

Figure 6.19: Unnotched Charpy fracture energies of LGF-PP hybrid samples. The exact formulations are given in Table 4.1.

All the aspects mentioned in the above discussion refer to a viewpoint of fracture-property relationships, but in reality the conditions during the testing of toughness are equally important. One of the principal parameters is whether the samples are notched or not. Notched impact tests depend mainly on the energy needed for a crack to propagate until final failure occurs. Unnotched impact tests, however, reflect the total energy including both crack initiation and propagation energies [26]. The notched Charpy impact energies for LGF-PP/filler hybrid composites are shown in Figure 6.20. As can be noticed, the addition of fillers only slightly affects the energy values, when notched specimens are considered. Therefore it can be concluded that the fillers used in the present study do not greatly influence the propagation of the existing notch. At the same time, the overall impact energy (unnotched samples) either remains unchanged (talc) or decreases ($CaCO_3$), due to the decreased energy required for crack initiation.

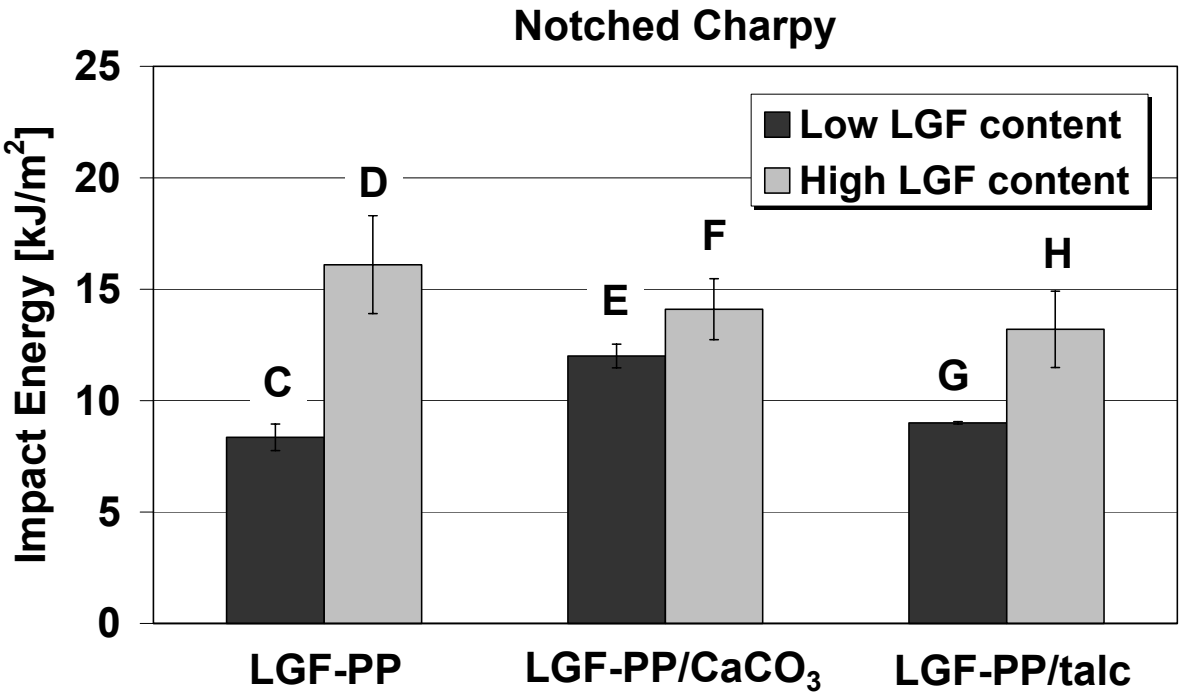

Figure 6.20: Notched Charpy impact energies of LGF-PP hybrid samples. The exact formulations are given in Table 4.1.

6.2.5 Fracture toughness of PP-LGF/filler hybrid composites

Linear elastic fracture mechanics offers a useful way of getting information about different fracture mechanisms which take place during the loading of composite specimens, especially if the mechanical testing is accompanied by other methods like acoustic emission or optical microscopy [18, 118, 136, 137]. One of the advantages of LEFM methods is the low testing speed, which allows different stages of fracture to be identified on the basis of load-elongation curves. Thus, a considerable amount of data about fracture modes can be collected, providing a good overall view of the fracture mechanical behaviour of the materials [138]. In the present work we used an LEFM approach to compare fracture behaviour of the LGF reinforced PP composites to that of the $CaCO_3$ filled PP and LGF-PP/$CaCO_3$ hybrid composites. The obtained fracture toughness values are shown in Table 6.3. Additionally, the literature values for the injection moulded SGF and LGF reinforced PP composites are shown [32]. It can be observed that the critical stress intensity factor K_c increases considerably when the materials are reinforced with LGF. As calcium carbonate is added to the

matrix, K_c remains almost unchanged in the case of unreinforced PP, but decreases slightly in the case of hybrid composites. Furthermore, the obtained values agree well with the literature data. It should be also noted that the LGF-PP composites reach much higher level of fracture toughness than the SGF-PP material [32].

Table 6.3: Fracture toughness of LGF-PP/$CaCO_3$ hybrid composites.

Formulation	*Reinforcement and filler type*	*Fibre loading [vol %]*	*Filler loading [vol %]*	K_c *[MPa√m]*
A	-	0	0	1.62
B	$CaCO_3$	0	7.7	1.52
C	LGF	3.7	0	2.95
D	LGF	12.9	0	4.49
E	LGF/$CaCO_3$	4.2	7.4	2.54
F	LGF/$CaCO_3$	14.6	6.6	3.96
Ref. [32]	LGF	13.4	0	4.4
Ref. [32]	SGF	13.4	0	2.7

It is widely accepted that the fracture toughness of PP can be increased by reinforcing with long glass fibres [58]. On the other hand, it has also been reported that filler inclusions may lead to a decreased fracture toughness when added to thermoplastics like polypropylene. For example, it has been observed that the fracture toughness of polypropylene decreases sharply above a 5 vol % addition of calcium carbonate, decreasing to half of the original value at 30 vol % filler content [139]. In this study, the amount of calcium carbonate was only 7.7 vol % of the matrix, and detrimental particle agglomeration was minimised by surface treatment of the filler used and by heavy mixing conditions during the compounding step. Consequently, the fracture toughness of neat PP was almost unaffected by the filler addition. However, in hybrid composites K_c values decreased, which suggests that there are effects that cannot be explained purely by the filler-matrix related mechanisms.

In order to get a deeper understanding of the failure mode and sequence, an *in situ* acoustic emission analysis was carried out during the fracture mechanical test. In the case of unreinforced polypropylene, the main mode of energy absorption during the fracture mechanical test is matrix deformation. However, as PP is reinforced with long glass fibres, several additional mechanisms are observed to occur in the fracture process; fibre debonding, fibre breakage, and pull-out of fibres and fibre bundles [18]. These different failure mechanisms can be distinguished by acoustic emission, because they give acoustic signals at certain characteristic amplitudes. Based on numerous AE studies performed with the same experimental set-up on discontinuous fibre-reinforced composites, the following correlation exists between the AE amplitude ranges and individual failure events: fibre/matrix debonding (< 35 dB) < fibre pull-out (35-55 dB) < fibre fracture (> 55 dB). These assumptions are based on the numerous studies where the amplitude distribution of the emitted acoustic signals was compared with the failure behaviour of various composite materials [58, 140].

The cumulative numbers of the AE events registered during loading of SEN-T specimens are summarized in Table 6.4. The loading curve was sectioned as follows: range I ends at 40 % of F_{max}, range II extends from 40 % of F_{max} to 80 % of F_{max}, range III extends from 80 % of F_{max} to F_{max}, and range IV covers the section from F_{max} downwards (Figure 6.21). A notable feature in the values of Table 6.4 is that the neat PP and its $CaCO_3$ modified version were acoustically much less active than LGF reinforced composites. Furthermore, the signals are of low amplitude, *i.e.* close to the threshold level (10 dB), which reflect the matrix related failure mechanisms [18]. The related signals may arise from matrix deformation (neat PP) and particle/matrix debonding (calcium carbonate filled PP). As the LGF content increases, so does the cumulative number of AE signals. The AE amplitude distribution remains practically the same in samples containing LGF reinforcement, in each loading section (I…IV), independent of fibre content. This means that the same failure occurs in the related loading sections.

Table 6.4: Relative distribution of amplitude during the acoustic emission analysis. Sectioning of the force-elongation curve: I = 0-0.4 F_{max}, II = 0.4-0.8 F_{max}, III = 0.8-1 F_{max}, IV = 1-0 F_{max}.

Relative distribution of amplitude [%]		*Amplitude interval [dB]*								*Number of AE signals*
		11-20	*21-30*	*31-40*	*41-50*	*51-60*	*61-70*	*71-80*	*81-90*	
Sample A: LGF/$CaCO_3$ 0/0 vol %	I									11
	II	100.0								
	III	87.5	12.5							
	IV	100.0								
Sample B: LGF/$CaCO_3$ 0/7.7 vol %	I									36
	II	100.0								
	III	100.0								
	IV	69.7	21.2	9.1						
Sample C: LGF/$CaCO_3$ 3.7/0 vol %	I	72.0	12.0	16.0						1097
	II	31.9	15.9	11.6	15.9	22.0	2.7			
	III	24.2	10.0	11.1	30.8	22.5	1.4			
	IV	62.1	16.7	1.5	1.5	10.6	7.6			
Sample E: LGF/$CaCO_3$ 4.2/7.4 vol %	I	70.9	21.8	7.3						833
	II	73.8	17.3	3.1	2.7	2.5	0.6			
	III	7.4	6.2	19.3	56.0	11.1				
	IV	16.5	6.4	13.8	52.1	11.2				
Sample D: LGF/$CaCO_3$ 12.9/0 vol %	I	82.8	14.8	2.4						2592
	II	73.8	17.3	3.1	2.7	2.5	0.6			
	III	51.3	12.5	6.3	12.6	14.4	2.8	0.1		
	IV	38.3	25.2	13.6	9.9	10.1	2.9			
Sample F: LGF/$CaCO_3$ 14.6/6.6 vol %	I	76.5	18.5	5.0						1717
	II	64.2	17.2	4.9	5.9	5.8	1.7	0.3		
	III	28.3	11.5	12.2	20.0	21.1	6.6	0.3		
	IV	41.3	31.9	15.9	7.2	2.2	1.5			

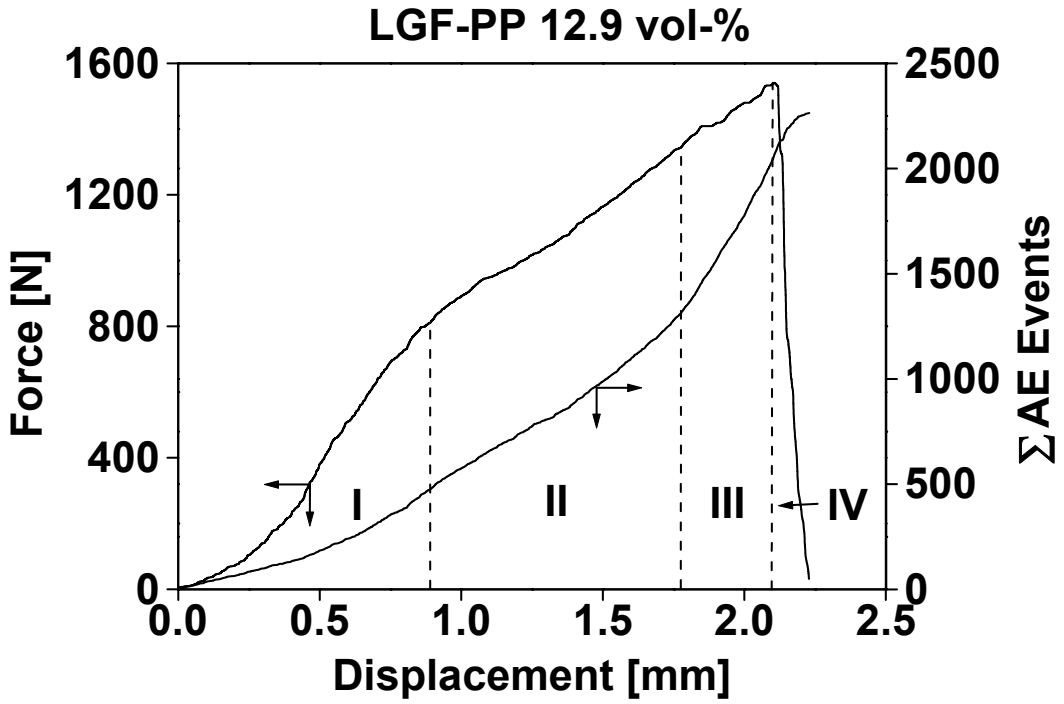

Figure 6.21: Load-displacement curve and cumulative AE signals of one SEN-T specimen (Sample D). Sectioning of the load-displacement curve is shown with Roman numbers I-IV.

In previous studies on fracture behaviour of LGF-PP composites it has been observed that crack initiation takes place before the maximum load is achieved [18]. A similar conclusion was reached using acoustic emission analysis in the present study. Figure 6.22 shows a distribution of the amplitudes at different stages of force-elongation curve of hybrid composite containing 14.6 vol % of LGF and 6.6 vol % of calcium carbonate. It can be seen that there is some AE activity already during the stage I of failure sequence. This indicates that some fibre debonding and related matrix deformation may take place at early stage of the loading. The activity increases considerably at stage II, indicating the start of the crack propagation. At stage II higher amplitude signals are emitted, which suggest that fibre pullout takes place. In stage III fibre debonding and pullouts are even more evident, and additionally fibre fractures occur suggested by signals emitted with amplitudes above 55 dB. Finally the activity decreases as the fracture terminates during the last stage IV. Thus, it can be concluded that fibre related mechanisms dominate the fracture of studied composites containing long glass fibres.

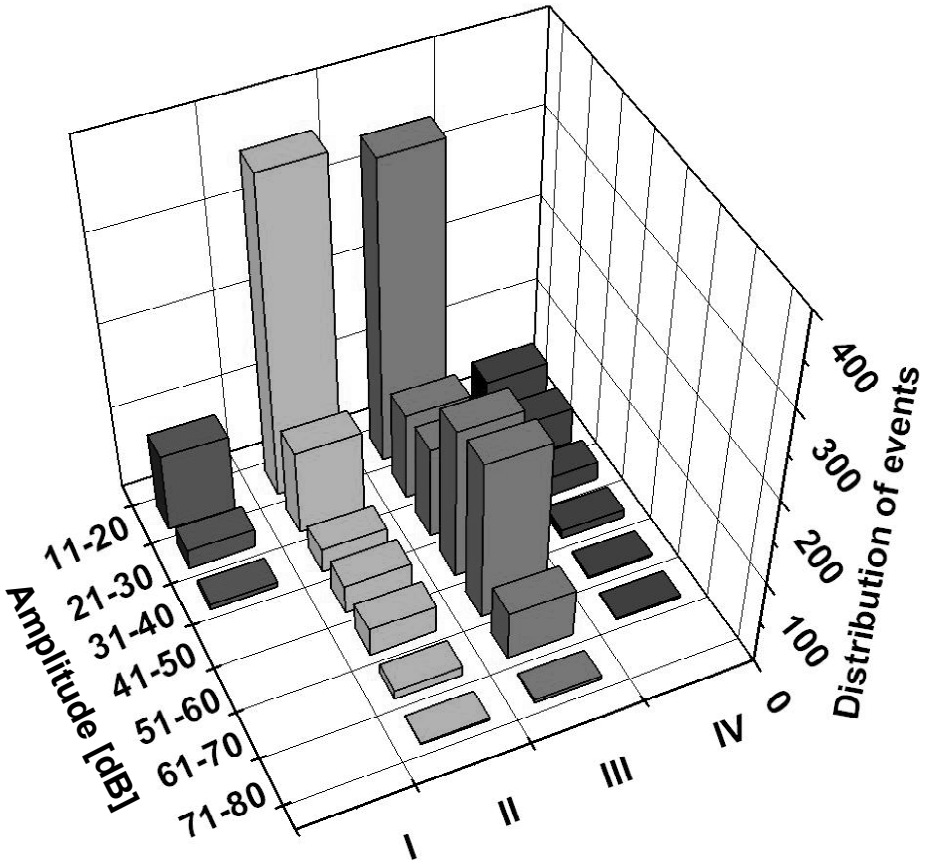

Figure 6.22: Distribution of amplitudes in acoustic emission analysis (LGF/$CaCO_3$ = 14.6/6.6 vol %).

It can be noted from the values in Table 6.3 that the addition of $CaCO_3$ to LGF reinforced composites results in a pronounced decrease of AE activity. Secondly, there are interesting changes in amplitude distribution when filler is added, especially evident at lower LGF contents. Firstly, the amplitude distribution at stages I and II indicates more frequent matrix deformation and fibre debonding related fracture incidents as filler is added to the LGF-PP composite, compared to samples without a filler. In the case of sample D (PP with 4.2 vol % of LGF and 7.4 vol % of calcium carbonate), more than 90 % of the incidents at stage II take place at amplitudes below 30 dB. However, in the case of sample C (PP with 3.7 vol % of LGF) these were less than 50 %. This means that filler particles increase the incidents of matrix deformation and fibre debonding. Secondly, at later phases of the failure (stages III and IV), the majority of the incidents in the case of hybrid samples take place at amplitudes reflecting fibre debonding. Thus, it seems that filler particles induce fibre debonding, which may explain the decreased mechanical properties like strength and

fracture toughness. This has already been suggested in other studies of SGF-ABS/$CaCO_3$ [75] and glass mat reinforced PP/mica [77] hybrid composites. These studies conclude that fillers may indeed cause premature fibre debonding due to void formation around particles during loading, or due to direct contact between particles and fibres. It should be noted that the increase of low amplitude signals at stages I and II in hybrid samples cannot be explained only by filler related events, since the number of acoustic emission arising from matrix deformation was only slightly increased as calcium carbonate was added to neat PP. Thus, it can be concluded that LGF-related failure incidents dominate also in hybrid systems, but the volume of the acoustic signals is less than in LGF composites without a filler. This can be explained by the fact that pullouts occur more easily due to reduced fibre-matrix adhesion (originating from the strong debonding at the early stage of failure sequence).

Finally, the fracture surfaces after fracture mechanical testing were analysed by a scanning electron microscope. In the case of LGF-PP composite with 12.9 vol % of fibres (Figure 6.23a) there is clear evidence of ductile matrix deformation, which is a result of the fibre debonding and pullout processes. On the other hand, a more irregular fracture surface is observed in the case of corresponding hybrid sample containing $CaCO_3$ (Figure 6.23b). In addition, there are more marks of pullout events as indicated by higher amount of voids (originating from fibres disconnected from the matrix) and also by higher pullout lengths. Figure 6.24 shows SEM micrographs at higher magnification, showing the clear difference in matrix deformation of LGF reinforced composites and hybrid materials. As calcium carbonate is added to the matrix, void formation around the filler particles take place during the loading. In Figure 6.24b it can be seen that the voids may come into contact with fibres and thus, induce early stage fibre debonding. Furthermore, it can be noted from both figures (6.23 and 6.24) that large scale ductility is reduced in filler filled samples. It can be concluded that this ductility reduction also contributes to the decrease of fracture toughness when calcium carbonate is added to LGF-PP.

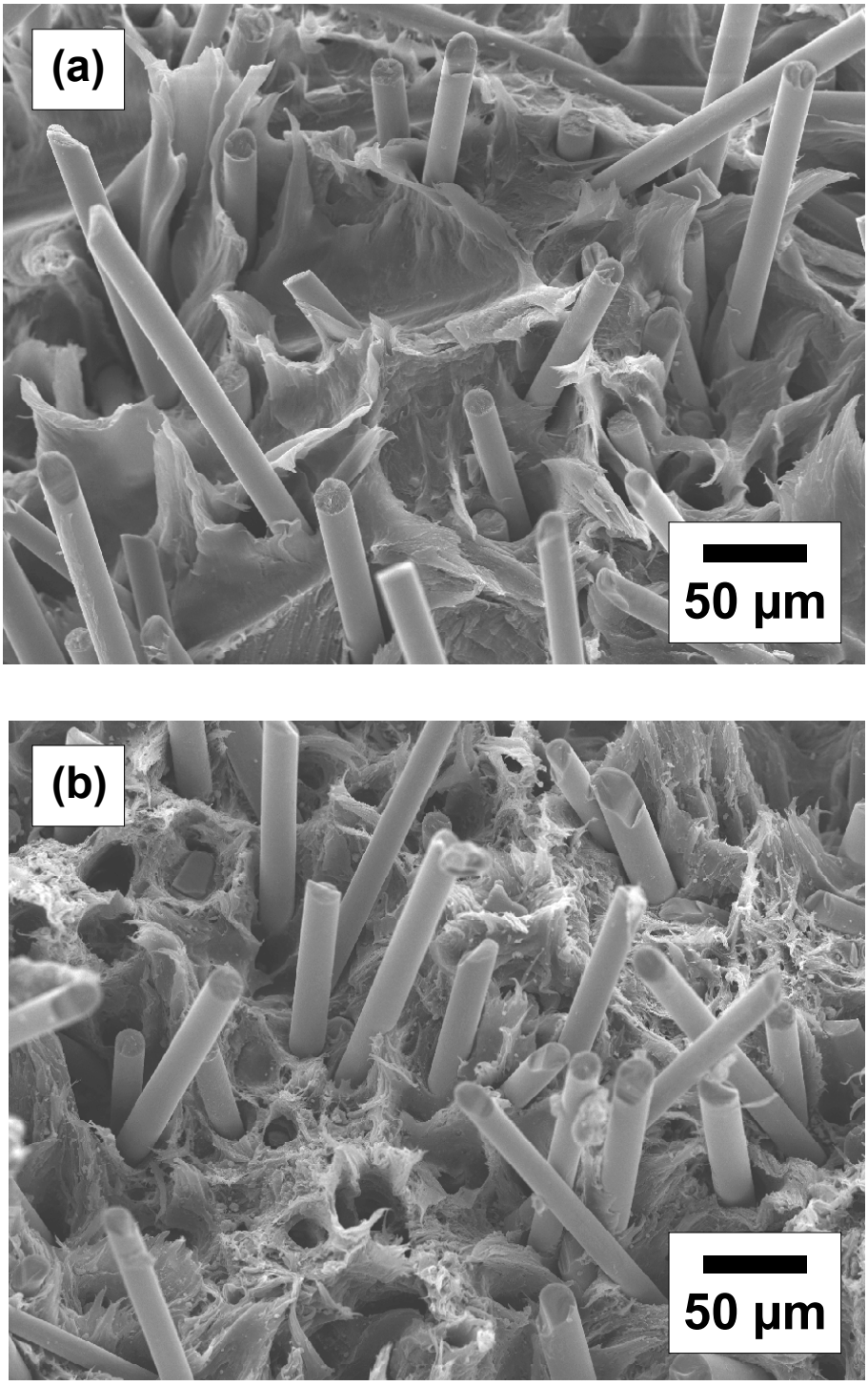

Figure 6.23: SEM micrographs of fracture surfaces after fracture mechanical test for PP hybrid composites at 350 times magnification:
a) LGF/$CaCO_3$ = 12.9/0 vol % and
b) LGF/$CaCO_3$ = 14.6/6.6 vol %.
Crack growth direction is from left to right in both cases.

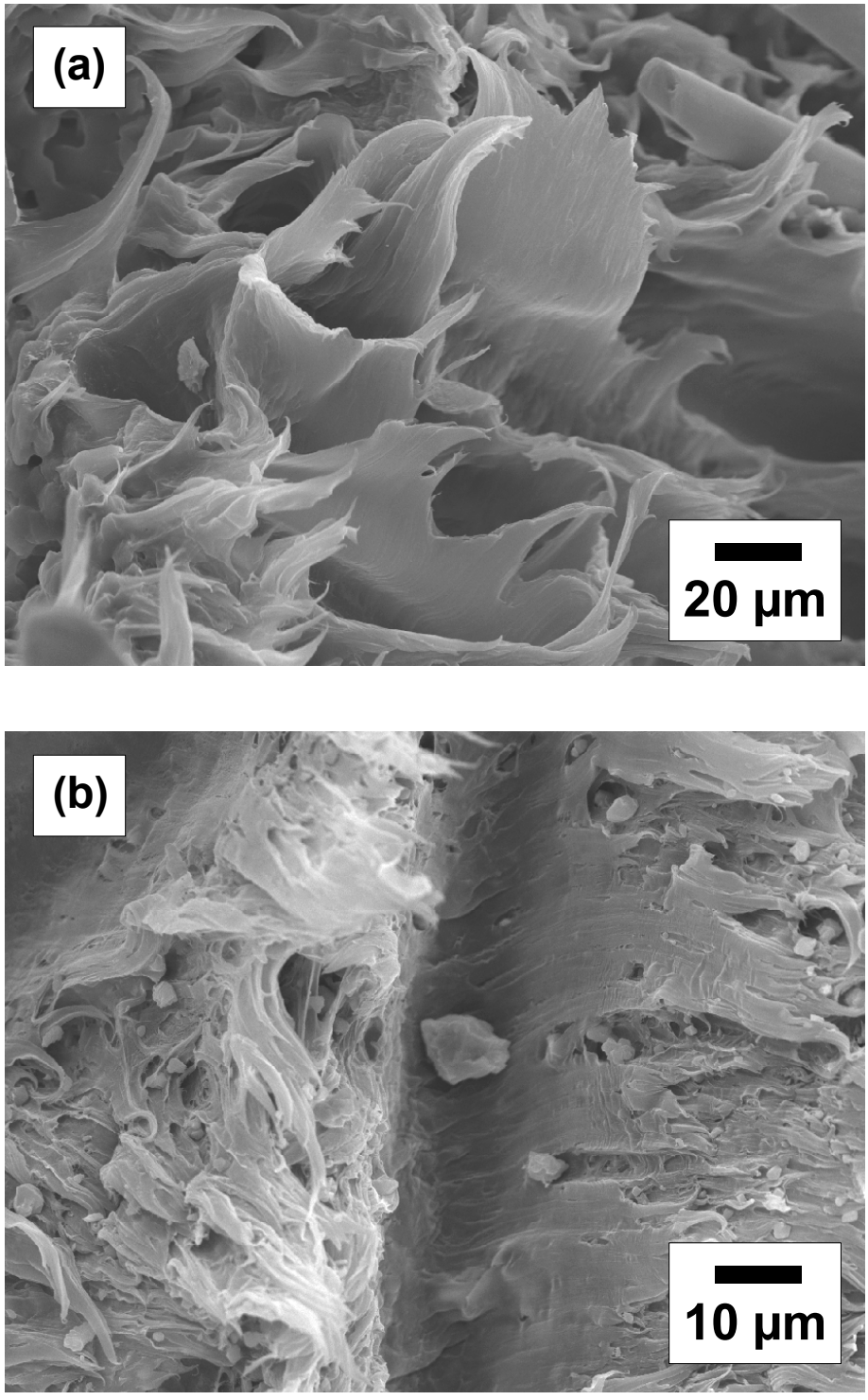

Figure 6.24: SEM micrographs of fracture surfaces after fracture mechanical test for PP hybrid composites:
a) LGF/$CaCO_3$ = 12.9/0 vol %, 750 x magnification and
b) LGF/$CaCO_3$ = 14.6/6.6 vol %, 1500 x magnification.
Crack growth direction is from left to right.

6.2.6 Conclusions

A useful way of modifying the mechanical properties of LGF reinforced polypropylene composites was found by adding a small amount of mineral fillers into the matrix. The modulus of the filler filled LGF composites was 40 % higher than in the unfilled LGF materials. Secondly, it was noted that the strength and fracture toughness values decreased when filler was added. However, it was found that calcium carbonate and talc filled materials caused different mechanical response; the modulus increase was larger and the strength and toughness values decreased less in the case of talc filled LGF-PP compared to $CaCO_3$.

Various analytical methods were used to investigate the mechanisms behind the property changes when filler is added to LGF-PP. Optical image analysis showed that the fillers do not considerably affect the orientation of fibres during injection moulding. However, the average length of the fibres was 25 % lower in the case of filler filled composites compared to unfilled LGF-PP. It must be noted that the average length of fibres in the injection moulded ISO specimens is typically 7 to 9 mm. This is above the 'critical' fibre length required to reach 90 % of the maximum, achievable composite strength. In the recent comprehensive study on this subject it was shown that this critical fibre length is different in the case of different properties [26]. For example, in the case of glass fibre reinforced PP with optimised interfacial properties it was possible to reach 90 % of the maximum composite stiffness at the fibre length of 1 mm [28]. On the other hand, to reach 90 % level of the maximum composite strength, the fibre length of 7 mm or longer was required [29]. In this work, the decrease of average fibre length when filler is added cannot be used as a primary explanation for the changes in mechanical properties. On the other hand, DSC and polarisation microscopy analyses showed that the effect of talc on the crystallinity of PP is stronger than the effect of calcium carbonate. Furthermore, SEM micrographs of the fracture surfaces indicated that talc particles became oriented during injection moulding. These findings explain the better mechanical properties of talc filled hybrid composites compared to $CaCO_3$ filled materials.

The fracture mode of the hybrid composites was studied using a linear elastic fracture mechanical test together with an *in-situ* acoustic emission analysis. It was shown that that the fracture toughness of unreinforced polypropylene remained unaffected as calcium carbonate was added. However, the fracture toughness of LGF reinforced PP decreased upon filler addition. The acoustic emission of the samples showed that the acoustic activity of LGF-PP/$CaCO_3$ hybrid samples was higher compared to LGF-PP without a filler. Secondly, the distribution of the amplitudes suggested that filler addition caused debonding of the fibres at early stage of loading. This results in fibre pull-out mechanism at an earlier phase of fracture sequence than when compared to unfilled samples. A second important observation was that the fracture surfaces showed decreased matrix ductility in the case of filler filled hybrid materials: the filled samples did not show the large plastic deformation patterns which were observed in unfilled samples. This may be one cause of a decrease in fracture toughness values when $CaCO_3$ is added.

In conclusion, the addition of fillers in LGF-PP composites offers a tool to modify the mechanical properties according to the requirements of applications. This is particularly relevant in the automobile interior parts where high stiffness, strength, toughness and good form stability are required. An example of such an application is given in Figure 7.1. However, the application is obviously not limited to automotive parts.

6.3 System C: Improved water resistance of LGF reinforced polyamide composites

6.3.1 Chemical structure and morphology of polyamide-phenolic resin blends

6.3.1.1 Calculations

Analysis of the fine chemical structure of polymeric systems is a relatively complex matter, especially if quantum mechanical calculations are considered. By using oligomeric model compounds including similar functionalities as in corresponding macromolecular system, it is possible to mimic changes taking place when two dissimilar polymers are blended. For instance, it was recently demonstrated in context of a conducting polymer, *i.e.* polyaniline complexed with dodecylbenzenesulfonic acid (DBSA) and Zinc$(DBSA)_2$ salt, that by using a model compound approach it is possible to avoid dealing with complexity of the corresponding macromolecular system. This provides detailed information about crystalline structures [141]. Similarly, quantum mechanical calculations for pyridine complexed with methane sulfonic acid gave a new insight to the protonation of conjugated polymers with sulfonic acids [142]. Also an interassociation equilibrium constant in PA6-phenolic resin blend has been recently determined by using *N*-propylacetamide complexed with 2,4-xylenol [105]. These examples show that modelling with low molecular weight analogues offers a useful method of providing a detailed structural analysis.

In the present work, *N*-methylacetamide was used as a model for polyamide, and phenol as a model for phenol formaldehyde resin. NMA and phenol were chosen due to their simple structures, which allowes high-quality calculations and interpretation of the FTIR spectra. Optimised geometries and hydrogen bonding energies in phenol dimer, NMA dimer and NMA-phenol complex were calculated by a Gaussian 03 software (by a group of Prof. O. Ikkala of Helsinki University of Technology, Finland). Additionally, because water molecules have a strong effect on the mechanical properties of various polar thermoplastics, as well as on polymer chain degradation *via* hydrolysis reaction, hydrogen bonding in water-NMA and water-phenol

complexes was investigated. In the case of NMA, hydrogen bonding with water molecules takes place essentially through CO (acceptor) or through NH (donor) functionalities of NMA. Similarly, in the case of phenol, water can be hydrogen bonded either directly to hydroxyl oxygen (acceptor) or hydroxyl proton (donor). These possibilities were analysed by calculating the interaction energies. The labelling of the atoms and chemical structures of the model compounds are given in Figure 6.25.

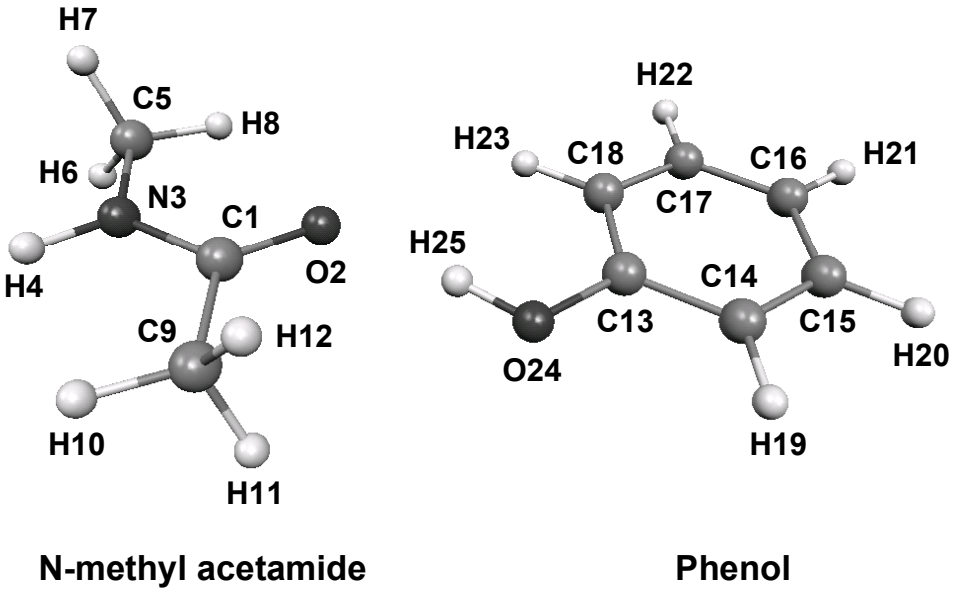

Figure 6.25: Chemical structure and labelling of atoms in *N*-methylacetamide-phenol complex.

Calculated minimum energy structures of NMA dimer, phenol dimer and NMA-phenol complex are shown in Figure 6.26, and the complexation energies using the MP2/6-31+G(d,p) and B3LYP/6-31+G(d,p) methods are given in Table 6.5. It can be seen that in the minimum energy structure of NMA-phenol complex (Figure 6.26c), hydrogen bonding occurs between carbonyl oxygen of NMA and hydroxyl proton of phenol. Both methods predicted that hydrogen bond strength is highest in NMA-phenol complex and weakest in phenol dimer. However, in NMA dimer the strength is somewhere in between, shown by the differences in counterpoise corrected complexation energies: -26 to -31 kJ/mol for NMA dimer, -19 to -24 kJ/mol for phenol dimer but -38 to -39 kJ/mol for NMA-phenol complex. These calculations indicate that NMA and phenol form a stable complex with a dissociation energy exceeding that of their dimers.

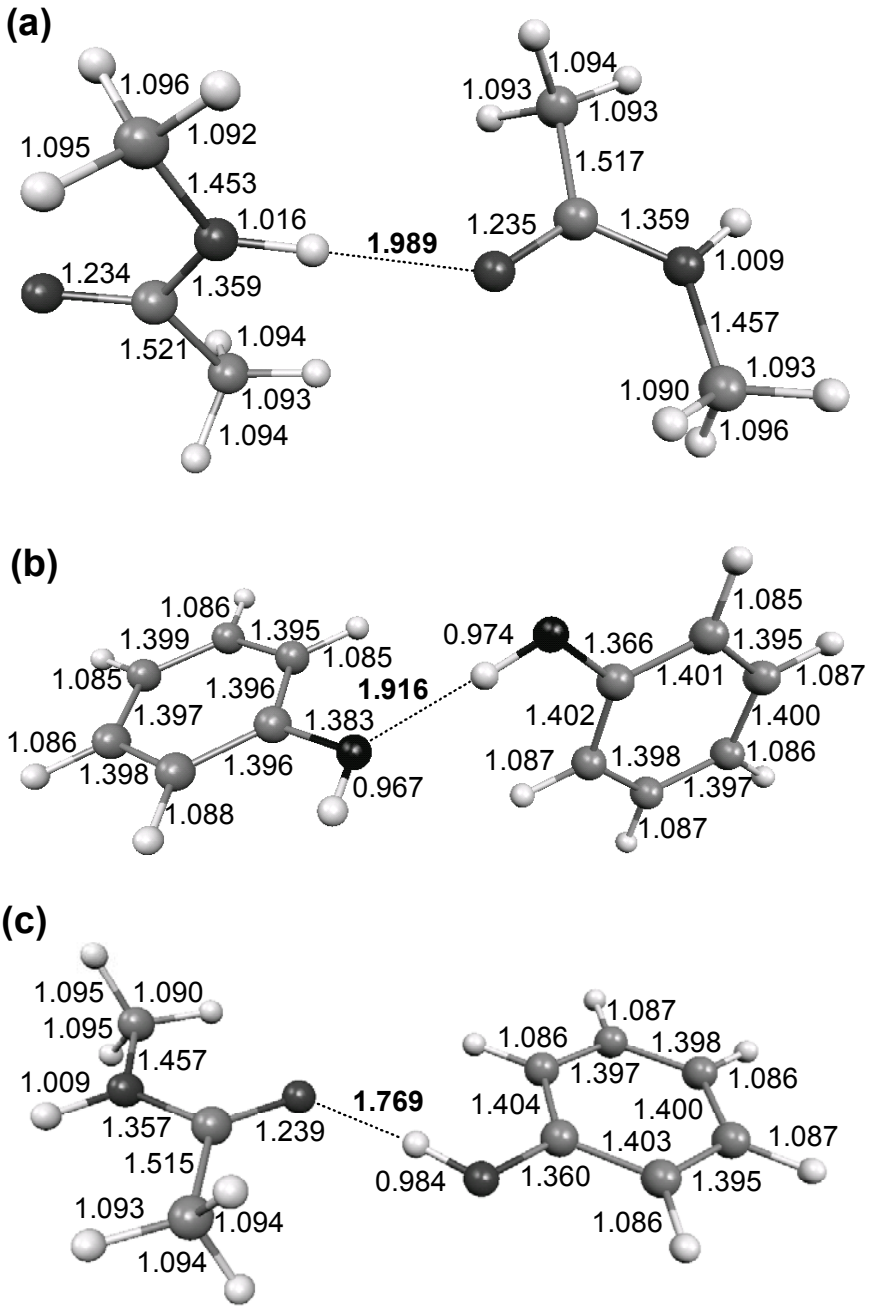

Figure 6.26: Optimised structure and calculated bond lengths (Å) in:
a) *N*-methylacetamide dimer
b) phenol dimer and
c) *N*-methylacetamide-phenol complex.

Table 6.5: Complexation energies, estimated basis set superposition errors (BSSE) and calculated counterpoise corrected complexation energies (unit kJ/mol) in *N*-methylacetamide dimer, phenol dimer and *N*-methylacetamide-phenol complex using the MP2/6-31+G(d,p) and B3LYP/6-31+G(d,p) methods.

			Method 1: B3LYP/6-31+G(d,p)		
Molecules	*Donor*	*Acceptor*	ΔE_1	$BSSE_1$	ΔE_1 *corr.*
NMA dimer	N H	O (NMA)	-27.3	1.4	-25.9
Ph. dimer	O H	O (phenol)	-22.6	3.4	-19.2
NMA-phenol	O H	O (NMA)	-40.0	2.3	-37.7
NMA-water	O H	O (NMA)	-32.5	2.0	-30.4
NMA-water	N H	O (water)	-21.6	3.4	-18.2
Ph.-water	O H	O (phenol)	-18.2	2.3	-15.9
Ph.-water	O H	O (water)	-30.9	4.8	-26.1
			Method 2: MP2/6-31+G(d,p)		
Molecules	*Donor*	*Acceptor*	ΔE_2	$BSSE_2$	ΔE_1 *corr.*
NMA dimer	N H	O (NMA)	-38.1	6.9	-31.2
Ph. dimer	O H	O (phenol)	-34.6	10.6	-24.0
NMA-phenol	O H	O (NMA)	-47.5	8.8	-38.8
NMA-water	O H	O (NMA)	-35.2	6.2	-29.0
NMA-water	N H	O (water)	-27.6	7.7	-19.9
Ph.-water	O H	O (phenol)	-23.4	6.2	-17.2
Ph.-water	O H	O (water)	-35.7	9.9	-25.8

It can be noticed from the values of Table 6.5 that one of the NMA-water complexes (CO…H) has a complexation energy of comparable magnitude to NMA dimer, enabling water molecules to break the intermolecular hydrogen bonds between the NMA monomers and to form a strong physical bonding with amide groups. On the other hand, in the NMA-phenol complex the hydrogen bond strength is 8 to 10 kJ/mol higher than in NMA-water complexes. Secondly, optimised geometries of the complexes (Figure 6.28) show that the hydrogen bond length is 1.989 Å in the case of NMA dimer, 1.916 Å in the case of phenol dimer, but only 1.769 Å in NMA-phenol complex. These findings suggest that there exists a strong interaction between NMA and phenol, exceeding that of the dimers, and therefore phenolic groups can protect amide moieties from water absorption.

The quantum mechanical calculations for the small molecular weight model compounds can be linked to macromolecular systems including amide functionalities. Water absorption and hydrolysis reactions in polyamides occur essentially in an amorphous region [117], though at elevated temperature erosion of the crystalline phase may take place too [115]. It is obvious that unbonded amide groups initially become connected with water molecules. However, it has been suggested that eventually the amide-amide hydrogen bonds in an amorphous region may be replaced by bonding with water, when the samples are treated in humid conditions [117]. Calculations for the model compounds carried out in the present work show that the complexation energy of the amide-amide hydrogen bond is close to the energy of the amide-water hydrogen bond, which indicates that a disruption of hydrogen bonds between polyamide chains may indeed take place. It is known that if polyamides are blended with oligomers, such as phenol formaldehyde resin, containing a high amount of hydroxyl groups that can bond with amide, water absorption decreases [106]. Although water is still able to break intermolecular hydrogen bonds between amide groups in this system, phenolic resins are able to form a network which binds different polymer chains together *via* hydrogen bonding. Due to the strong interaction between amide and hydroxyl groups, water is, to a large extent, unable to damage these hydrogen bonds. Therefore, the modelling results suggest that water uptake of polyamides should decrease when blended with PFR type oligomers or polymers.

6.3.1.2 Fourier transform infrared spectroscopy of PA66-PFR blends

In order to study if hydrogen bonding exists between a carbonyl group of NMA and a hydroxyl group of phenol (as proposed by the calculated minimum energy state), Fourier transform infrared spectroscopy was used. Figure 6.27 shows FTIR spectra of the model compounds in the 1350-1750 cm^{-1} wavenumber range. In pure NMA, a split band is observed in the amide I region, with peaks of 1662 cm^{-1} and 1634 cm^{-1}. The latter one is caused by the characteristic C=O stretching vibration (self-associated). A second characteristic mode of amides known as amide II band is observed at 1568 cm^{-1} in pure NMA.

Upon complexation with phenol, the intensity of the amide I fundamental peak increases considerably, and it shifts to 1640 cm^{-1}. An amide II band is found at 1564 cm^{-1} in a complex, and its intensity remains essentially unchanged compared to the spectrum of pure NMA. These observations in amide I and amide II regions suggest that self-association of NMA molecules is replaced by (stronger) hydrogen bonding between carbonyl and phenol groups, which supports the quantum mechanical calculations for the same molecules in a model compound.

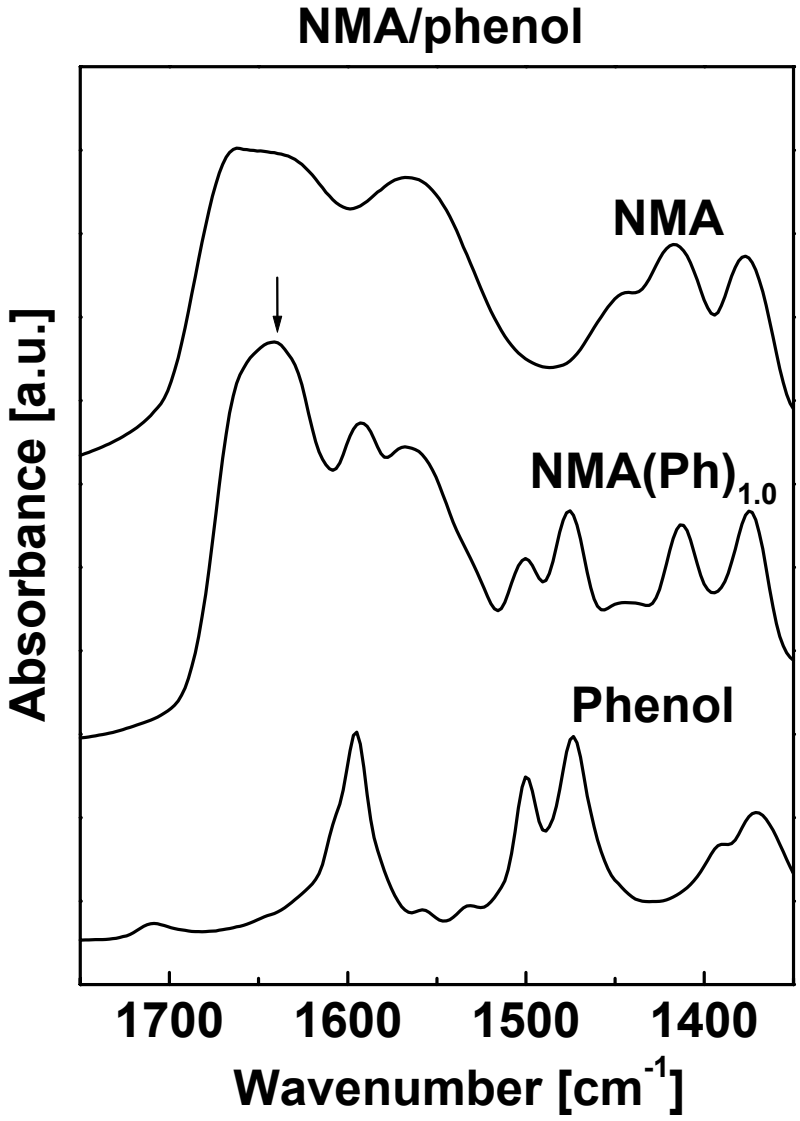

Figure 6.27: FTIR spectra of *N*-methylacetamide, phenol and *N*-methylacetamide-phenol complex at the region of 1350-1750 cm^{-1}. The amide I absorption band is marked with an arrow in the case of NMA-phenol complex (arbitrary units).

An FTIR analysis was carried out also for the polymeric blend of PA66 and phenol formaldehyde resin (without PFR crosslinking), in order to study hydrogen bonding in the macromolecular system. Figure 6.28 depicts FTIR spectra of PA66-PFR blends as well as those of neat PA66 and PFR at the 1350-1650 cm^{-1} region. Neat PA66 has an amide I band of 1640 cm^{-1} and an amide II band of 1537 cm^{-1}, caused by the C=O stretching and N-H bending vibrations, respectively. It can be noticed that the relative intensity of the amide I peak increases from 0.79 to 1.08, with a simultaneous peak broadening, when PFR is added to PA66. This indicates that hydrogen bond formation between PA66 and PFR takes place.

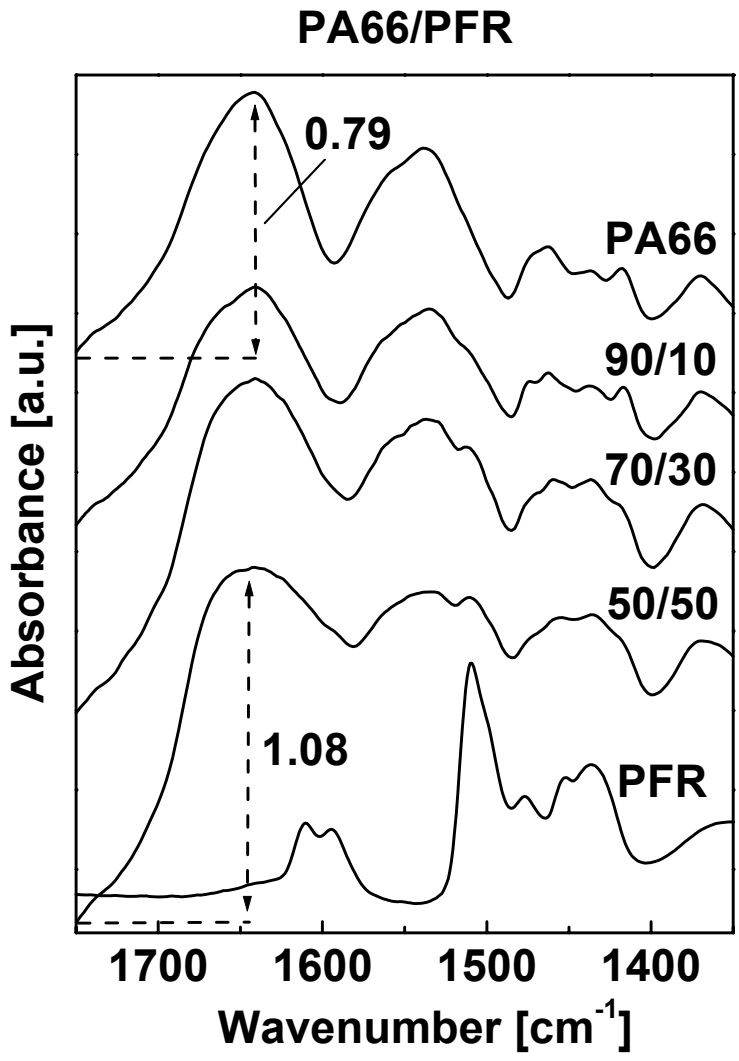

Figure 6.28: FTIR spectra of polyamide 66-phenol formaldehyde resin blends at the region of 1350-1750 cm^{-1} (arbitrary units).

Further evidence of complexation is obtained by analysing higher frequencies of the spectra of the polymer blends (Figure 6.29). Neat PA66 shows N-H stretching vibrations of 3307 cm^{-1} and 3500 cm^{-1} (amide A), caused by self-associated and free amide functionalities. Pure PFR shows a broad band with a peak of 3380 cm^{-1}, which has been assigned to the self associated hydroxyl groups. In blends of PA66 and PFR, intensities of the free and self-associated N-H stretching bands decrease and the amide A band broadens at lower frequencies. Additionally, there emerges a new peak at 3400 cm^{-1}, which is probably a result of newly hydrogen bonded O-H. These findings together with the quantum chemical calculations demonstrate a hydrogen bond formation between the carbonyl group of PA66 and the hydroxyl group of PFR.

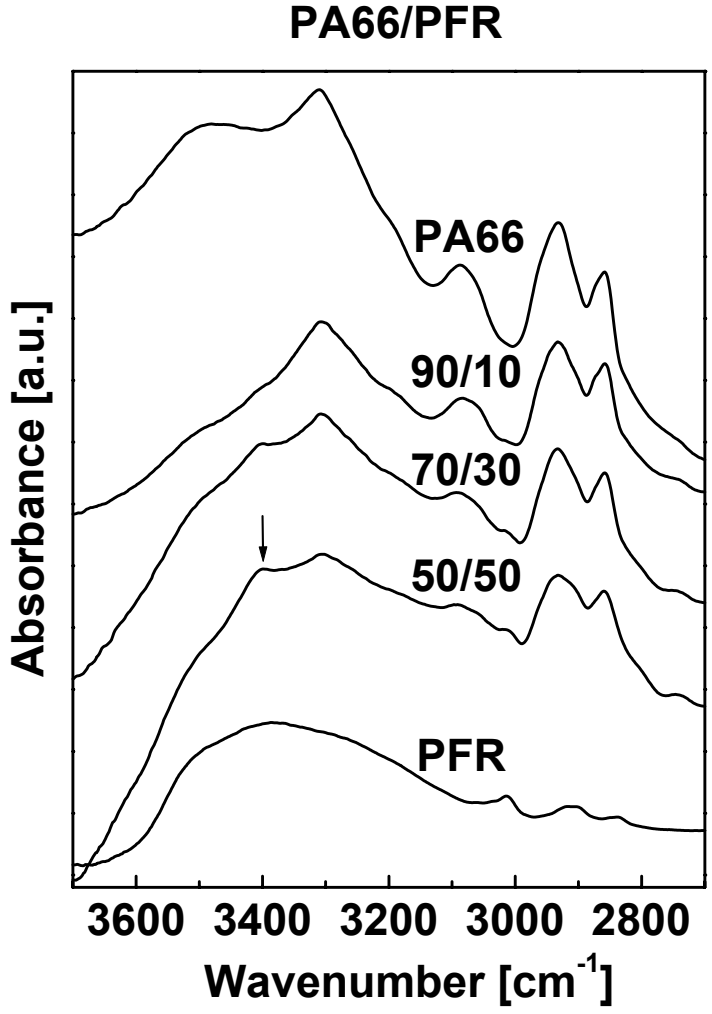

Figure 6.29: FTIR spectra of polyamide 66-phenol formaldehyde resin blends at 2900-3700 cm^{-1} region (arbitrary units).

6.3.1.3 Differential scanning calorimetry of PA66-PFR blends

Differential scanning calorimetry (DSC) has been successfully used to study the morphological changes when thermoplastics and phenolic resins are blended [104, 105, 108]. In the present work DSC was used to study glass transition temperatures (T_g) and the melting points (T_m) of the blends, in order to analyse the miscibility of the components at different blend compositions. Additionally, the effect of crosslinking of a PFR part using HMTA on T_g and T_m was investigated. Figure 6.30 presents DSC scans of the PA66/PFR blends without HMTA at a temperature range of 0-150 °C, showing a glass transition change upon blending, and Figure 6.31 shows the DSC curves at a temperature range of 200-280 °C. Observed T_g and T_m temperatures are given in Table 6.6.

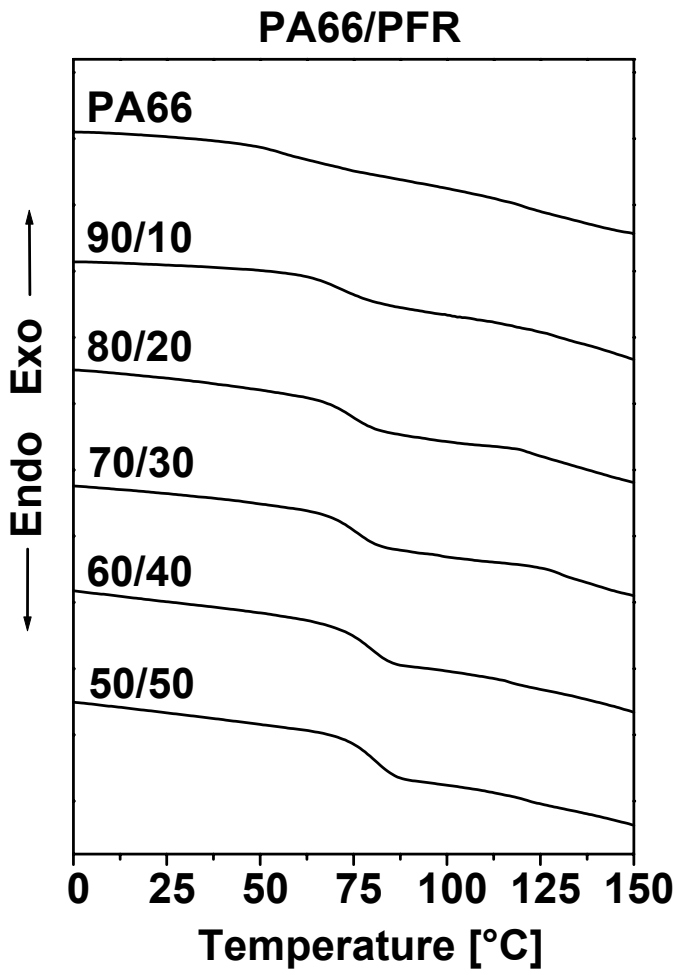

Figure 6.30: DSC thermograms of polyamide 66-phenol formaldehyde resin blends at the region of 0-150 °C (without crosslinking).

Table 6.6: T_g and T_m temperatures of the studied blends at different ratios of PA66/PFR.

Formulation	*HMTA crosslinking*	T_g *[°C]*	T_m *[°C]*
PA66	No	56	261
95/5	No	67	261
90/10	No	72	259
80/20	No	74	256
70/30	No	75	251
60/40	No	79	241
50/50	No	80	243
PFR	No	77	-
95/5	Yes	55 / 128	261
95/10	Yes	61 / 127	261
PFR	Yes	134	-

A generally accepted criterion for the miscibility of a polymer blend is a single glass transition temperature, determined, for example, by DSC. In the present work a single T_g value was obtained for all the blends when the crosslinking agent hexamethylene tetramine (HMTA) was not used. Figure 6.30 illustrates how the glass transition temperature T_g increases with increasing PFR content. The T_g of phenolic resin is 77 °C, which is a high value for such a compound of low molecular weight. This can be explained by the hydroxyl groups in PFR, which are capable of forming strong hydrogen bonds with each other. Due to the high hydrogen bond density, the mobility of the PFR molecules is restricted, resulting in an unexpected high T_g value. As PFR is mixed with PA66 (T_g 56 °C), the T_g of the blend is shifted to the intermediate temperatures between the T_g values of PFR and PA66. Interestingly, when the PFR content is higher than 40 wt %, the T_g values are even higher than the T_g of PFR. This phenomenon is discussed in connection with Figure 6.32.

A second important finding is shown in Figure 6.31: melting temperature depression takes place in the case of all PA66-PFR samples under study, as long as HMTA is not added. This finding has also been observed in other blend systems of PFR like PA6-PFR, and it reflects a strong interaction between the blend components [108, 143]. These experimental results show that the strong interaction between the blend components, as suggested by the theoretical modelling and by the FTIR spectroscopy, leads to a molecular level miscibility in blends of PA66 and phenol formaldehyde resin.

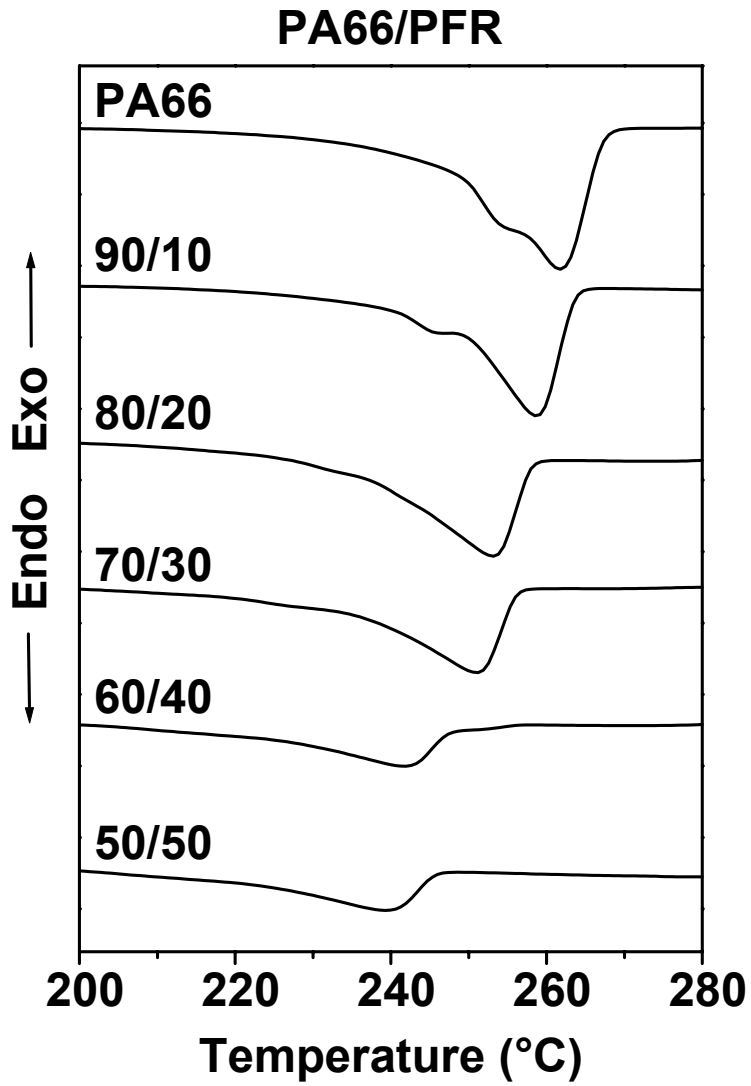

Figure 6.31: DSC thermograms of polyamide 66-phenol formaldehyde resin blends at the region of 0-150 °C (without crosslinking).

The weight average T_g of the blends can be calculated using the so called Fox equation [144]:

$$\frac{1}{T_g} = \frac{\omega_1}{T_{g1}} + \frac{\omega_2}{T_{g2}} \qquad (11)$$

where ω_i is the weight fraction and T_{gi} is the glass transition temperature of the component *i*. Figure 6.32 shows the observed and calculated T_g as a function of PFR content in the blends. It can be noticed that the deviation of the glass transition temperature of the blends from the weight average values is (in synergistic sense) strongly positive, which has been observed in several other thermoplastic-PFR blend systems [94, 95, 145]. This phenomenon is based on a supposition that the newly formed hydrogen bonds between PFR and polyamide are physical cross-links, which form a network. This results in a decreased molecular mobility of the polymer chains and therefore an unexpectedly high T_g is observed.

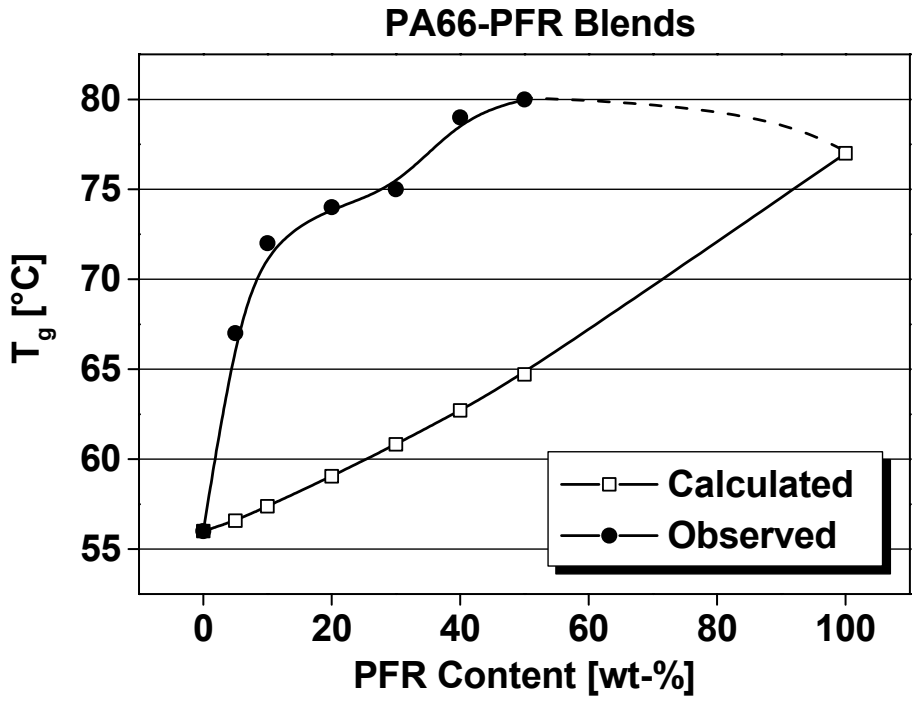

Figure 6.32: Deviation of the observed T_g from the calculated values.

As the PFR part of the blends is cross-linked by HMTA, minor changes in T_g and T_m temperatures are observed in the blends compared to the neat PA66. Figure 6.33 shows the DSC scan of PA66-PFR containing HMTA crosslinking agent. As a comparison, DSC scans of PA66 and cross-linked PFR are also shown. In addition to the primary T_g value, a weak secondary glass transition temperature is detected slightly below 130 °C. This suggests that a phase separation of PFR takes place. From the T_g values given in Table 6.6 it can be seen that at 10 wt % PFR content the T_g temperature changes more than at lower PFR content, which shows that not all of the PFR has reacted during the crosslinking. In this case, part of the PA66-PFR blend is still at a miscible state at molecular level. The phase separation was also clearly shown by optical microscopy of cross-linked film samples (Figure 6.34). These findings show that the morphology of PA66-PFR blends can be controlled firstly by changing the component ratio and, secondly, by crosslinking PFR with HMTA. It can be assumed that this will result in different macromechanical properties, thermal behaviour and water absorption in blends.

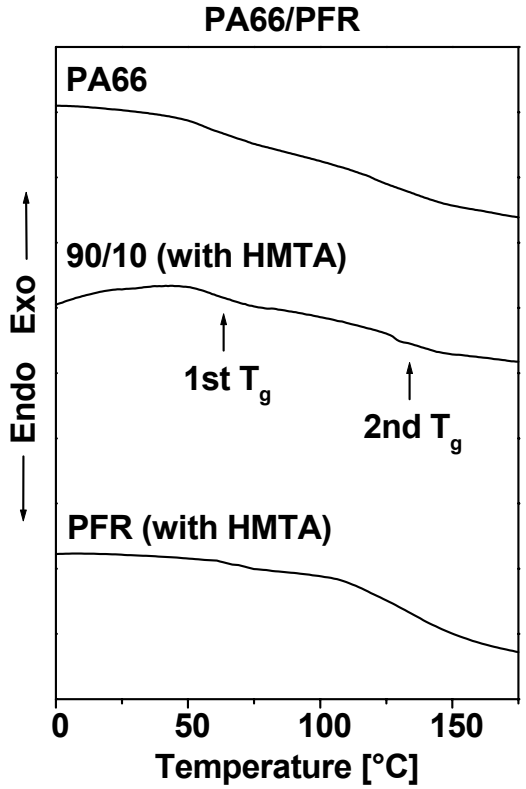

Figure 6.33: DSC scans of PA66, PA66-PFR blend containing HMTA and cross-linked phenol-formaldehyde resin.

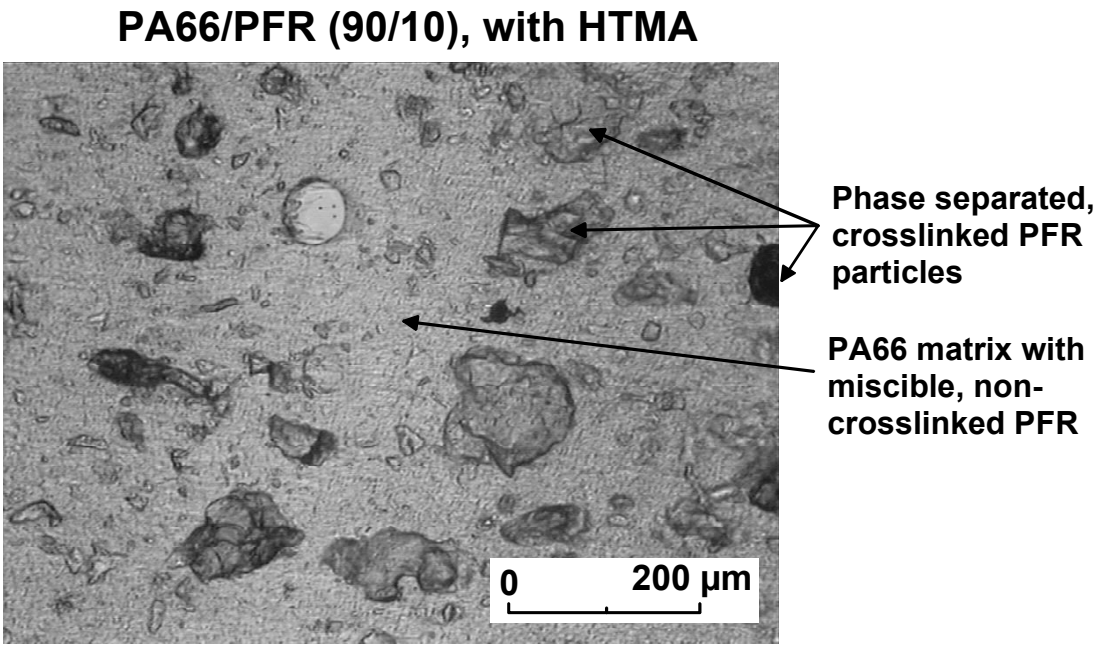

Figure 6.34: Optical micrograph of PA66-PFR blend showing the phase separation.

6.3.1.4 Microscopy studies of PA66-PFR blends

Also microscopic methods (optical microscopy and transmission electron microscopy) were used to study the morphology of the blends. Optical micrographs of PA66-PFR films with different phenolic resin contents are presented in Figure 6.35, showing that all samples are birefringent. The morphology becomes coarser with spherulite type structure as phenolic resin is added, which was also observed in recent studies with poly(ε-carpolactone)-PFR [100] and PA6-PFR [106] blends. The phenomenon can be seen also by transmission electron microscopy analysis, which was used to study a blend containing 30 wt % of phenolic resin (Figure 6.36), showing the spherulitic structure. Microscopic analysis indicated that there was no phase separated PFR phase present in samples without HTMA. However, it is known that PFR is an amorphous material and is rejected from the crystalline lattice of PA during the crystallisation process, as indicated by the SAXS patterns of PA6-PFR blends [108]. Therefore, PFR is probably located in amorphous phase of PA66. On the basis of the microscopy studies, it is suggested that PFR coarsens the lamellar structure of the PA66 spherulites and hinders the nucleation.

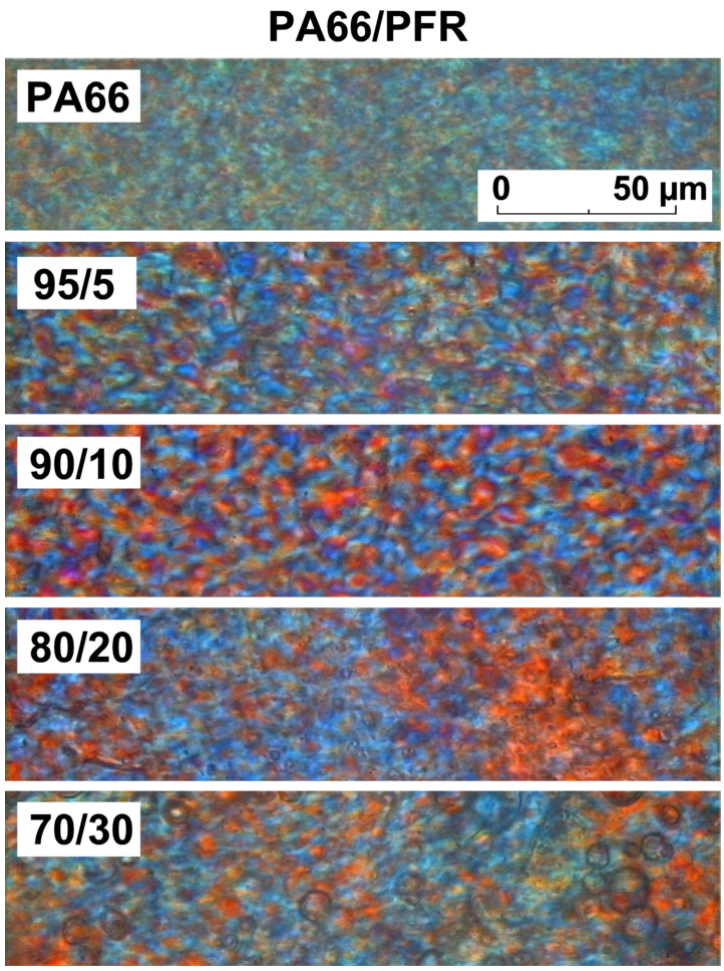

Figure 6.35: Cross polarized optical micrographs of PA66-PFR blends.

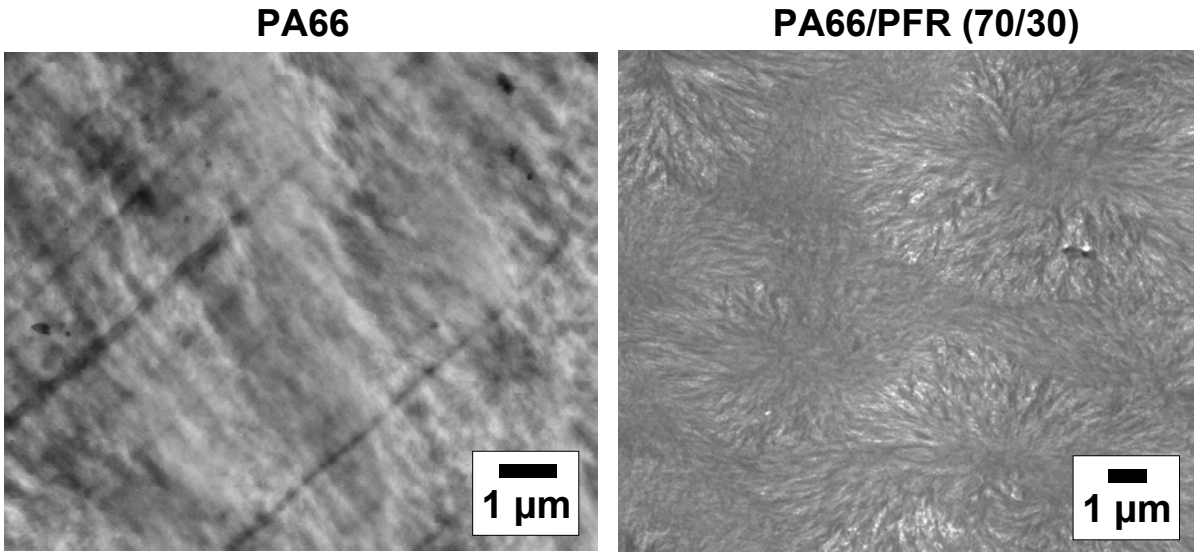

Figure 6.36: TEM micrographs of polyamide 66 and its blend with phenol formaldehyde resin.

6.3.2 Properties of LGF reinforced polyamide-phenolic resin blends

6.3.2.1 Water absorption of LGF reinforced PA66-PFR blends

In the next phase, the developed PA66-PFR blends were used as a matrix for LGF reinforced composites to study the effect of PFR on mechanical properties, water absorption and thermal behaviour. HMTA was added to the blends in order to crosslink the PFR part, since it was expected that this will result in an increased modulus due to the formation of rigid thermoset particles. However, as it was noticed in the structural study, even in cross-linked blends not all of the PFR reacted but part of it remained still in a miscible state with PA66. As indicated by the theoretical calculations, it can be expected that water absorption of PA66 is decreased upon addition of PFR. Figure 6.37 shows the water uptake of the matrix against exposure time in the LGF-PA66 composites with and without PFR (75 % relative humidity and 23 °C).

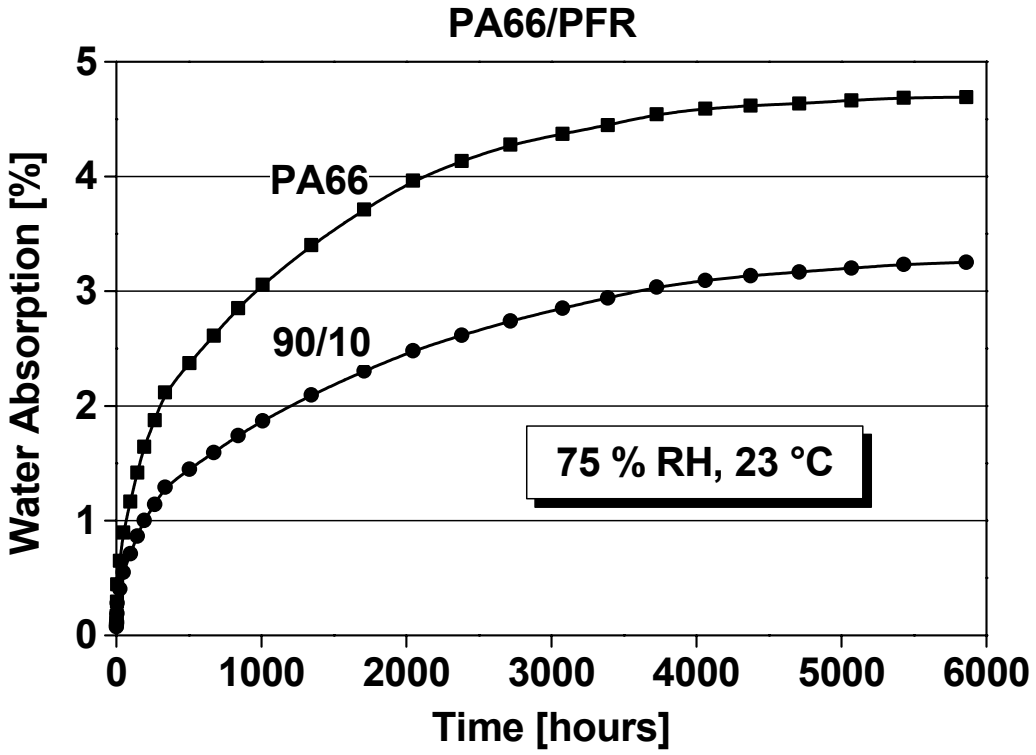

Figure 6.37: Water absorption of PA66 and PA66-PFR blend with 10 wt % of PFR as a function of time. PFR part was crosslinked with HMTA (LGF content was 20 vol %).

Figure 6.37 shows that there is a large difference in absorption rate of the PA66 and PA66-PFR samples. At the equilibrium state, a mass gain of *ca.* 4.7 wt % is observed for PA66 and *ca.* 3.3 wt % for the PA66-PFR blend sample. This experimental result demonstrates the protective effect of phenolic groups as predicted by the quantum chemical calculations. The calculations suggested that the strength of the hydrogen bonding between phenolic groups and amide groups is higher than the strength of amide-water hydrogen bonds (Table 6.5). Therefore, the water molecules are not able to brake the intermolecular bonding between PA66 and PFR. The DSC analysis showed that PA66 and PFR form a miscible or partly miscible blend, depending whether crosslinking agent was used or not. Thus, as water has less available groups for bonding in blends, decreased water absorption is observed when compared to the neat PA66 matrix.

6.3.2.2 Tensile properties of LGF reinforced PA66-PFR blends

The tensile properties of LGF reinforced PA66-PFR composites were analysed at dry state, but also after exposure in humid climate of 75 % humidity for 9000 hours, as well as after immersion in water-glycol 1:1 mixture for 250 hours. The values gained were normalised to 20 vol % fibre content to distinguish the effect of PFR addition on properties. The matrix systems analysed were crosslinked PA66-PFR blends. Figure 6.38 shows the tensile modulus of the studied blends as a function of PFR concentration in matrix. At dry state, the modulus was almost unaffected by the addition of PFR. Therefore, the phase separated PFR did not result in increase of the stiffness, which was somewhat unexpected. After conditioning in humid climate, the stiffness of the all formulations decreased considerably. However, the modulus of blends containing PFR was somewhat higher, presumably due to the lower amount of absorbed water. During the aging of the samples, the modulus of PA66 decreases 50 % as compared to the dry state values, whereas in the case of blend samples the decrease is about 43 % in best. This is an indication of the protective effect of PFR addition against water and chemicals in LGF PA66 composites.

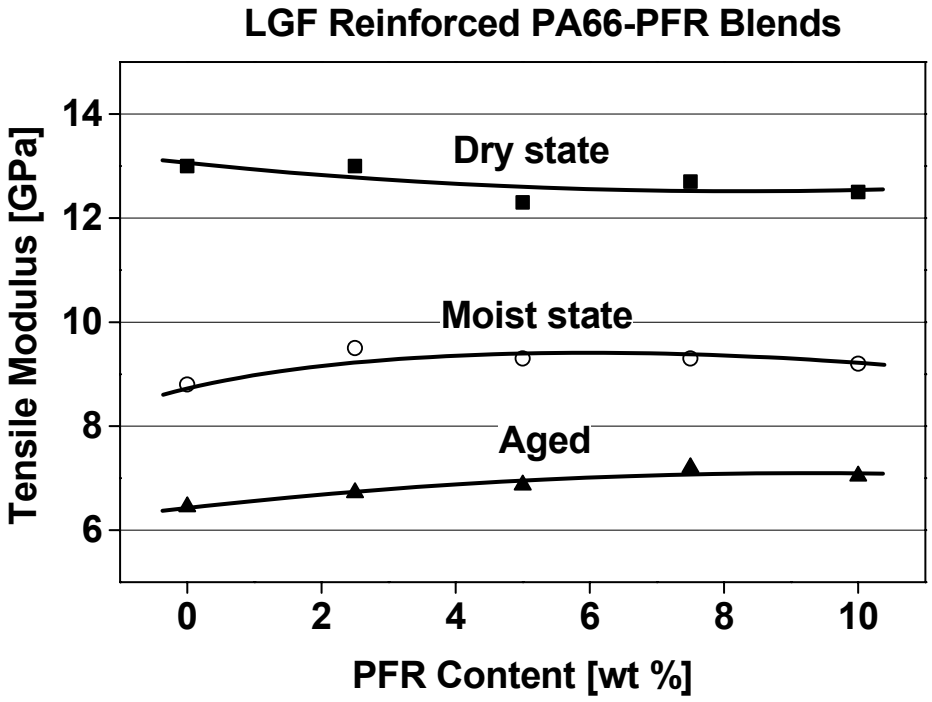

Figure 6.38: Normalised tensile modulus of LGF reinforced PA66-PFR blends containing 20 vol % of fibres in average: in dry state, after 9000 hours storing at humid conditions (75 % RH, 23 °C, moist state), and after 250 hours immersion in water-glycol mixture at 130 °C (aged). PFR component was cross-linked with HMTA.

Normalised tensile strength values of PA66-PFR blends are shown in Figure 6.39 as a function of PFR content. As shown, the dry state strength of the composites decreases by *ca.* 25 MPa upon PFR addition. However, at moist state there is nearly no difference between the samples with and without PFR. After aging, there seems to be a slight improvement in the strength in the blend samples compared to LGF-PA66 (0 % sample). The decrease in strength values at dry state is most probably related to the phase separation process taking place in the blends, resulting in PFR particle formation (Figure 6.34), since it has been observed in previous studies that particulate inclusions like calcium carbonate added to polyamide cause loss of the strength compared to unfilled materials [146] (see also Table 6.2). It can be also noticed that the strength after aging of the blend samples is on the same level as that of the LGF-PA66, which shows the protective effect of the PFR under the severe conditions used.

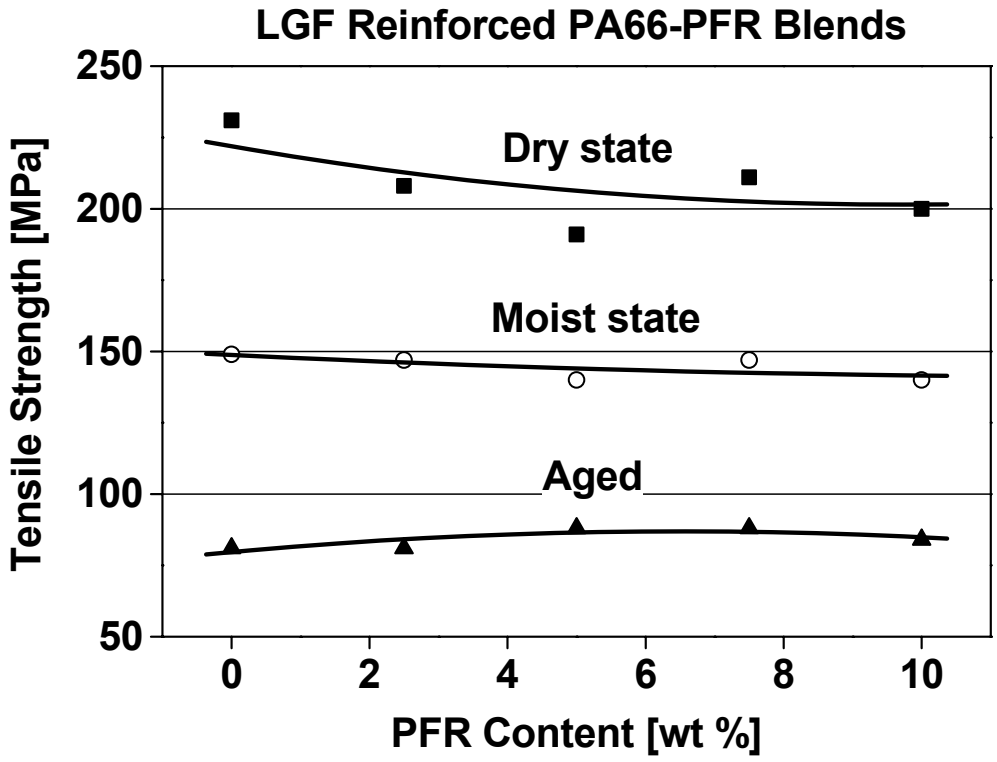

Figure 6.39: Normalised tensile strength values of LGF reinforced PA66-PFR blends containing 20 vol % of fibres in average: in dry state, after 9000 hours storing at humid conditions (75 % RH, 23 °C, moist state), and after 250 hours immersion in water-glycol mixture at 130 °C (aged). PFR component was cross-linked with HMTA.

6.3.2.3 Impact energy of LGF reinforced PA66-PFR blends

It is widely reported that water molecules enhance the impact toughness of polyamide due to the plasticization effect, which 'softens' the polymer and improves its capability to absorb energy during the impact loading. In this work the effect of water uptake on unnotced Charpy impact energy of PA66-PFR blends was analysed by using both unreinforced and reinforced samples, in order to distinguish the influence of PFR from fibre related factors. The water treatment was in this case carried out by immersing the specimens in water for 200 hours at 50 °C. Results of the impact toughness tests are collected in Table 6.7. As it can be seen, the toughness of the unreinforced blends containing HMTA is considerably lower compared to the corresponding samples without crosslinking agent. This can be

explained by the phase separation process of the cross-linked samples, since the formed PFR particles may work as crack initiation points in PA66 during the impact loading. Upon water treatment of the samples without HMTA, the impact energy of the blend with 5 wt % of PFR increased considerably but the impact energy of the sample with 10 wt % of PFR even decreased. It may well be that this difference is due to the higher water absorption rate of the sample containing 5 wt % of PFR, since there are more available amide groups in this sample. This ‘softens’ the polymer more and leads to the higher impact energy values in the composite. Increase of the impact energy after the water treatment was observed also in the case of 5 wt % samples, when PFR was cross-linked with HMTA. In this case there are less oligomeric PFR molecules available that can hydrogen bond to amide groups, on a molecular level, compared to the samples without HMTA; this is due to the reason that part of the PFR is in phase separated, particulate form. Therefore, this sample presumably absorbs more water than the uncrosslinked samples (not determined in this work, however), resulting in a 4-fold increase of the impact energy after immersion in water.

As PA66-PFR blends are reinforced with 30 vol % of LGF, impact energy is on a much higher level compared to unreinforced samples. Secondly, in this case there are only small differences between the different formulations. However, it can be seen that, similarly as in the case of unreinforced samples, the crosslinking of the PFR components with HMTA results in decreased toughness. After immersion of the reinforced PA66-PFR samples in water for 200 hours at 50 °C, the toughness values increase but not as dramatically as in the case of unreinforced blends. The explanation for this behaviour is the fact that the long glass fibres dominate the fracture process of reinforced samples more than the matrix.

Table 6.7: Unnotched Charpy impact energy of PA66-PFR blends without reinforcement and with 30 vol % of LGF at dry state and after water immersion for 200 hours at 50 °C. Formulations are given as PA66/PFR (wt %).

Formulation	*Crosslinking with HTMA*	*LGF reinforcement*	*Charpy at dry state [kJ/m^2]*	*Charpy at moist state [kJ/m^2]*
PA66	No	No	n.b.	n.b.
95/5	No	No	40 ± 11	78 ± 20
90/10	No	No	38 ± 6	30 ± 11
95/5	Yes	No	21 ± 3	33 ± 13
90/10	Yes	No	12 ± 4	16 ± 1
PA66	No	Yes	84 ± 10	105 ± 6
95/5	No	Yes	88 ± 9	111 ± 6
90/10	No	Yes	78 ± 4	101 ± 10
95/5	Yes	Yes	79 ± 8	103 ± 6
90/10	Yes	Yes	77 ± 6	97 ± 3

n.b. = not breaking

6.3.2.4 Thermal behaviour of LGF reinforced PA66-PFR blends

Molecular weight changes after immersion of the PA66-PFR blends in water-glycol mixture were studied by a solution viscosity method, in order to see the effect of blending on the hydrolysis rate. Table 6.8 presents the measured solution viscosity values and the corresponding viscosity averaged molecular weights, M_V. As shown, molecular weight of the samples decreases clearly during the immersion. However, PFR did not affect the molecular weight and hydrolysis reaction of PA66, which is probably due to the high temperature (130 °C) during the treatment; it is known that the hydrogen bonding density in blends of thermoplastics and phenolic resins decreases clearly above T_g temperature [95].

Table 6.8: Solution viscosity and molecular weight of PA66 and PA66-PFR blend with 5 wt % of PFR, before and after immersion in water-glycol mixture at 130 °C for 250 hours. The PFR part of the blend was cross-linked with HMTA.

Formulation	*Aging*	*Solution viscosity [dl/g]*	M_v *[kg/mol]*
PA66	No	1.22	35.1
95/5	No	1.11	30.7
PA66	Yes	0.65	14.9
95/5	Yes	0.64	14.7

More understanding of the thermal behaviour of the blends can be obtained by dynamic mechanical thermal analysis, DMTA. Figure 6.40 shows the DMTA spectra of unreinforced PA66 and its blend with 5 wt % of PFR. At room temperature the complex modulus |*E**| is somewhat higher in the case of the PA66-PFR blend compared to the neat PA66, which can be explained by the hydrogen bonding network taking place upon blending. However, as temperature is increased, the differences between the samples become minor so that the curves coincide at a temperature of *ca.* 110 °C. This phenomenon shows that the hydrogen bonding density decreases upon heating.

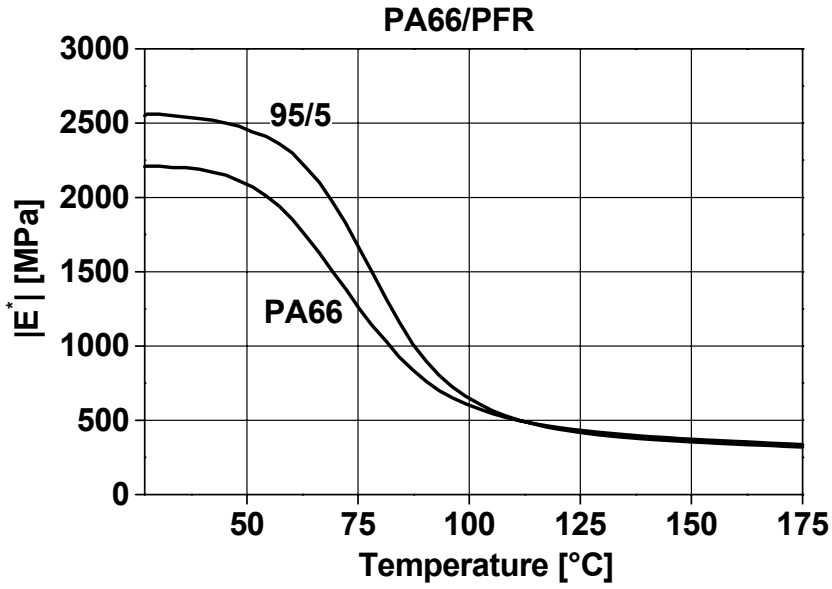

Figure 6.40: DMTA spectra of unreinforced PA66 and a PA66-PFR blend.

6.3.2.5 Electron microscopy studies of LGF reinforced PA66-PFR blends

Scanning electron microscopy was used to study the fracture surfaces of LGF reinforced PA66 and PA66-PFR blends after Charpy impact test. Figure 6.41 shows SEM micrograph of the impact fracture surface of an LGF reinforced PA66 composite. The fibre surfaces are well covered with the matrix, which is an indication of a good fibre-matrix adhesion. Secondly, the matrix shows a brittle failure mode, as indicated by the low amount of deformation patterns. Upon blending of PA66 with PFR, this morphology did not change noticeably.

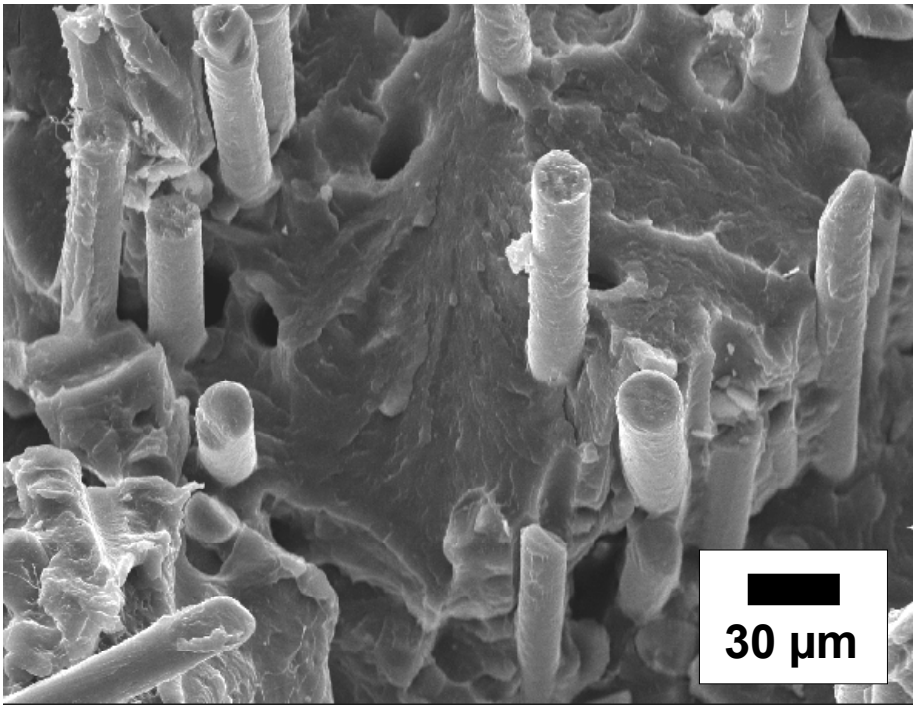

Figure 6.41: SEM fractographs after unnotched Charpy impact toughness test for dried samples of LGF reinforced PA66.

Figure 6.42 illustrates SEM micrographs of impact fracture surfaces after treatment of LGF PA66 and LGF PA66-PFR composites in a water glycol mixture for 250 hours at 130 °C. In the case of LGF PA66 the fibres were poorly connected to the matrix, and the fibre surfaces were not any more covered with polyamide (Figure 6.42a). This indicates that the immersion in water-glycol mixture has disrupted the adhesion between the fibres and the matrix. Also in PA66-PFR blends the fibre-matrix adhesion is poorer than in the case of untreated composites, but in this case the fibres are still connected to the matrix (Figure 6.42 b). Additionally, there is still some

matrix which is covering the fibre surfaces. This observation provides an explanation for the better mechanical properties of LGF reinforced PA66-PFR composites after immersion, as compared to the corresponding LGF-PA66 samples. Due to the better adhesion, the stresses can be better transferred to the fibres, which results in improved mechanical response (Figures 6.38 and 6.39).

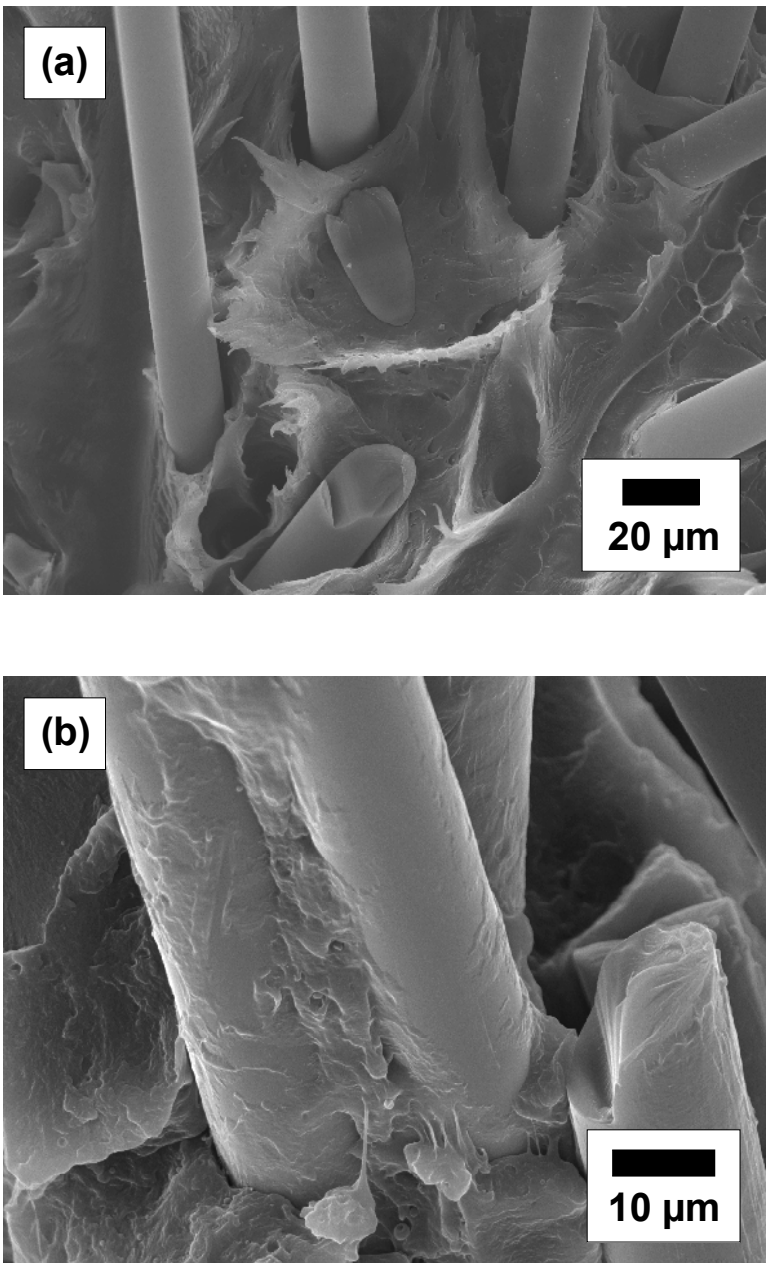

Figure 6.42: SEM fractographs after Charpy impact toughness test for aged samples (250 hours immersion in water-glycol mixture at 130 °C):
a) LGF reinforced PA66 and
b) LGF reinforced PA66-PFR blend with 5 wt % of PFR part (cross-linked with HMTA).

6.3.3 Conclusions

The present work has shown that polymers containing amide functionalities can form strong physical bonds with compounds including hydrogen bonding donors. This idea was illustrated by using a phenolic formaldehyde type resin including hydroxyl groups. As has been shown, the strong hydrogen bonding between the amide groups and the hydroxyl groups resulted in miscibility at a molecular level. Additionally, quantum mechanical calculations, as well as the spectroscopic analysis, predicted that the blending of PA with hydrogen bonding substances, such as PFR, reduces water absorption. Since PFR is chemically a thermoset prepolymer, the morphology of the blends can be modified by hexamethylene tetramine, which induces a crosslinking reaction in PFR. This was observed to lead to a phase separation of PFR, as indicated by DSC and optical microscopy studies.

When PA66-PFR blends were used as a matrix in LGF reinforced composite materials, water absorption was decreased by 30 % compared to LGF-PA66. This decrease was also reflected in the mechanical properties, particularly in the tensile modulus, which was higher in the case of blend samples compared to LGF-PA66 (after treatment in humid conditions). Treatment of the samples in water-glycol mixture at elevated temperature resulted in decreasing mechanical properties of the LGF reinforced composites. However, by using a PA66-PFR blend as a matrix, the decrease was smaller compared to composites using PA66 only. Solution viscosity and DMTA analyses showed that blending cannot protect the matrix from polymer chain degradation during the immersion test at elevated temperature. This is because the hydrogen bonding density between PA66 and PFR is reduced. On the other hand, SEM micrographs showed that the fibre-matrix adhesion in LGF-PA66 composites disappeared upon aging, whereas in the case of LGF reinforced PA66-PFR blends there was still some interfacial adhesion left. Therefore, it seems that PFR can protect the interface between long glass fibres and the polyamide matrix, leading to better overall stability of the composite in a hydrolytic environment. Applications of these developed composite materials could be in parts of automobile cooling systems, where the materials are subjected to high temperatures, as well as to a chemical environment.

7 CONCLUDING REMARKS

The results of this study have demonstrated how the properties of LGF reinforced thermoplastic composites can be modified by using different concepts of polymer materials science. The basic approach throughout the work has been to systematically analyse the materials: the molecular level phenomena, the mechanical properties of the composites, and their characteristics needed in potential applications of the commercial market. It was shown that by applying the basic principles of chemistry and physics (*e.g.* analysing the chemical structures of components) provides a useful platform from which to realise required properties in final composite parts. Furthermore, understanding these fundamental factors can enhance macroscale properties leading to novel applications containing improved or new property combinations. The development of novel tools to tailor the properties of LFT composites has been illustrated in this work by three case studies. In the first one of them it was demonstrated how the properties of thermoplastic styrenic based LGF composites can be tailored by using a compatibilising agents, and by a novel LGF concentrate concept. In the second case study, LGF reinforced PP composites were modified by adding mineral fillers to the matrix. Finally, a novel matrix system based on PA66 and oligomeric thermosets was developed for LGF composites. Some final remarks on each of the three case studies are reported below.

Remarks on material system A: LGF composites based on thermoplastic styrenic resins:

The first case study of the present work dealt with LGF composites based on thermoplastic styrenic resins. Thermoplastic styrenics are frequently used in automotive applications such as instrumental panels and decorative components, both without reinforcement and in fibre reinforced form (usually short glass fibres). Therefore, it can be assumed that LGF reinforced thermoplastic styrenics have a commercial potential in such a market. However, there are some technological issues which must be resolved before the commercial applications can be realised. The compatibility of the glass fibres with thermoplastic styrenics is one of the most

important of these issues. In the present work the adhesive strength between the reinforcing fibres and the SAN or PS matrix was improved by adding a small amount of functionalised styrenic resins into to the matrix. As a consequence, improvements in the mechanical properties of LGF composites were obtained. A second important aspect of LFT styrenics is the variety of the possible matrix resins available. It is possible to use neat PS, its co-polymers (*e.g.* SAN, ABS, SMA) and blends with other thermoplastics (*e.g.* PC/ABS, PA/ABS). It was demonstrated that the use of LGF concentrate as a base material offers a novel, flexible way of manufacturing final parts: the fibre concentration can be modified according to the application by mixing the concentrate with neat thermoplastic styrenic resins.

The present work has demonstrated that functionalised thermoplastic styrenics can be successfully applied as coupling agents in LGF styrenic composites. However, the concept can be further developed by changing the amount of functional groups in the coupling agent (in the present work: maleic acid anhydride). The type of the carrier polymer could also have an affect on the final properties. Therefore, it would make sense to cross-mix the different functional polymers (like SAN-*co*-MAH, PS-*co*-MAH, ABS-*co*-MAH) with different LGF reinforced thermoplastic styrenics. In the case of a concentrate concept a possibility for future development work is to further optimise the material properties by selecting the most suitable raw materials (matrix system, additive *etc.*). Such a research work would be of both a considerable academic and commercial interest.

Remarks on material system B: LGF-PP/filler hybrid composites:

Initially, the reason for adding fillers in thermoplastics was to reduce material costs. However, nowadays it is known that fillers can be used to improve several properties in polymers such as stiffness and form stability. From the processing point of view, fillers can also be used to reduce the cooling times of the parts since the thermal conductivity of the mineral fillers is much higher compared to thermoplastics like PP. The results of the present work have shown that the addition of fillers in LGF-PP

results in higher stiffness, without compromising strength or toughness. In the targeted automotive applications this means a decreased tendency for warpage, which is a big advantage in the case of large but relatively thin parts, such as the one presented in Figure 7.1. The part shown is a trunk cover of Mercedes Benz SL, illustrating the potential of the hybrid concept in such applications.

Figure 7.1: An application of the hybrid concept: a cover of a trunk of Mercedes Benz SL. Material is FACTOR LGF reinforced PP with a mineral filler (moulder: Intier Automotive).

The results of the present work show that the final properties of LGF-PP/filler hybrid composites are not only determined by the filler content, but also by the type of filler used. This work provides the basic data necessary to understand this material behaviour. However, there are many technological aspects which could be interesting subjects for future research. Firstly, as was shown in this study, the L/D ratio of the filler has a pronounced effect on the mechanical properties of hybrid composites. Therefore, fillers that have a high aspect ratio (*e.g.* magnesium

hydroxide, MgOH) might result in interesting property combinations when being used as a hybrid “reinforcement” in LFT materials. Secondly, the reduction of warpage in final parts, as well as the processing related aspects (*e.g.* cooling time), are also issues which might be potential subjects for future studies.

Remarks on material system C: LGF composites based on PA-thermoset blends:

The concept of blending PA66 with hydrogen bonding oligomers is rather general. Therefore one can assume that this method can be applied to any similar materials containing chemical groups which form strong hydrogen bonds with amide functionalities. In this work, phenolic based oligomers were used as an example to demonstrate the principles of this concept, and to illuminate a basic understanding of the chemical structure, the morphology and the macroscale properties of the material. As it was shown, strong hydrogen bonding between the blend components resulted in a molecular level miscibility. However, the miscibility can be controlled easily by using a crosslinking agent: the addition of HMTA to the blend of PA66 and phenolic formaldehyde resin resulted in phase separation.

The use of the developed blend system as a matrix in LFT composites revealed that the blending remarkably decreased the absorption of moisture compared with conventional LGF-PA66 composites. It was also noted that the LGF reinforced blends had better mechanical properties than LGF-PA66 without PFR after treatment in moist conditions, or after aging in water-glycol mixture at higher temperatures. These results suggest that the developed material could be used under the hood of a car, such as in parts of the cooling system. However, it should be noted that the main purpose of the present study was to offer an understanding of the chemical structure, morphological features and mechanical properties of this novel matrix system and its LGF composites. The final optimisation regarding the applications is a subject of future studies, and of commercial interest. It is assumed that the mechanical properties of the LGF reinforced PA66/oligomer blends can be further enhanced by selecting the most suitable thermoset oligomer, as well as by optimising the amount

of the crosslinking agent. The blending of polyamides with other oligomeric substances is also of academic interest and offers an interesting thematic area for future studies. After optimisation, the developed material concept may find use in automotive cooling system parts, such as the one shown in Figure 7.2.

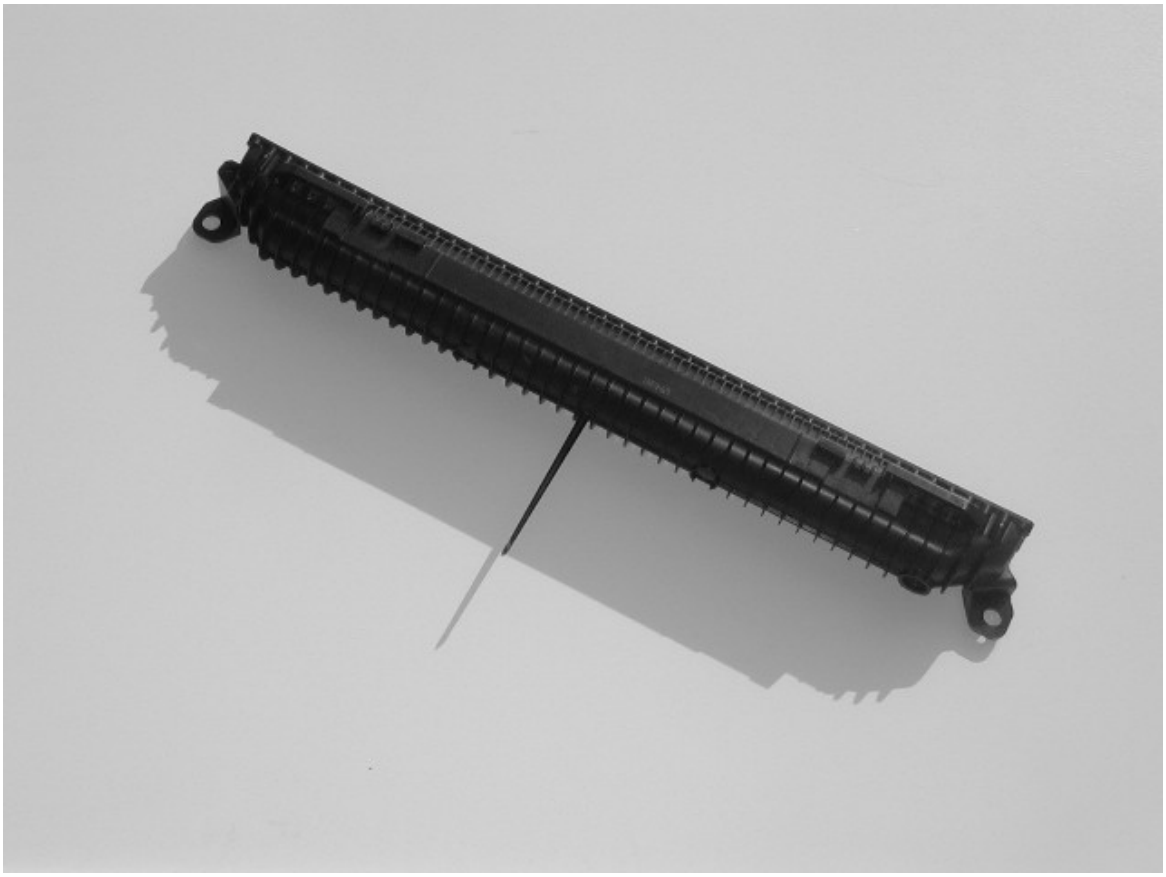

Figure 7.2: A typical, targeted application of the PA-thermoset concept: an air duct of a truck (MAN). The material is a special, tailored grade of FACTOR PA66 LGF 50.

8 REFERENCES

1. Menges, G.: The reinforcement of plastics. Kunststoffe 56 (1966), p. 818-823.
2. Harmia, T.: Aufbau, mechanische Eigenschaften und Bruchverhalten von unverstärkten, kurzfaser- und diskontinuierlich langfaserverstärkten Polymeren und Blends. Doctoral thesis, University of Kaiserslautern 1996.
3. Lutz, A.: Beitrag zur entwicklung innovativer Fertigungstechniken für die verarbeitung thermoplastischer Faserverbundwerkstoffe. Doctoral thesis, University of Kaiserslautern 1999.
4. Berglund, L.A.: Thermoplastic resins. In Handbook of Composites (Ed. S.T. Peters). New York: Chapman & Hall. 1998, p. 115-130.
5. Friedrich, K. and M. Hou: On stamp forming of curved and flexible geometry components from continuous glass. Composites A 29 (1998), p. 217-226.
6. Haffner, S.M., K. Friedrich, P.J. Hogg, and J.J.C. Busfield: Finite-element-assisted modelling of a thermoplastic pultrusion process for powder-impregnated yarn. Compos. Sci. Technol. 58 (1998), p. 1371-1380.
7. Steenkamer, D.A. and J.L. Sullivan: On the recyclability of a cyclic thermoplastic composite material. Composites B 29 (1998), p. 745-752.
8. Savadori, A. and J. Schuster: Thermoplastic composites. In Polymeric Materials Encyclopedia (Ed. J.C. Salamone). Boca Raton: CRC Press Inc. 1996, p. 8326-8343.
9. Truckenmueller, F. and H.-G. Fritz: Injection moulding of long fibre-reinforced thermoplastics: a comparison or extruded and pultruded materials with direct addition of roving strands. Polym. Eng. Sci. 31 (1991), p. 1316-1329.
10. Miller, A. and A.G. Gibson: Impregnation techniques for thermoplastic matrix composites. Polym. Polym. Compos. 4 (1996), p. 459-481.
11. Lutz, A. and T. Harmia: Impregnation techniques for fiber bundles or tows. In Polypropylene: An A-Z Reference (Ed. J. Karger-Kocsis). Dordrecht: Kluwer . 1999, p. 301-306.

12. Gibson, A.G.: Continuous molding of thermoplastic composites. In Comprehensive Composite Materials (Ed. A. Kelly and C. Zweben). Amsterdam: Elsevier. 2000, p. 979-998.

13. Bates, P.J. and X.P. Zou: Polymer melt impregnation of glass fibres. Int. Polym. Proc. 17 (2002), p. 376-386.

14. Karger-Kocsis, J.: Swirl mat- and long discontiunuous fiber mat-reinforced polypropylene composites-status and future trends. Polym. Compos. 21 (2000), p. 514-522.

15. Krause, W., F. Henning, S. Tröster, O. Geiger, and P. Eyerer: LFT-D - A process technology for large scale production of fiber reinforced thermoplastic composites. J. Thermoplast. Compos. Mater. 16 (2003), p. 289-302.

16. Månson, J.-A.E., M.D. Wakeman, and N. Bernet: Composite processing and manufacturing - an overview. In Comprehensive Composite Materials (Ed. A. Kelly and C. Zweben): Elsevier. p. 577-607.

17. Stokes, V.K., L.P. Inzinna, E.W. Liang, T.G. G, and J.T. Woods: A phenomenological study of the mechanical properties of long-fiber filled injection-molded thermoplastic composites. Polym. Compos. 21 (2000), p. 696-710.

18. Karger-Kocsis, J., T. Harmia, and T. Czigány: Comparison of the fracture and failure behavior of polypropylene composites reinforced by long glass fibers and by glass mats. Compos. Sci. Technol. 54 (1995), p. 287-298.

19. Lee, N.-J. and J. Jang: The effect of fibre content on the mechanical properties of glass fibre mat/polypropylene composites. Composites A 30 (1999), p. 815-822.

20. Toll, S. and P.-O. Andersson: Microstrucutre of long- and short-fiber reinforced injection molded polyamide. Polym. Compos. 14 (1993), p. 116-125.

21. Akay, M. and D. Barkley: Fibre orientation and mechanical behaviour in reinforced thermoplastic injection mouldings. J. Mater. Sci. 26 (1991), p. 2731-2742.

22. Skourlis, T.P., C. Chassapis, and S. Manoochehehri: Fiber orientation morphological layers in injection molded long fiber reinforced thermoplastics. J. Thermoplast. Compos. Mater. 10 (1997), p. 453-475.

23. Harmia, T. and K. Friedrich: Local fracture resistance based on microstructural efficiency concept and simulation of injection molding. Theor. Appl. Fract. Mech. 26 (1997), p. 47-52.

24. Hollin, J., D. Miller, and D. Vautour: A comparison of transverse properties of 50% short and long glass fiber reinforced nylon 6/6 resin. J. Reinf. Plast. Compos. 17 (1998), p. 1617-1624.

25. Mouzakis, D.E., T. Harmia, and J. Karger-Kocsis: Fracture behaviour of discontinuous long glass fibre reinforced injection moulded polypropylene. Polym. Polym. Compos. 8 (2000), p. 167-175.

26. Thomason, J.L.: The influence of fibre length and concentration on the properties of glass fibre reinforced polypropylene: 5. Injection moulded long and short fibre PP. Composites A 33 (2002), p. 1641-1652.

27. Thomason, J.L. and W.M. Groenewoud: The influence of fibre length and concentration on the properties of glass fibre reinforced polypropylene: 2. Thermal properties. Composites A 27 (1996), p. 555-565.

28. Thomason, J.L. and M.A. Vlug: Influence of fibre length and concentration on the properties of glass fibre-reinforced polypropylene: 1. Tensile and flexural modulus. Composites, Part A, 27 (1996), p. 477-484.

29. Thomason, J.L., M.A. Vlug, G. Schipper, and H.G.L.T. Krikor: Influence of fibre length and concentration on the properties of glass fibre-reinforced polypropylene: Part 3. Strength and strain at failure. Composites A 27 (1996), p. 1075-1084.

30. Thomason, J.L. and M.A. Vlug: Influence of fibre length and concentration on the properties of glass fibre-reinforced polypropylene: 4. Impact properties. Composites A 28 (1997), p. 277-288.

31. Pechulis, M. and D. Vautour: The effect of thickness on the tensile and impact properties of reinforced thermoplastics. J. Reinf. Plast. Compos. 17 (1998), p. 1580-1586.

32. Spahr, D.E., K. Friedrich, J.M. Schulz, and R.S. Bailey: Microstructure and fracture behaviour of short and long fibre-reinforced polypropylene composites. J. Mater. Sci. 25 (1990), p. 4427-4439.

33. Peltonen, P., E.J. Pääkkönen, P.K. Järvelä, and P. Törmälä: The influence of adhesion promoters on the properties of injection moulded long-glass-fibre polypropylene. Plast. Rubber Compos. Process. Appl. 23 (1995), p. 111-126.

34. Mäder, E., E. Moos, and J. Karger-Kocsis: Role of film formers in glass fibre reinforced polypropylene - new insights an relation to mechanical properties. Composites A 32 (2001), p. 631-639.

35. Chou, S., L.-S. Lin, and J.-T. Yeh: Effect of surface treatment of glass fibres on adhesion to polypropylene resin. Polym. & Polym. Compos. 8 (2000), p. 131-138.

36. Mäder, E. and E.V. Pisanova: Characterization and design of interphases in glass fiber reinforced polypropylene. Polym. Compos. 21 (2000), p. 361-368.

37. Hamada, H., K. Fujihara, and A. Harada: The influence of sizing conditions on bending properties of continuous glass fiber reinforced polypropylene composites. Composites, Part A , 31 (2000), p. 979-990.

38. Lee, N.-J. and J. Jang: The use of a mixed coupling agent system to improve the performance of polypropylene-based composites reinforced with short-glass-fibre mat. Compos. Sci. Technol. 57 (1997), p. 1559-1569.

39. Gao, P., K.B. Su, Y. Ward, and L.T. Weng: Effects of chemical composition and thermal stability of finishes on the compatibility between glass fiber and high melting temperature thermoplastics. Polym. Compos. 21 (2000), p. 312-321.

40. Han, C.D., C. Sanford, and H.J. Yoo: Effects of titanate coupling agents on the rheological and mechanical properties of filled polyolefins. Polym. Eng. Sci. 18 (1978), p. 849-854.

41. Wade, G.A. and W.J. Cantwell: Adhesive bonding and wettability of plasma treated, glass fiber-reinforced nylon-6,6 composites. J. Mater. Sci. Lett. 19 (2000), p. 1829-1832.

42. Karger-Kocsis, J. and T. Czigány: Interfacial effects on the dynamic mechanical behavior of weft-knitted glass fiber fabric-reinforced polypropylene composites produced of commingled yarns. Tensile and flexural response. Appl. Compos. Mater. 4 (1997), p. 209-218.

43. Jang, J., Y.J. Lee, and J.K. Jeong: Performance improvement of glass-fiber-reinforced polystyrene composite using a surface modifier. I. Synthesis and characterization of poly(γ-MPS-*co*-styrene). J. Appl. Polym. Sci. 56 (1995), p. 1561-1660.

44. Jang, J., Y.J. Lee, and J.K. Jeong: Performance improvement of glass-fiber-reinforced polystyrene composite using a surface modifier. II. Mechanical properties of composites. J. Appl. Polym. Sci. 59 (1996), p. 2069-2077.

45. Tjong, S.C., R.K.Y. Li, and X.L. Xie: Compatibilizing effect of styrene-maleic anhydride copolymer on the properties of poylamide-6/liquid crystalline copolyester composites. J. Appl. Polym. Sci. 77 (2000), p. 1964-1974.

46. Guest, M.J.: Styrene Copolymers. In Handbook of Thermoplastics (Ed. O. Olabisi). New York: Dekker. 1997, p. 161-175.

47. Sosa, J.M. and K.P. Blackmon: Styrenic resins. In Polymeric Materials Encyclopedia (Ed. J.C. Salamone). Boca Raton: CRC Press Inc. 1996, p. 8032-8041.

48. Yokouchi, M., S. Seto, and Y. Kobayashi: Comparison of polystyrene, poly(styrene/acrylonitrile), high-impact polystryrene, and poly(acrylonitrile/-butadiene/styrene) with respect to tensile and impact properties. J. Appl. Polym. Sci. 28 (1983), p. 2209-2216.

49. Chen, C.-H. and W.-S. Wang: The development of glass fiber reinforced polystyrene for pultrusion. I: Process feasibility, dynamic mechanical properties, and postforming. Polym. Compos. 19 (1998), p. 415-422.

50. Chen, C.-H. and W.-S. Wang: The development of glass fiber reinforced polystyrene for pultrusion. II: Effect of processing parameters for optimizing the process. Polym. Compos. 19 (1999), p. 423-430.

51. Chrysostomou, A. and S. Hashemi: Effect of reprocessing on mechanical properties of short glass fibre reinforced styrene maleic anhydride. Plast. Rubber Compos. 29 (2000), p. 235-242.

52. Devaux, E., S.-H. Pak, and C. Caze: Effects of the structure of styrene-co-maleic anhydride oligomers on the interfacial properties in a glass fibre reinforced polystyrene composite material. Polym. Test. 21 (2002), p. 773-779.

53. Maldas, D. and B.V. Kokta: Effect of fiber treatment on the mechanical properties of hybrid fiber reinforced polystyrene composites: IV. Use of glass fiber and sawdust as hybrid fiber. J. Compos. Mat. 25 (1991), p. 375-389.

54. Chrysostomou, A. and S. Hashemi: Mechanical properties of injection moulded styrene maleic anhydride (SMA). Part II: Influence of short glass fibres and weldlines. J. Mater. Sci. 33 (1998), p. 4491-4501.

55. Nabi, Z.U. and S. Hashemi: Influence of short glass fibres and weldlines on the mechanical properties of injection-moulded acrylonitrile-styrene-acrylate copolymer. J. Mater. Sci. 33 (1998), p. 2985-3000.

56. Billmeyer, F.W.: Textbook of polymer science. Singapore: John Wiley & Sons. 1984.

57. Wolfsberger, A., M. Gahleitner, and M. Wachholder: Polypropylene (PP). Kunststoffe Plast Europe 92 (10) (2002), p. 14-17.

58. Karger-Kocsis, J.: Microstructural aspects of fracture in polypropylene and in its filled, chopped fiber and fiber mat reinforced composites. In Polypropylene: Structure, blends and composites (Ed. J. Karger-Kocsis). London: Chapman & Hall. 1995, p. 142-201.

59. Harmia, T. and K. Friedrich: Mechanical and thermomechanical properties of discontinuous long glass fiber reinforced PA66/PP blends. Plast. Rubber Compos. Process. Appl. 23 (1995), p. 63-69.

60. Gibson, A.G.: Processing and properties of reinforced polypropylenes. In Polypropylene: Structure, blends and composites (Ed. J. Karger-Kocsis). London: Chapman & Hall. 1995, p. 73.

61. Thomason, J.L.: The influence of fibre properties of the performance of glass-fibre-reinforced polyamide 6,6. Compos. Sci. Technol. 59 (1999), p. 2315-2328.

62. Fu, S.-Y. and B. Lauke: The elastic modulus of misaligned short-fiber-reinforced polymers. Compos. Sci. Technol. 58 (1998), p. 389-400.

63. Dweib, A., C.F. Vahlund, and C.M.Ó. Brádaigh: Fibre structure and anisotropy of glass reinforced thermoplastics. Composites A 31 (2000), p. 235-244.

64. Hine, P.J., N. Davidson, R.A. Duckett, and I.M. Ward: Measuring the fibre orientation and modelling the elastic properties of injection-moulded long-glass-fibre-reinforced Nylon. Compos. Sci. Technol. 53 (1995), p. 125-131.

65. Thomason, J.L.: Micromechanical parameters from macromechanical measurements on glass reinforced polyamide 6,6. Compos. Sci. Technol. 61 (2001), p. 2007-2016.

66. Pukanszky, B.: Particulate filled polypropylene: structure and properties. In: Karger-Kocsis, J. (Ed.): Polypropylene: Structure, blends and composites. London: Chapman & Hall. 1995, p. 1-70.

67. Friedrich, K. and U.A. Karsch: Failure processes in particulate filled polypropylene. J. Mater. Sci. 16 (1981), p. 2167-2175.

68. Pukanszky, B., K. Belina, A. Rockenbauer, and F.H.J. Maurer: Effect of nucleation, filler anisotropy and orientation on the properties of PP composites. Composites 25 (1994), p. 205-214.

69. Kowalewski, T. and A. Galeski: Influence of chalk and its surface treatment on crystallization of filled polypropylene. J. Appl. Polym. Sci. 32 (1986), p. 2919-2934.

70. Rybnikár, F.: Interactions in the system isotactic polypropylene-calcite. J. Appl. Polym. Sci. 42 (1991), p. 2727-2737.

71. Thio, Y.S., A.S. Argon, R.E. Cohen, and M. Weinberg: Toughening of isotactic polypropylene with $CaCO_3$ particles. Polymer 43 (2002), p. 3661-3674.

72. Zuiderduin, W.C.J., C. Westzaan, J. Huetink, and R.J. Gaymans: Toughening of polypropylene with calcium carbonate particles. Polymer 44 (2003), p. 261-275.

73. Kim, G.-M. and G.H. Michler: Micromechanical deformation processes in toughened and particle-filled semicrystalline polymers: Part 1. Characterization of deformation processes in dependence on phase morphology. Polymer 39 (1998), p. 5689-5697.

74. Hargarter, N., K. Friedrich, and P. Catsman: Mechanical properties of glass fiber/talc/polybutylene-terephtalate composites as processed by the radlite technique. Compos. Sci. Technol. 46 (1993), p. 229-244.

75. Fu, S.-Y. and B. Lauke: Characterization of tensile behaviour of hybrid short glass fibre/calcite particle/ABS composites. Composites A 29 (1998), p. 575-583.

76. Fu, S.-Y. and B. Lauke: Fracture resistance of unfilled and calcite-particle-filled ABS composites reinforced by short glass fibers (SGF) under impact load. Composites A 29 (1998), p. 631-641.

77. Zhao, R., J. Huang, B. Sun, and G. Dai: Study of the mechanical properties of mica-filled polypropylene-based GMT composite. J. Appl. Polym. Sci. 82 (2001), p. 2719-2728.

78. Acosta, J.L., E. Morales, M.C. Ojeda, and A. Linares: Effect of addition of sepiolite on the mechanical properties of glass fiber reinforced polypropylene. Angew. Makromol. Chem. 138 (1986), p. 103-110.

79. Twigg, G., A. Poursartip, and G. Fernlund: Tool-part interaction in composites processing. Part I: experimental investigation and analytical model. Composites A 35 (2004), p. 121-133.

80. Kohan, M.I.: Nylon plastics handbook. Cincinnati: Hanser/Gardner Publications. 1995.

81. Valkama, S.: Self-organised nanostructures based on polyamides and polypeptides. Master's Thesis, Helsinki University of Technology 2000.

82. Evstatiev, M.: Polyamides. In Handbook of Thermoplastics (Ed. O. Olabisi). New York: Marcel Dekker. 1997, p. 641-663.

83. Magill, J.H.: Spherulites: A personal perspective. J. Mater. Sci. 36 (2001), p. 3143-3164.

84. Paul, D.R. and C.B. Bucknall, eds: Polymer Blends. Volume 1: Formulation. New York: John Wiley & Sons. 1999.

85. Collyer, A.A., ed. Rubber toughened engineering plastics. 1st ed. Cambridge: Chapman & Hall. 1994.

86. Utracki, L.A.: Polymer alloys and blends: Thermodynamics and rheology. Nördlingen: Hanser. 1989.

87. Gadekar, R., A. Kulkarni, and J.P. Jog: Blends of Nylon with Polyethylene: Effect of Compatibilization on Mechanical and Dynamic Mechanical Properties. J. Appl. Polym. Sci. 69 (1998), p. 161-168.

88. Puffr, R. and J. Stehlicek: Polyamides, lactam-based. In Polymeric Materials Encyclopedia (Ed. J.C. Salamone). Boca Raton: CRC Press Inc. 1996, p. 5432-5440.

89. Anttila, U., K. Hakala, T. Helaja, B. Lofgren, and J. Seppala: Compatibilization of Polyethylene/polyamide 6 Blends with Functionalezed Polyethylenes Prepared with Metallocene Catalyst. J. Polym. Sci. 37 (1999), p. 3099-3108.

90. Park, S.J., B.K. Kim, and H.M. Jeong: Morphological, thermal and rheological properties of the blends polypropylene/nylon-6, polypropylene/nylon-6/(maleic anhydride-g-polypropylene) and (maleic anhydride-g-polypropylene)/nylon-6. Eur. Polym. J. 26 (1990), p. 131-136.

91. Ohlsson, B., H. Hassander, and B. Tornell: Improved compatibility between polyamide and polypropylene by the use of maleic anydride grafted SEBS. Polymer 39 (1998), p. 6705-6714.

92. Greco, R., M. Malinconico, E. Martuscelli, G. Ragosta, and G. Scarinzi: Rubber modification of polyamide-6 effected concurrently with caprolactam

polymerization: influence of blending conditions and degree of grafting of rubber. Polymer 29 (1988), p. 1418-1425.

93. van der Wal, A., J.J. Mulder, J. Oderkerk, and R.J. Gaymans: Polypropylene-rubber blends: 1. The effect of the matrix properties on the impact behaviour. Polymer 39 (1998), p. 6781-6787.

94. Fahrenholtz, S.R. and T.K. Kwei: Compatibility of polymer mixtures containing novolac resins. Macromolecules 14 (1981), p. 1076-1079.

95. Pennacchia, J.R., E.M. Pearce, T.K. Kwei, B.J. Bulkin, and J.-P. Chen: Compatibility of substituted phenol condensation resins with poly(methyl methacrylate). Macromolecules 19 (1986), p. 973-977.

96. Kim, H.-I., E.M. Pearce, and T.K. Kwei: Miscibility Control by Hydrogen Bonding in Polymer Blends and Interpenetrating Networks. Macromolecules 22 (1989), p. 3374-3380.

97. Zhang, X. and D.H. Solomon: Phase structures of hexamine cross-linked novolac blends. 1. blends with poly(methyl methacrylate). Macromolecules 27 (1994), p. 4919.

98. Coleman, M.M., C.J. Serman, and P.C. Painter: Effect of cross-linking on the degree of molecular level mixing in a polymer blend. Macromolecules 20 (1987), p. 226-232.

99. Mekhilef, N. and P. Hadjiandreou: Miscibility behaviour of ethylene vinyl acetate/Novolac blends. Polymer 36 (1995), p. 2165-2171.

100. Zhong, X. and Q. Guo: The miscibility and morphology of hexamine cross-linked novolac/poly(ε-caprolactone) blends. Polymer 38 (1997), p. 279.

101. Ma, C.-C.M., H.-D. Wu, P.P. Chu, and H.-T. Tseng: Prediction of Thermodynamic Properties of Novolak-Type Phenolic Resin and Aliphatic Polyester Blends: Painter-Coleman Association Model Study of Compositional Homogeneity. Macromolecules 30 (1997), p. 5443-5449.

102. Kosonen, H., J. Ruokolainen, P. Nyholm, and O. Ikkala: Self-organized cross-linked phenolic thermosets: thermal and dynamic mechanical properties of novolac/block copolymer blends. Polymer 42 (2001), p. 9481-9486.

103. Kosonen, H., J. Ruokolainen, P. Nyholm, and O. Ikkala: Self-Organized Thermosets: Blends of Hexamethyltetramine Cured Novolac with Poly(2-vinylpyridine)-block-poly(isoprene). Macromolecules 34 (2001), p. 3046-3049.

104. Yang, T.P., E.M. Pearce, T.K. Kwei, and N.L. Yang: Complexation of poly(N,N-dimethylacrylamide) and phenol-formaldehyde resins. Macromolecules 22 (1989), p. 1813-1818.

105. Wang, F.-Y., C.-C.M. Ma, A.Y.C. Hung, and H.-D. Wu: The interassociation equilibrium constant and thermodynamic properties of phenolic resin/poylamide 6 blend. Macromol. Chem. Phys. 202 (2001), p. 2328-2334.

106. Huang, M.W., K.J. Zhu, E.M. Pearce, and T.K. Kwei: The modification of Nylon 6 by a phenol-formaldehyde resin. J. Appl. Polym. Sci. 48 (1993), p. 563-573.

107. Huang, P.T., J.L. Lee, S.C. Chiu, T.K. Kwei, and E.M. Pearce: Modification of Nylon 6 by phenol-containing polymers. J. Appl. Polym. Sci. 73 (1999), p. 295-300.

108. Huang, P.-T., T.K. Kwei, E.M. Pearce, and S.V. Levchik: Blends of Nylon-6 with phenol-containing polymers. J. Polym. Sci., Part A: Polym. Chem. 39 (2001), p. 841-850.

109. Voelker, M.J.: Low temperature impact properties of long fiber thermoplastic composite molding materials. Polym. Compos. 12 (1991), p. 119-121.

110. Auerbach, I. and M.L. Carnicom: Sorption of water by nylon 66 and kevlar 29. Equilibria and kinetics. J. Appl. Polym. Sci. 42 (1991), p. 2417-2427.

111. Paterson, M.W.A. and J.R. White: Effect of water absorption on residual stresses in injection-moulded nylon 6,6. J. Mater. Sci. 27 (1992), p. 6229-6240.

112. Dlubek, G., M. Stolp, C. Nagel, H.M. Fretwell, M.A. Alam, and H.-J. Radusch: Effect of crystallization and of water uptake on the free-volume hole size in polyamides 6 and 66. J. Phys: Condens. Matter 10 (1998), p. 10443-10450.

113. Hutchison, J.L., N.S. Murthy, and E.T. Samulski: Deuterium NMR studies of water in oriented nylon 6 fibers. Macromolecules 29 (1996), p. 5551-5557.

114. Adriaensens, P., A. Pollaris, R. Carleer, D. Vanderzande, J. Gelan, V.M. Litvinov, and J. Tijssen: Quantitative magnetic resonance imagingstudy of water uptake by polyamide 4,6. Polymer 42 (2001), p. 7943-7952.

115. Chaupart, N., G. Serpe, and J. Verdu: Molecular weight distribution and mass changes during polyamide hydrolysis. Polymer 39 (1998), p. 1375-1380.

116. Akay, M.: Moisture absorption and its influence on the tensile properties of glass-fibre reinforced polyamide 6,6. Polym. & Polym. Compos. 2 (1994), p. 349-354.

117. Murthy, N.S., M. Stamm, J.P. Sibilia, and S. Krimm: Structural changes accompanying hydration in Nylon 6. Macromolecules 22 (1989), p. 1261-1267.

118. Czigány, T., Z.A. Mohd Ishak, and J. Karger-Kocsis: On the failure mode in dry and hygrothermally aged short fiber-reinforced injection-molded polyarylamide composites by acoustic emission. Appl. Compos. Mater. 2 (1995), p. 313-326.

119. Valentin, D., F. Paray, and B. Guetta: The hygrothermal behaviour of glass fibre reinforced PA66 composites: a study of the effect of water absorption on their mechanical properties. J. Mater. Sci. 22 (1987), p. 46-56.

120. Liou, W.J.: Effects of moisture content on the creep behavior of Nylon-6 thermoplastic composites. J. Reinf. Plast. Compos. 17 (1998), p. 39-50.

121. Roeder, J., R.V.B. Oliveira, M.C. Goncalves, V. Soldi, and A.T.N. Pires: Polypropylene/polyamide-6 blends: influence of compatibilizing agent on interface domains. Polym. Test. 21 (2002), p. 815-821.

122. Anderson, T.L.: Fracture Mechanics - Fundamentals and Applications. 2nd ed. Boca Raton: CRC Press Inc. 1995.

123. Harris, D.O.: Stress Intensity Factors for Hollow Circumferentially Notched Round Bars. Journal of Basic Engineering 89 (1967), p. 49-54.

124. Szabó, J.S. and T. Czigány: Investigation of static and dynamic fracture toughness on short ceramic fiber reinforced polypropylene composites. J. Macromol. Sci., Phys. B41 (2002), p. 1191-1204.

125. Solomon, O. and I. Ciuta: Determination de la ciscosite intrinsique de solutions de polymeres par une simple determination de la viscosite. J. Appl. Polym. Sci. 6 (1962), p. 683-686.

126. Aharoni, S.M.: n-Nylons: Their synthesis, structure, and properties. New York: John Wiley & Sons. 1997.

127. Frisch, M.J., G.W. Trucks, H.B. Schlegel, G. Scuseria, M.A. Robb, J.R. Cheeseman, J.A. Montgomery, T.J. Vreven, K.N. Kudin, J.C. Burant, J.M. Millam, S.S. Iyengar, J. Tomasi, V. Barone, B. Mennucci, M. Cossi, G. Scalmani, N. Rega, G.A. Petersson, H. Nakatsuji, M. Hada, M. Ehara, K. Toyota, R. Fukuda, J. Hasegawa, M. Ishida, T. Nakajima, Y. Honda, O. Kitao, H. Nakai, M. Klene, X. Li, J.E. Knox, H.P. Hratchian, J.B. Cross, C. Adamo, J. Jaramillo, R. Gomperts, R.E. Stratmann, O. Yazyev, A.J. Austin, R. Cammi, C. Pomelli, J.W. Ochterski, P.Y. Ayala, K. Morokuma, G.A. Voth, P. Salvador, J.J. Dannenberg, V.G. Zakrzewski, S. Dapprich, A.D. Daniels, M.C. Strain, O. Farkas, D.K. Malick, A.D. Rabuck, K. Raghavachari, J.B. Foresman, J.V. Ortiz, Q. Cui, A.G. Baboul, S. Clifford, J. Cioslowski, B.B. Stefanov, G. Liu, A. Liashenko, P. Piskorz, I. Komaromi, R.L. Martin, D.J. Fox, T. Keith, M.A. Al-Laham, C.Y. Peng, A. Nanayakkara, M. Challacombe, P.M.W. Gill, B. Johnson, W. Chen, M.W. Wong, C. Gonzalez, and J.A. Pople: Gaussian 03 (Revision B.02). Pittsburgh PA: Gaussian, Inc. 2003.

128. Becke, A.D.: Density-functional thermochemistry. III. The role of exact exchange. J. Chem. Phys. 98 (1993), p. 5648-5652.

129. Boys, S.F. and F. Benardi: The calculation of small molecular interactions by the differences of separate total energies. Some procedures with reduced errors. Mol. Phys. 19 (1970), p. 553-566.

130. van Duijneveldt, F.B., J.G.C.M. van Duijneveldt-van de Rijdt, and J.H. van Lenthe: State of the Art in Counterpoise Theory. Chem. Rev. 94 (1994), p. 1873-1885.

131. Qiu, W., K. Mai, and H.M. Zeng: Effect of macromolecular coupling agent on the property of PP/GF composites. J. Appl. Polym. Sci. 71 (1999), p. 1537-1542.

132. Demjen, Z., B. Pukanszky, and J. Nagy: Evaluation of interfacial interaction in polypropylene/surface treated $CaCO_3$ composites. Composites A 29 (1998), p. 323-329.

133. Rockenbauer, A., L. Jokay, B. Pukansky, and F. Tudos: Electron paramagnetic resonance investigation of orientation produced by mechanical processing in the fillers of polymer composites. Macromolecules 18 (1985), p. 918-923.

134. Argon, A.S. and R.E. Cohen: Toughenability of polymers. Polymer 44 (2003), p. 6013-6032.

135. Friedrich, K.: Crazes and shear bands in semi-crystalline thermoplastics. In Crazing in polymers (Ed. H.H. Kausch). Berlin: Springer-Verlag. 1983, 225-274.

136. Czigány, T. and J. Karger-Kocsis: Comparison of the failure mode in short and long glass fiber-reinforced injection-molded polypropylene composites by acoustic emission. Polym. Bull. 31 (1993), p. 495-501.

137. Czigány, T., J. Marosfalvi, and J. Karger-Kocsis: An acoustic emission study of the temperature-dependent fracture behavior of polypropylene composites reinforced by continuous and discontinuous fiber mats. Compos. Sci. Technol. 60 (2000), p. 1203-1212.

138. Hashemi, S. and M. Koohgilani: Fracture toughness of injection molded glass fiber reinforced polypropylene. Polym. Eng. Sci. 35 (1995), p. 1124-1132.

139. Levita, G., A. Marchetti, and A. Lazzeri: Fracture of ultrafine calcium carbonate/polypropylene composites. Polym. Compos. 10 (1989), p. 39-43.

140. Benevolenski, O. and J. Karger-Kocsis: Fracture and failure behavior of partially consolidated discontinuous glass fiber mat-reinforced polypropylene composites (Azdel SuperLite®). Macromol. Symp. 170 (2001), p. 165-179.

141. Hartikainen, J., M. Lahtinen, M. Torkkeli, R. Serimaa, J. Valkonen, K. Rissanen, and O. Ikkala: Comb-shaped supramolecules based on protonated polyaniline and their self-organization into nanoscale structures: polyaniline sulfonates/zinc sulfonates. Macromolecules 34 (2001), p. 7789-7795.

142. Lehtonen, O., J. Hartikainen, K. Rissanen, O. Ikkala, and L.-O. Pietilä: Hydrogen bonding and protonation in acid-base complexes: methanesulfonic acid-pyridine. J. Chem. Phys. 116 (2002), p. 2417-2424.

143. Flory, P.J.: Principles of polymer chemistry. Ithaca, New York: Cornell University Press. 1953.

144. Fox, T.G.: Influence of diluent and of copolymer composition on the glass temperature of a polymer system. Bull. Am. Phys. Soc. 1 (1956), p. 123.

145. Kwei, T.K.: The effect of hydrogen bonding on the glass transition temperatures of polymer mixtures. J. Polym. Sci., Polym. Lett. Ed. 22 (1984), p. 307-313.

146. Wilbrink, M.W.L., A.S. Argon, R.E. Cohen, and M. Weinberg: Toughenability of Nylon-6 with $CaCO_3$ filler particles: new findings and general principles. Polymer 42 (2001), p. 10155-10180.

LIST OF PUBLICATIONS

This thesis is based on the following publications:

A. Publications in reviewed international journals

A1. Hartikainen, J., Lehtonen, O., Harmia, T., Lindner, M., Valkama, S., Ruokolainen, J. and Friedrich, K.: Structure and morphology of polyamide 66 and oligomeric phenolic resin blends: molecular modelling and experimental investigations, *Chemistry of Materials* (in press).

A2. Hartikainen, J., Lindner, M., Harmia, T. and Friedrich, K.: Mechanical properties of polypropylene composites reinforced with long glass fibres and mineral fillers, *Plastics, Rubber and Composites* 33 (2004), p. 77-84.

A3. Hartikainen, J., Hine, P., Szabó, J. S., Lindner, M., Harmia, T., Duckett, R. A., Friedrich, K.: Polypropylene Hybrid Composites Reinforced with Long Glass Fibres and Particulate Filler: Fibre Orientation and Fracture Behaviour, *Composites Science and Technology* (in press).

B. Publications in conference proceedings

B1. Hartikainen, J., Lindner, M., Harmia, T., Friedrich, K.: Mechanical properties of long glass fibre reinforced thermoplastic styrenic resins, Proceedings of *Verbundwerkstoffe und Werkstoffverbunde*, 2.-4.7.2003, Vienna, Austria.

B2. Hartikainen, J., Lindner, M., Harmia, T.: Long glass fibre reinforced styrene based thermoplastics, Proceedings of *5th International AVK-TV Conference for Reinforced Plastics and Thermoset Moulding Compounds*, 17-18.9.2002 Baden-Baden, Germany.

LIST OF STUDENT WORKS

Ikonen, A.: Hydrolysis stabilisation of long glass fibre reinforced polyamide 6,6. Thesis required for a diploma of Bachelor of Science (Eng.), North Karelia Polytechnic, Finland 2003.